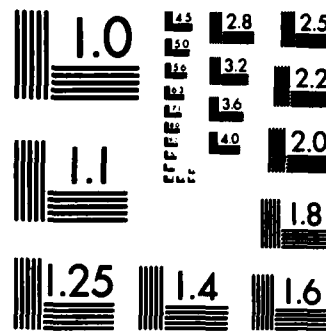
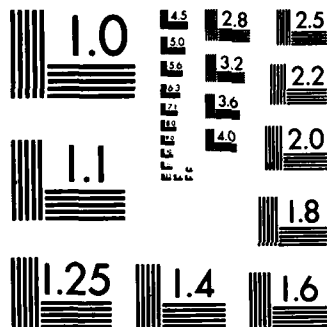


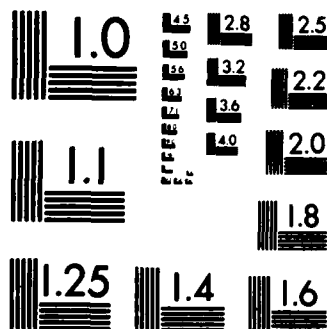
MICROCOPY RESOLUTION TEST CHART
NATIONAL BUREAU OF STANDARDS-1963-A



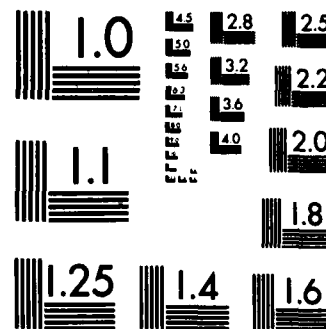
MICROCOPY RESOLUTION TEST CHART
NATIONAL BUREAU OF STANDARDS-1963-A



MICROCOPY RESOLUTION TEST CHART
NATIONAL BUREAU OF STANDARDS-1963-A



MICROCOPY RESOLUTION TEST CHART
NATIONAL BUREAU OF STANDARDS-1963-A



MICROCOPY RESOLUTION TEST CHART
NATIONAL BUREAU OF STANDARDS-1963-A

12

AD A120407

AFGL-TR-82-0207

A RESEARCH PROGRAM FOR ATMOSPHERIC CHEMISTRY,
RADIATION AND DYNAMICS

N. D. Sze
M. K. W. Ko
M. Livshits
W. C. Wang
P.B. Ryan

Atmospheric and Environmental Research, Inc.
840 Memorial Drive
Cambridge, Massachusetts 02139

Final Report
December 1980 - June 1982

DTIC
OCT 18 1982
H

July 1982

Approved for public release; distribution unlimited

DTIC FILE COPY

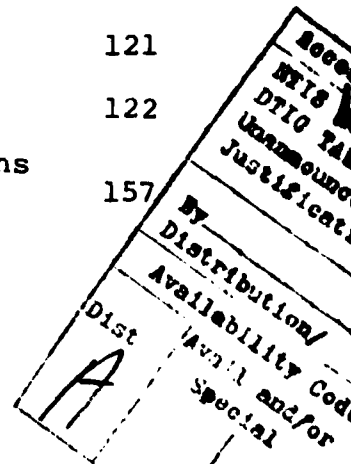
AIR FORCE GEOPHYSICS LABORATORY
AIR FORCE SYSTEMS COMMAND
UNITED STATES AIR FORCE
HANSCOM AFB, MASSACHUSETTS 01731

82 10 18 090

REPORT DOCUMENTATION PAGE		READ INSTRUCTIONS BEFORE COMPLETING FORM
1. REPORT NUMBER AFGL-TR-82-0207	2. GOVT ACCESSION NO. AD-A120407	3. RECIPIENT'S CATALOG NUMBER
4. TITLE (and Subtitle) A Research Program for Atmospheric Chemistry, Radiation and Dynamics		5. TYPE OF REPORT & PERIOD COVERED Final Report December 1980 - June 1982
		6. PERFORMING ORG. REPORT NUMBER
7. AUTHOR(s) N. D. Sze, M.K.W. Ko, M. Livshits W. C. Wang, P.B. Ryan		8. CONTRACT OR GRANT NUMBER(s) F19628-81-C-0016
9. PERFORMING ORGANIZATION NAME AND ADDRESS Atmospheric and Environmental Research, Inc. 840 Memorial Drive Cambridge, Massachusetts 02139		10. PROGRAM ELEMENT, PROJECT, TASK AREA & WORK UNIT NUMBERS 62101F 668708AB
11. CONTROLLING OFFICE NAME AND ADDRESS Air Force Geophysics Laboratory Hanscom AFB, Massachusetts 01731 Monitor/William Swider/LKD		12. REPORT DATE July 1982
		13. NUMBER OF PAGES 164
14. MONITORING AGENCY NAME & ADDRESS (if different from Controlling Office)		15. SECURITY CLASS. (of this report) Unclassified
		15a. DECLASSIFICATION/DOWNGRADING SCHEDULE
16. DISTRIBUTION STATEMENT (of this Report) Approved for public release; distribution unlimited		
17. DISTRIBUTION STATEMENT (of the abstract entered in Block 20, if different from Report)		
18. SUPPLEMENTARY NOTES		
19. KEY WORDS (Continue on reverse side if necessary and identify by block number) atmospheric chemistry, two-dimensional zonal-mean model, atmospheric ozone, ozone perturbation, model simulated trace gas concentrations, atmospheric lifetimes, meteoric metal		
20. ABSTRACT (Continue on reverse side if necessary and identify by block number) This report presents major accomplishments and significant findings of atmospheric research performed under AFGL contract F19628-81-C-0016 for the period December 1980 - June 1982. The following topics are discussed: <ul style="list-style-type: none"> . Review of recent developments in stratospheric chemistry . Modeling results on ozone perturbation studies . Results of the zonal-mean model calculations covering calculated species concentrations and atmospheric lifetimes . Role of meteoric metal in atmospheric chemistry. 		

TABLE OF CONTENTS

	Page
1. INTRODUCTION AND SUMMARY	4
2. STRATOSPHERIC CHEMISTRY: GENERAL REVIEW	8
3. OZONE PERTURBATION STUDIES	23
3.1 Single Perturbation Studies	23
3.2 Multiple Perturbation Studies	33
3.3 2-D Perturbations	35
4. RESULTS FROM 2-D MODEL	40
4.1 Introduction	40
4.2 Comparison with Observations	41
4.2a Long-Lived Species	44
4.2b Short-Lived Species	57
4.2c Ozone	77
4.2d Summary of Comparisons	88
4.3 Model Predictions of Atmospheric Lifetimes for N ₂ O, CFC-11 and CFC-12	91
4.4 Summary of Model Developments	97
5. THE ROLE OF METEORIC METAL IN ATMOSPHERIC CHEMISTRY	99
5.1 Background	99
5.2 Model Study	102
5.3 Recent Developments	106
REFERENCES	110
ACKNOWLEDGEMENTS	121
APPENDIX A - Documentation of 2-D Model	122
APPENDIX B - Latitude-Altitude Cross-Sections for Radical Species	157



1. INTRODUCTION AND SUMMARY

This report presents major accomplishments and significant findings of atmospheric research performed under AFGL Contract F19628-81-C-0016 for the period December 1980 - June 1982. Most of the findings presented here are based on the AER one- and two-dimensional models, although selective findings from other modeling groups are also included for comparison purposes. Part of the modeling effort is also funded by the CMA modeling program.

This report is organized into five sections together with two supporting appendices. Section 2 gives a brief overview of stratospheric chemistry with emphasis on the impact of recent rate data revisions on the quantitative understanding of various stratospheric chemical processes. The new rates for the reactions of OH with HNO_3 and HNO_4 introduce additional coupling between HO_x and NO_x species with the effect of reducing the OH and HO_2 concentrations in the lower stratosphere. Calculations are shown to illustrate the impact of the new rates on the vertical distributions of those trace gases that participate either directly or indirectly in various stratospheric O_3 removal processes.

Section 3 presents the results on the potential ozone perturbations due to various human activities. It is found that mainly because of the rate data revision, the calculated steady state O_3 depletion due to continued release of CFCs at 1977 production level is 6.1 percent, compared to

the previous depletion calculation of 16.4 percent based on the NASA (1979) rates. Sensitivity studies of O_3 perturbed by increasing N_2O and CO_2 have also been performed. It is pointed out that O_3 perturbations due to various human activities may interact in a non-linear fashion. Increase in atmospheric CO_2 for instance, may partially offset the CFC's-induced O_3 perturbation, particularly on an intermediate time scale (year 1980-2010).

Section 4 presents the results from our 2-D model calculation. We began with a comprehensive comparison of the calculated trace gas distribution with observations. In general, good agreement is found between calculated and observed distribution of long-lived species, except for CFC-11 and 12. The calculated latitudinal and seasonal column O_3 agrees well with observations, although the calculated latitudinal and seasonal gradients in column O_3 are less pronounced than those observed.

Much better agreement between calculated and observed distributions of radical species in the lower stratosphere (15-30 km) is achieved when the new kinetic rate data set is used. Agreement between calculated and observed distributions of Cl, ClO, NO and HNO_3 in the 35-40 km region, however, is rather poor. The situation is worth noting, since the discrepancies occur in the region where the largest impact of CFCs on O_3 is predicted; where the uncertainty in transport is thought to have minimal effect on model calculation, and where the chemistry appears to be relatively

simple because of the reduced role of larger molecules (e.g., ClNO_3 , HNO_4 , HNO_3) in stratospheric coupling processes.

We also calculated the atmospheric lifetimes for N_2O , CFC-11 and CFC-12 using the 2-D model. The behavior of these gases is typical of the upward diffusing gases which enter the stratosphere by upward diffusion from the troposphere and are removed in the stratosphere by photolytic reactions. Although direct comparison of the 2-D and 1-D results is difficult, our analysis points to the problem associated with the interpretation of the 1-D model calculated lifetimes. Because of the inability of the 1-D models to incorporate latitudinal covariance effect, 1-D models tend to overestimate the lifetimes of upward diffusing trace gases.

In Section 4 we also summarized the areas where significant improvement has been made to the 2-D model. These include the development of the diurnal code and a semi-implicit scheme for solving the trace gas equation. Other ways for improving the present model will also be discussed.

Recently, interests on meteoric metals in the atmosphere were renewed because of the possibility that trace metals may react with the chlorine species in the atmosphere. In Section 5 we report on our modeling study of the subject. We conclude that metal species have the potential to couple to other chemical cycles and change radical species concentrations. However, quantification of its effect remains difficult because of the lack of kinetic data. Nevertheless,

further modeling work should be helpful in identifying the role of the reactions and suggest priority for their measurements.

2. STRATOSPHERIC CHEMISTRY: GENERAL REVIEW

This section is intended to review the recent developments in stratospheric chemistry. We shall attempt in what follows to provide a simple account of stratospheric chemistry and focus on several recent revisions in kinetic rate data that have changed our quantitative understanding of several key chemical cycles responsible for ozone removal.

Ozone is formed by photolysis of O_2 , followed by the three-body reaction



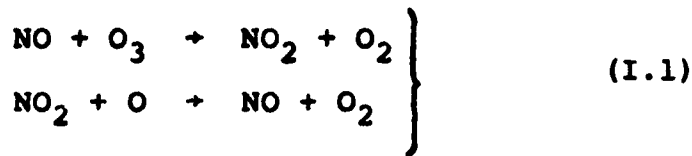
Loss of O_3 is affected by processes such as:



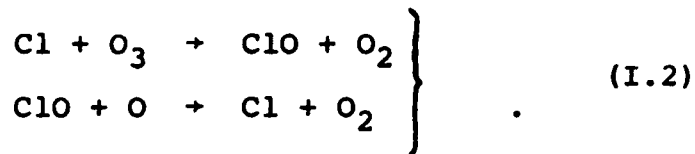
and



Both processes (I) and (II) may be catalyzed by a complex suite of reactions involving a variety of trace gases. Key examples for process (I) are:

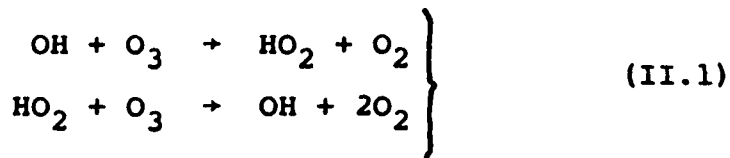


and

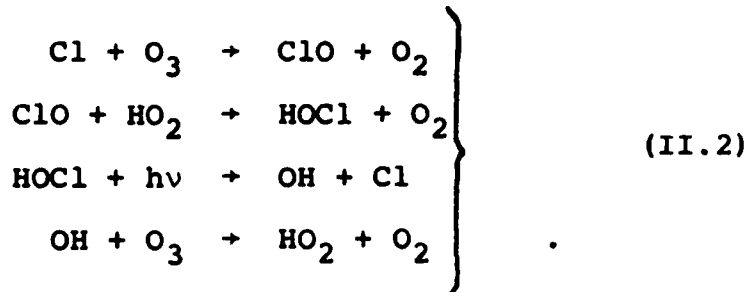


The efficiency of catalytic cycles (I.1) and (I.2) depends on the availability of O atoms as well as the radicals NO and Cl. Since the concentration of O decreases rapidly with decreasing altitude, the importance of processes such as (I.1) and (I.2) as sinks for O₃ is often restricted to altitudes above 25 km. The availability of stratospheric NO and Cl is, in part, limited by the supply of source molecules (e.g., N₂O, CFCs) from the troposphere, and, in part, regulated by HO_x chemistry, an area that has been affected most by recent changes in rate data.

In contrast to process (I), recombination of O₃ with O₃ (process II) does not depend on O atoms, but either involves slower reactions which are difficult to study at the laboratory or a longer sequence of reactions. Key examples of (II) are:



and

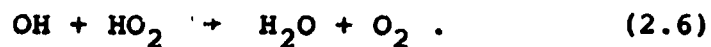


According to our present knowledge, the NO_x catalytic cycle (I.1) is the major sink for stratospheric O_3 in the region 25-36 km. Removal by (I.2) constitutes less than 10% of (I.1) below 30 km but approaches 20% of (I.1) at around 40 km. One major concern is the possibility that this sink (I.2) for O_3 might grow in time as the CFCs continue to increase in the atmosphere.

Ozone removal by (II.1) and (II.2) is restricted in the lower stratosphere and depends very much on the availability of HO_x radicals. These radicals are mainly produced by the reaction of $\text{O}(^1\text{D})$ with H_2O ,



and are removed by the following reactions:



Prior to 1979, reaction (2.6) was thought to be the major sink for stratospheric HO_x . Because of the complete lack of data on OH and HO_2 below 30 km, there is no direct way to test model predictions of HO_x in this region. Instead, Sze (1978, 1980) and McConnell and Evans (1978) have chosen an indirect approach to validate HO_x models. They

noted that certain model features (such as gradients of ClO and C₂H₆, HF/HCl, HNO₃/NO₂) would agree well with observations if it was assumed that the models (prior to 1979) had overestimated the OH abundance below 30 km. New laboratory measurements lend support to the "low OH" hypothesis. Specifically, the new rates for (2.3) and (2.4) are found to be much faster than formerly believed (see Table 2-1). The dominant sinks for HO_x below 30 km are now effected by (2.3) and (2.4) and the importance of (2.6) is restricted altitudes above 30 km, as indicated in Figure 2-1.

Mainly as a result of new laboratory studies of (2.3), (2.4), and of the cross-section of HO₂NO₂, the calculated altitude distributions of many key radical species have undergone significant changes of the past 18 months. Some of the examples based on the AER one-dimensional model are shown in Figures 2-2 through 2-7. Note that the OH concentration is about a factor of 2 to 3 smaller than that predicted by 1979 models for reasons discussed above. A somewhat larger reduction is calculated for HO₂ (Figure 2-3).

Figures 2-4 and 2-5 show the calculated changes in chlorine species (ClO, HCl, HOCl, ClNO₂) in the stratosphere. Many of the changes are related to the reduced stratospheric abundances of OH and HO₂ predicted by the present model. The concentration of ClO with 1981 rate data is lower than that of the 1979 model by factors of about ten and two at 20 and 30 km respectively. The calculated changes for HCl (Figure 2-4)

TABLE 2-1

Rate Constants for Key HO_x Reactions Given in
NASA (1979) vs. NASA/WMO (1981)

Reaction	Rate Constant	
	NASA (1979)	NASA/WMO (1981)
OH + HNO ₃ → product	8.5 (-14)	1.5 (-14) exp($\frac{650}{T}$)
OH + HO ₂ NO ₂ → product	5.0 (-13)	4 (-12)
OH + HO ₂ → H ₂ O + O ₂	3.0 (-11)	8.0 (-11)
OH + H ₂ O ₂ → H ₂ O + HO ₂	1.0 (-11) exp($-\frac{750}{T}$)	2.7 (-12) exp($-\frac{145}{T}$)

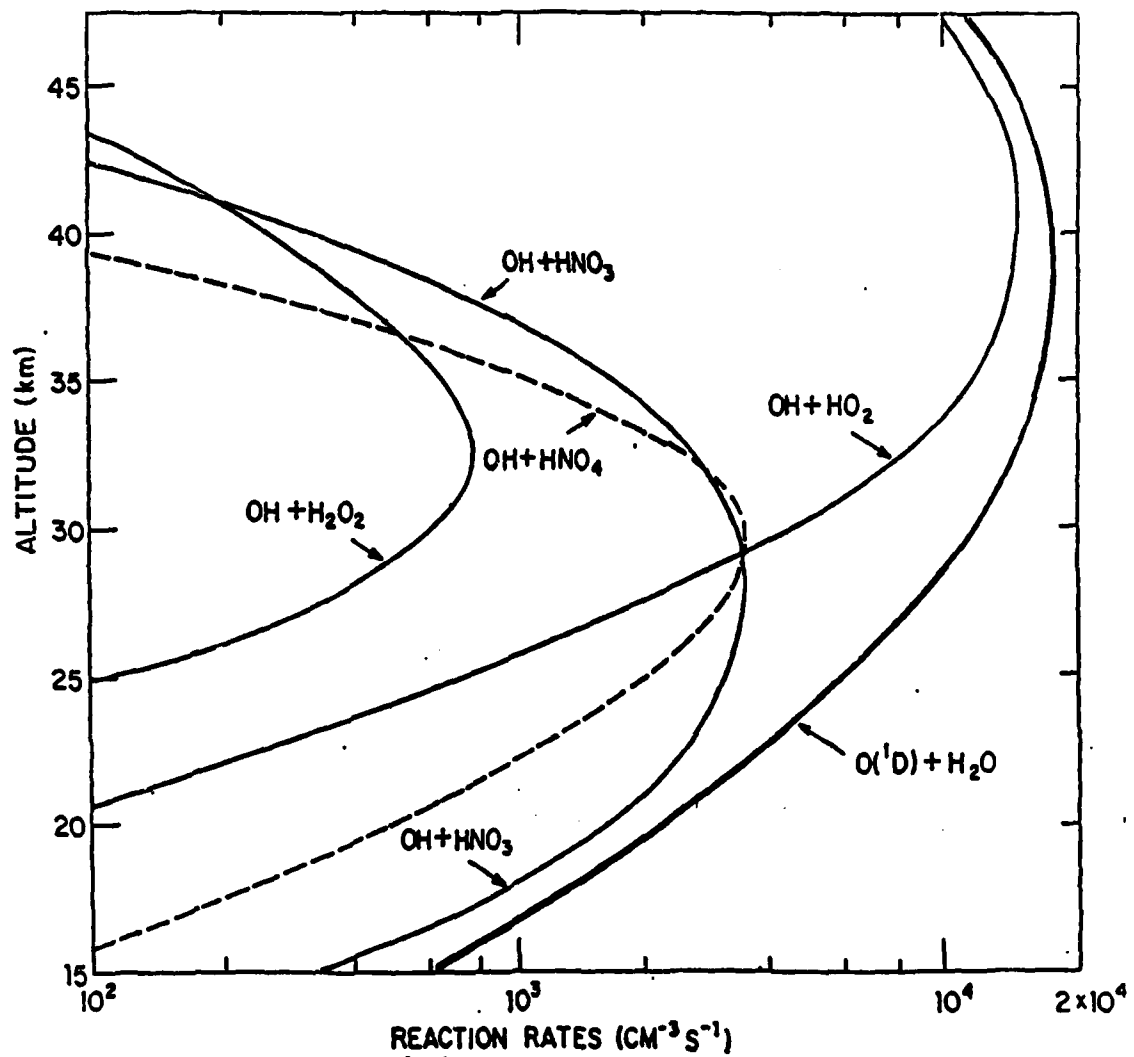


Figure 2-1

Stratospheric budget for odd hydrogen radicals showing the production and removal rates due to various chemical reactions. The calculation was performed using the reaction rate constants from JPL 81-3 (1981).

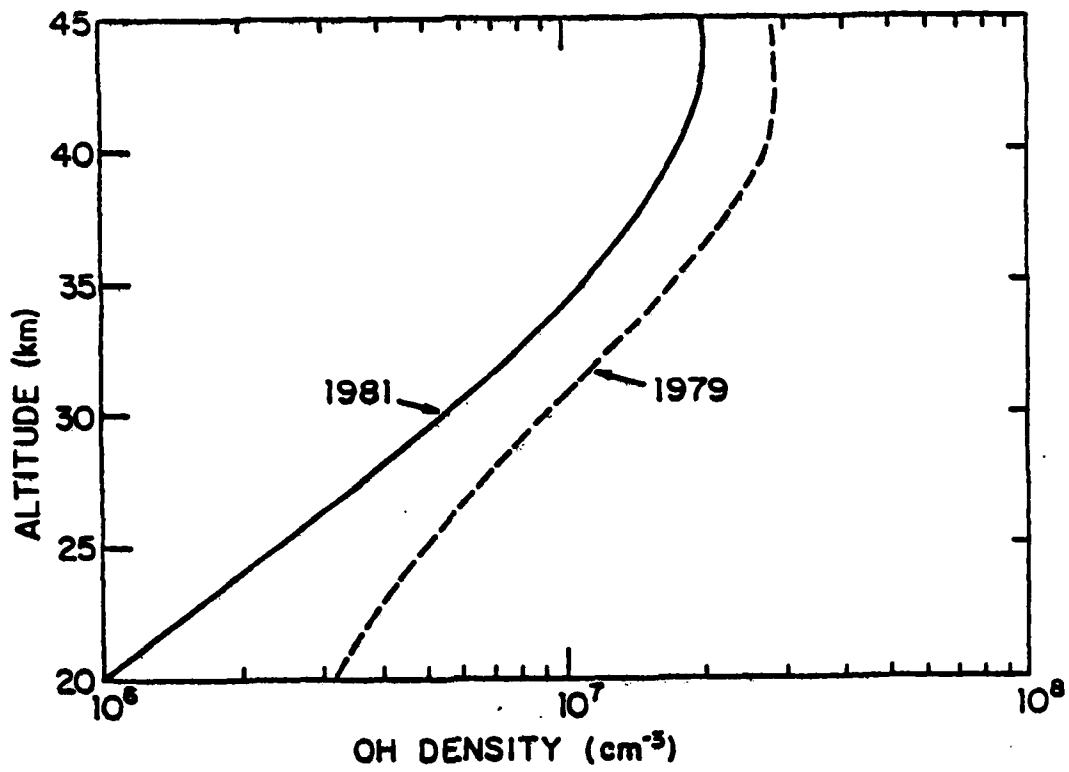


Figure 2-2

Comparison of 1-D model calculated OH concentrations using reaction rate constants from NASA (1979) and NASA/WMO (1981)

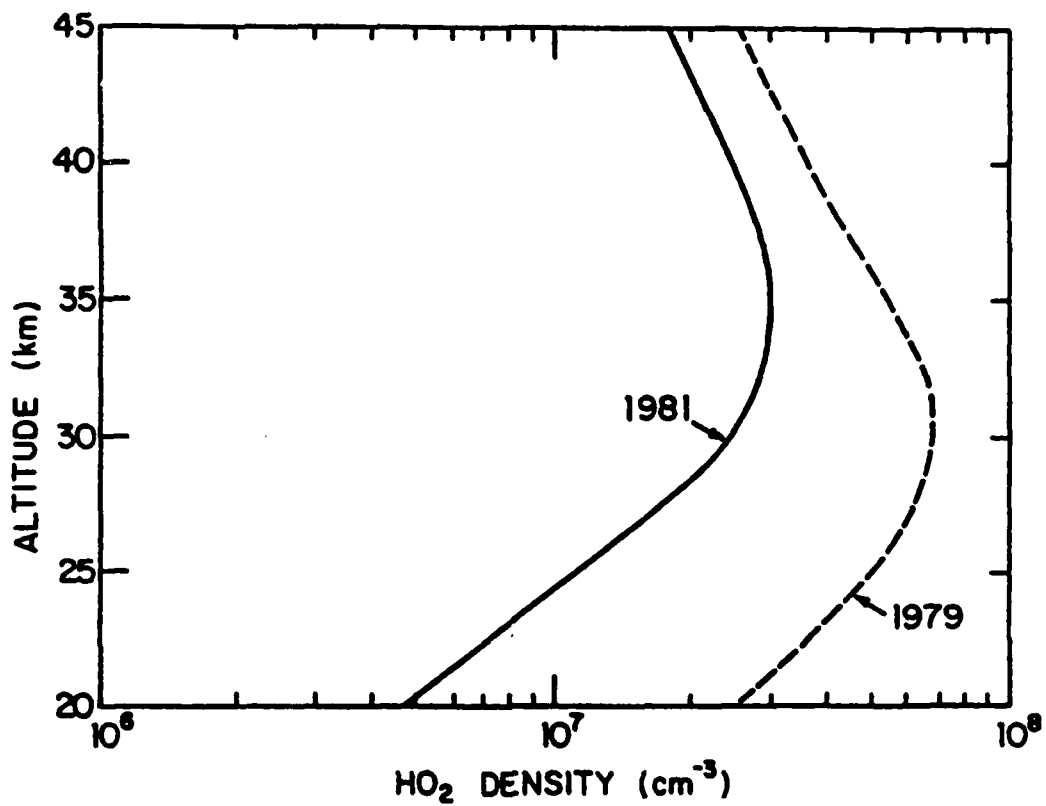


Figure 2-3

Comparison of 1-D model calculation concentrations of HO₂ using reaction rate constants from NASA (1979) and NASA/WMO (1981).

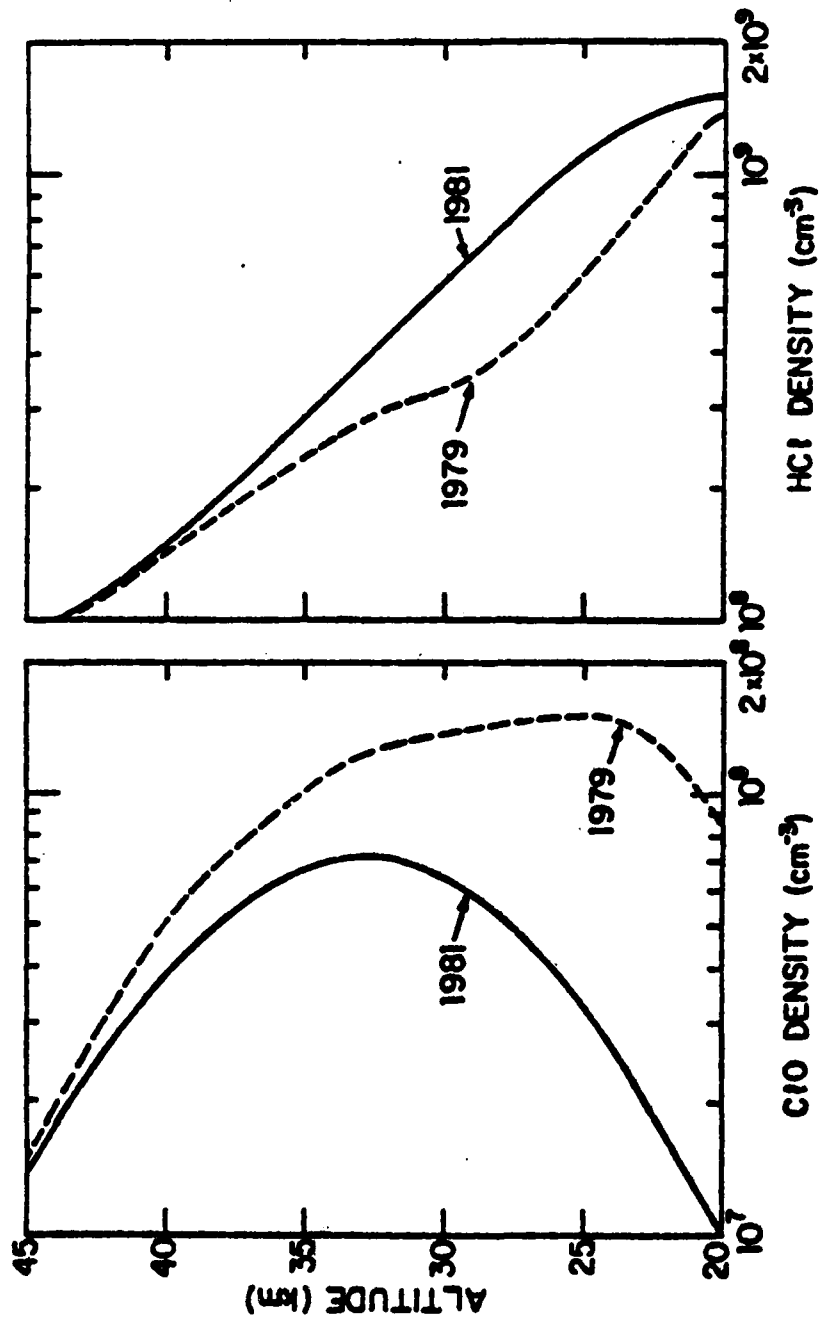


Figure 2-4
 Comparisons of 1-D model calculated ClO and HCl concentrations using reaction rate constants from NASA (1979) and NASA/WMO (1981).

are less dramatic, since HCl is a major component of ClX, which is mainly controlled by atmospheric transport and the supply of Cl-source molecules such as CFCs, CH_3CCl_3 , CCl_4 and CH_3Cl from the troposphere.

Major changes also are found in the calculated ClNO_3 and HOCl concentrations. The much lower value calculated for ClNO_3 (Figure 2-5) is mainly attributed to the use of a slower formation rate for ClNO_3 as recommended recently by NASA/WMO (1981). It should be noted that there are still considerable uncertainties regarding the ClNO_3 chemistry. Further laboratory studies together with atmospheric measurements are needed to resolve the issue. The largest calculated change among all species occurs in HOCl, a molecule formed by the reaction of HO_2 with ClO. The more than a factor of 10 reduction in HOCl concentration (Figure 2-5) around 20 km reflects lower concentration of both ClO and HO_2 in the stratosphere. As a result, HOCl should play a much lesser role in O_3 removal through (II.2).

Data on HOCl are currently non-existent. Since HOCl is sensitive to relatively small changes in rate constants, a detection of this molecule should provide an important check to current models.

Figure 2-6 shows the calculated NO and NO_2 profiles calculated with 1979 and 1981 rate data. The model with the recent rate data predicts significantly higher NO and NO_2 concentrations in the stratosphere ($z < 30$ km), where OH is a major sink for NO_2 through the reaction of $\text{OH} + \text{NO}_2$.

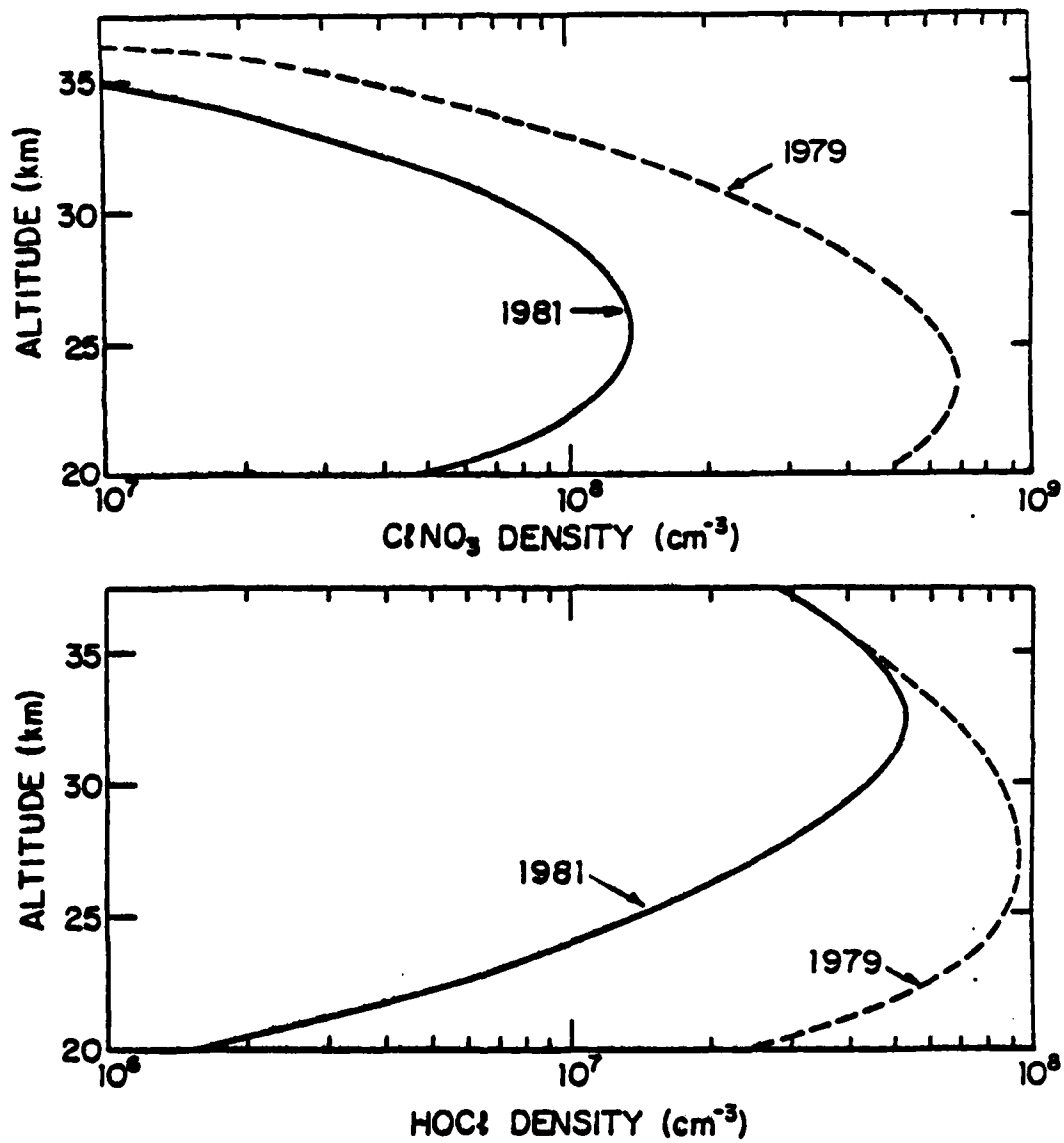


Figure 2-5

Comparison of 1-D model calculated ClNO₂ and HOCl using reaction rates from NASA (1979) and NASA/WMO (1981).

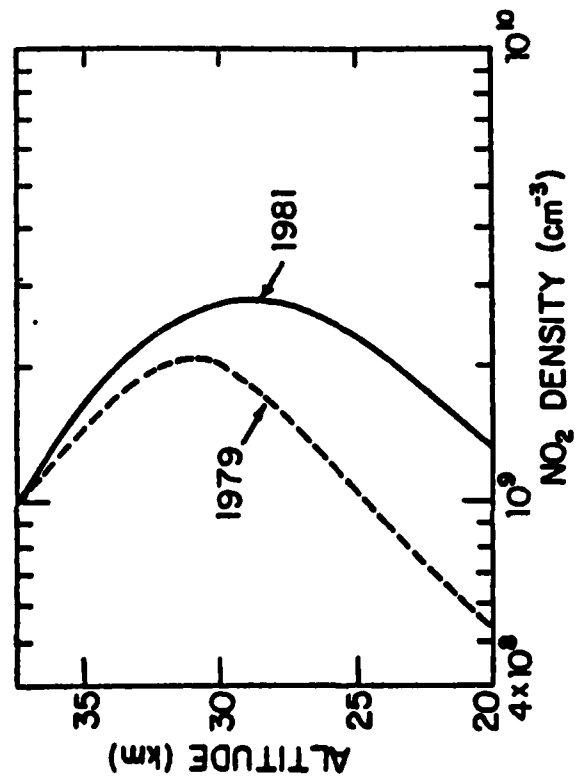
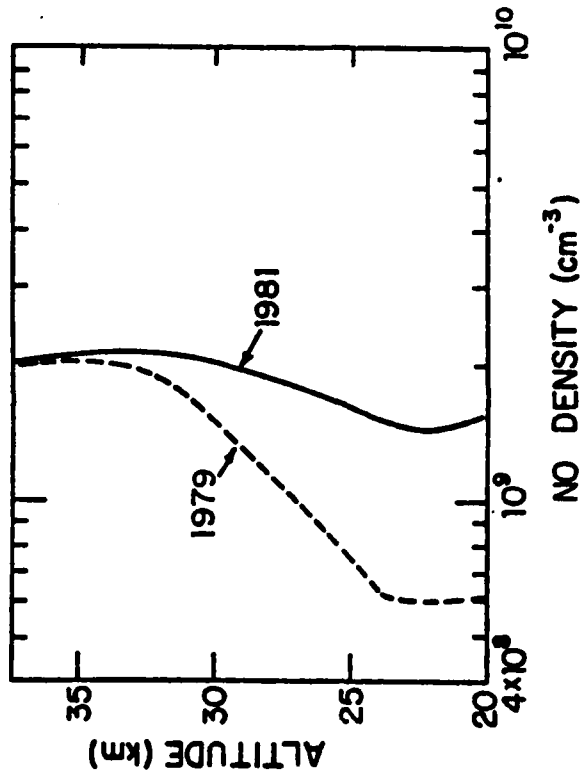


Figure 2-6
 Comparison of 1-D model calculated NO and NO₂ concentrations using reaction rate constants from NASA (1979) and NASA/WMO (1981).

The higher concentrations of NO and NO₂ would imply a more efficient NO_x cycle (I.1) in ozone removal.

Figure 2-7 shows the vertical profiles of C₂H₆ calculated with 1979 and 1981 rate data. The observed vertical gradient of C₂H₆ was identified as a sensitive indicator for stratospheric OH and Cl (Rudolph et al., 198; Sze et al., 1981). Our models with 1979 rate data predict a much steeper gradient than observations. The 1981 model which calculates lower stratospheric OH and Cl predicts substantially higher C₂H₆ concentration around 20-25 km, although the new model profile above 25 km still lies below observations by factors of 3 to 6. Further improvement between observation and model is possible by further reducing the stratospheric OH and Cl concentrations predicted by the current models. Alternately, a faster vertical eddy diffusion coefficient may also improve the agreement although this approach would further degrade the already poor agreement between observed and calculated CFC-11, as discussed in Section 4.

The calculated changes in the stratospheric distributions of the above species have several important implications for atmospheric models. First, in regards to the process of comparing observations with models, a change in model results can either improve the agreement or introduce additional discrepancies. On balance, the profiles predicted by models with 1981 chemistry agree with observation better than earlier calculations (NASA, 1979), though difficulties

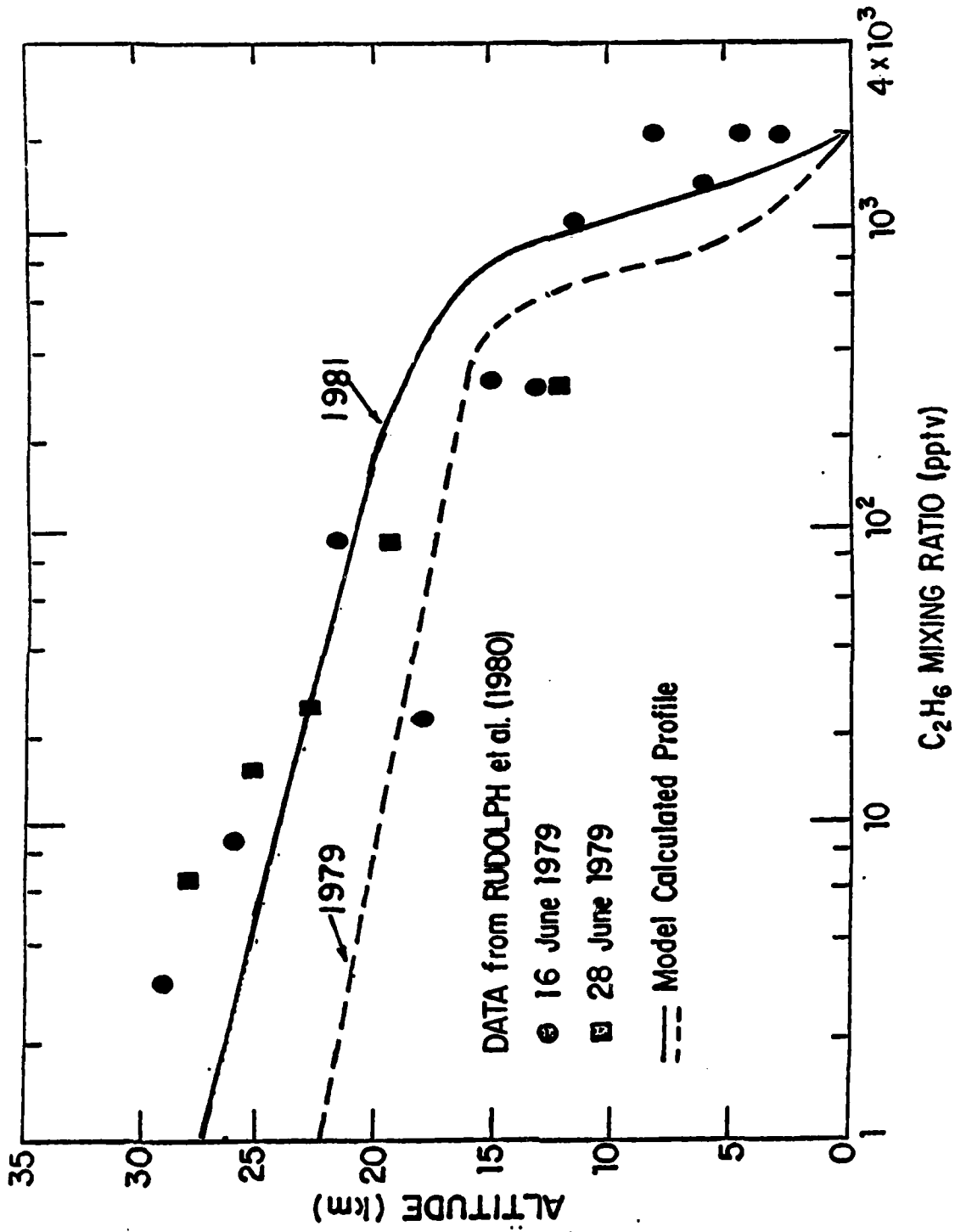


Figure 2-7

Comparison of 1-D model calculated C_2H_6 concentrations using different reaction rate constants taken from NASA (1979) and NASA/WMO (1981).

still remain, particularly in the upper stratosphere (~40 km). A detailed comparison of models with observations is given in Section 4.

The second implication concerns the chemistries of certain large molecules (ClNO_3 , HOCl , HNO_3 and HNO_4) formed by various coupling processes. The use of new rates reduces the roles of ClNO_3 and HOCl in stratospheric chemistry but enhances those of HNO_4 and HNO_3 in the removal of HO_x .

The third implication concerns models' sensitivity to perturbation studies. This issue will be addressed in detail in Section 3. Briefly stated, the recent revisions in rate data reduce the potential impact of CFCs but increase that of N_2O on stratospheric ozone.

3. OZONE PERTURBATIONS STUDIES

3.1 Single Perturbation Studies

There are various man's activities that may potentially alter the global distributions of atmospheric ozone. Among the more important ones that have been identified are:

- 1) Injection of NO_x from hypothetical high flying supersonic aircraft.
- 2) Release of CFCs due to their widespread use as a refrigerant and plastic foam manufacturing.
- 3) Release of N_2O due to the application of nitrogen fertilizers.
- 4) Increase of CO_2 due to the combustion of fossil fuels.
- 5) Injection of NO_x from subsonic aircraft operating in the upper troposphere.
- 6) Increase of CH_4 due to agricultural practice and tropospheric OH reduction.

In addition to the above possible anthropogenic influences, ozone also may be perturbed by a variety of natural phenomena such as volcanic eruptions, solar proton events, variability of the solar flux and the water vapor in the stratosphere. The quantitative effects of these natural events on O_3 is very uncertain and their assessment is beyond the scope of the present report.

Table 3-1 presents the calculated perturbations to ozone due to various man's activities. Also included in Table 3-1 are the corresponding model results based on the

TABLE 3-1

Calculated Change in Column O₃
due to Individual Perturbation

Scenario	Change in Column O ₃ (%)	
	1979*	1981**
1. NO _x injection of 2 x 10 ⁸ at 20 km	+ 4.0	- 6.2
2. CFC's release at 1977 production rates	-16.4	- 6.1
3. Doubling N ₂ O flux	+ 1.6	- 9.5
4. Doubling CO ₂ †		
narrow band model	-	+ 2.5
wide band model	-	+ 3.9

* Based on NASA (1979) rate data.

** Based on NASA/WMO (1981) rate data.

† The narrow band and wide band models refer to different treatments of radiation transport calculations in two separate model simulations.

earlier rate data recommendations (NASA, 1979). For the CFC's constant release scenario, we summarize the impact of individual revision in rate data on ozone depletion calculation in Table 3-2.

As discussed in Section 2, the recent revisions in rate constants for several HO_x reactions have changed the quantitative understanding of several key chemical cycles that control the removal rates of stratospheric ozone. In brief, the reduced stratospheric OH level calculated by current models, implies a less efficient HO_x and ClX cycle but a more efficient NO_x cycle for ozone removal, particularly in the lower stratosphere (20-30 km).

The calculated steady state column ozone reduction is now 6.1% compared to the corresponding figure 16.4% based on the earlier NASA (1979) rate data. Much of the drastic change in the depletion calculation occurs below 32 km as indicated in Figure 3-1. Note that a small increase in O₃ around 20 km is predicted by the 1981 model. It should, however, be noted that the new rate data have relatively little impact on the depletion calculation above 32 km. The largest percentage change in local ozone under steady state condition is predicted to occur at around 40 km with a magnitude of about 42%. The calculated changes in column O₃ on an intermediate time scale (year 1970-2000) are given in Figure 3-2. The predicted present day (1980) O₃ depletion is 0.65%, compared to the corresponding value of 1.7% predicted by our 1979 model. Based on a constant release

TABLE 3-2

Change in AER 1-D Model Calculation since
1979 of Calculated Effect on Total Ozone
from Constant Release of CFC-11 and CFC-12*

Model	Change in O ₃ (%)	
	Present Day	Steady State
A. NASA (1979) Chem	- 1.7	- 16.4**
B. Same as A with $k(\text{OH} + \text{H}_2\text{O}_2) = 2.5(-12)\exp\left(\frac{-126}{T}\right)$	- 1.6	- 16.0
C. Same as B with $k(\text{OH} + \text{HNO}_3) = 1.5(-14)\exp\left(\frac{649}{T}\right)$	-	- 11.0
D. NASA (1980) Chem (JPL Publ. 81-3)	-	- 8.2
E. Same as D with $k(\text{OH} + \text{HNO}_4) = 4(-12)$ $k(\text{OH} + \text{HO}_2) = 8(-11)$	-	- 4.7
F. NASA/WMO (1981) Chem	- 0.65	- 6.1

* The constant release rates of CFC-11 and CFC-12 are set at 1977 production levels.

** All calculations (except for model F) use fast rate for ClNO₃ formation.

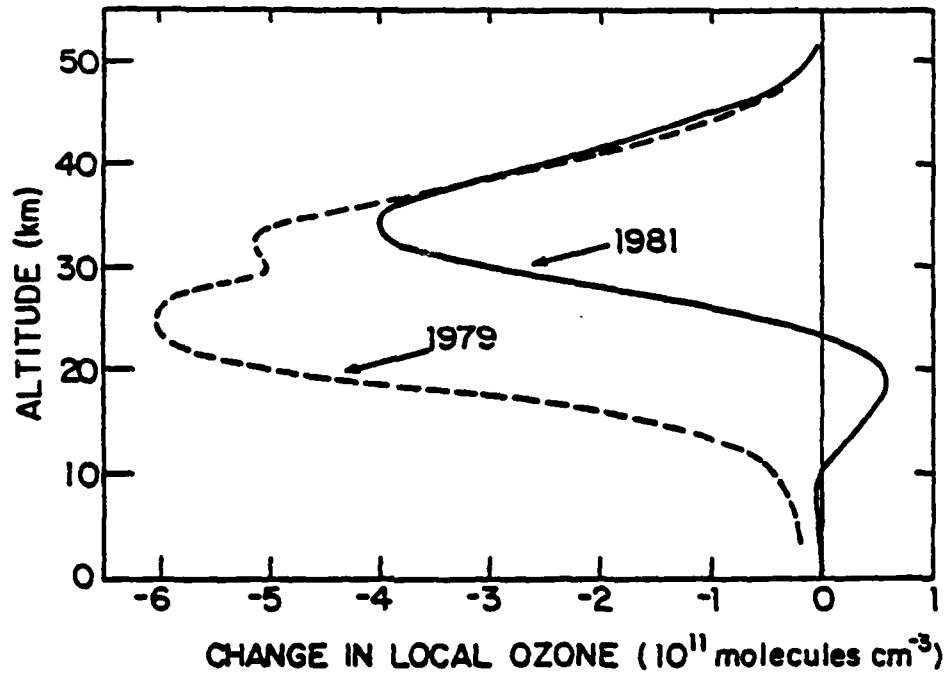


Figure 3-1

Comparison of 1-D calculated changes in local ozone due to CFCs' perturbation at steady state using different reaction rate constants from NASA (1979) and NASA/WMO (1981).

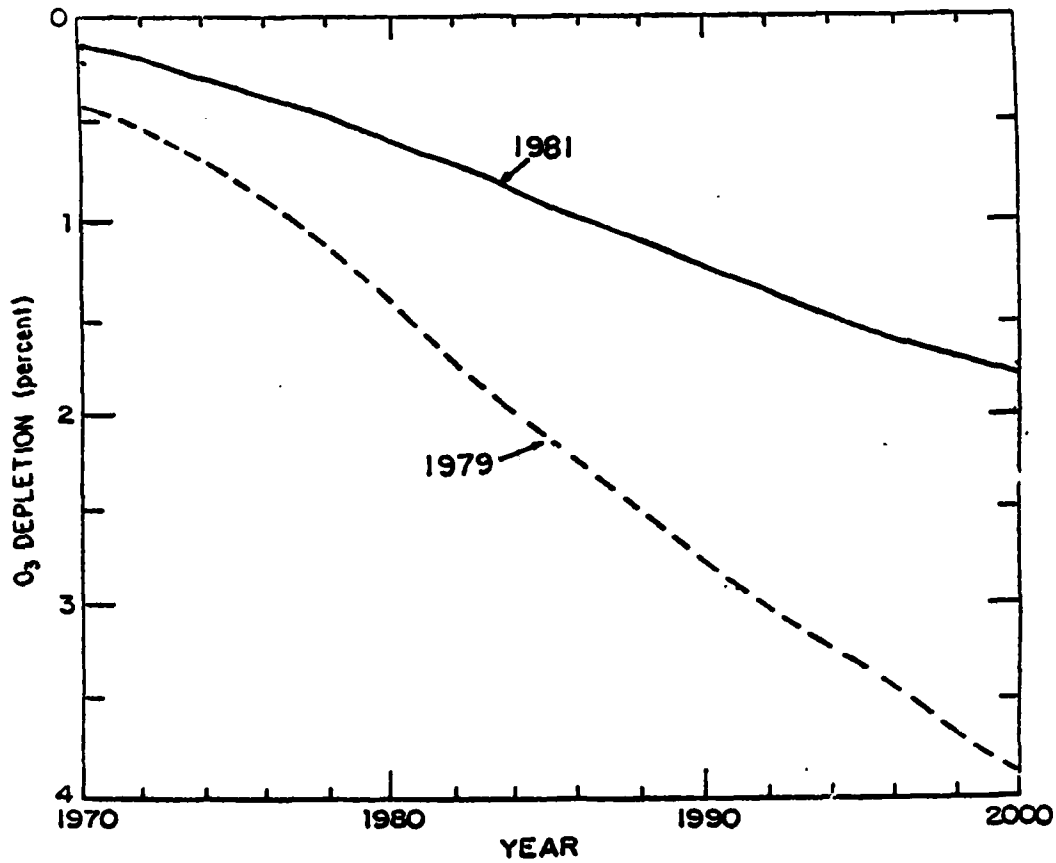


Figure 3-2

Comparison of 1-D model calculated time-dependent column ozone depletions due to CFC's release using reaction rate constants from NASA (1979) and NASA/WMO (1981).

scenario of CFCs at 1979 release rates after 1980, our model with 1981 rates projects that the column O_3 reduction will reach 1.7% by year 2000.

Figures 3-3 and 3-4 show the possible changes in O_3 caused by a doubling of N_2O and CO_2 respectively. In contrast to CFCs and N_2O , an increase in CO_2 is believed to increase column O_3 (Luther et al., 1977; Boughner, 1978; Groves et al., 1978) as the CO_2 -induced cooling effect reduces the efficiency of several O_3 removal processes. The quantitative effect of CO_2 on O_3 depends on the absorption band treatment used in the radiative calculation as well as the treatment of hydrostatic adjustment. The narrow band model predicts a smaller increase of column O_3 (2.5%) than that (3.9%) predicted by the wide band model due to CO_2 doubling (Wang et al., 1982). It is interesting to note that the maximum CO_2 impact on O_3 (Figure 3-4) is predicted to occur at around 40 km, a region where CFC's impact on O_3 is also found to be the greatest though opposite in sign.

Ozone may also be perturbed by the emission of NO_x into the upper troposphere by subsonic aircraft. Injection of NO_x into this region (9-11 km) may promote ozone production through processes such as:

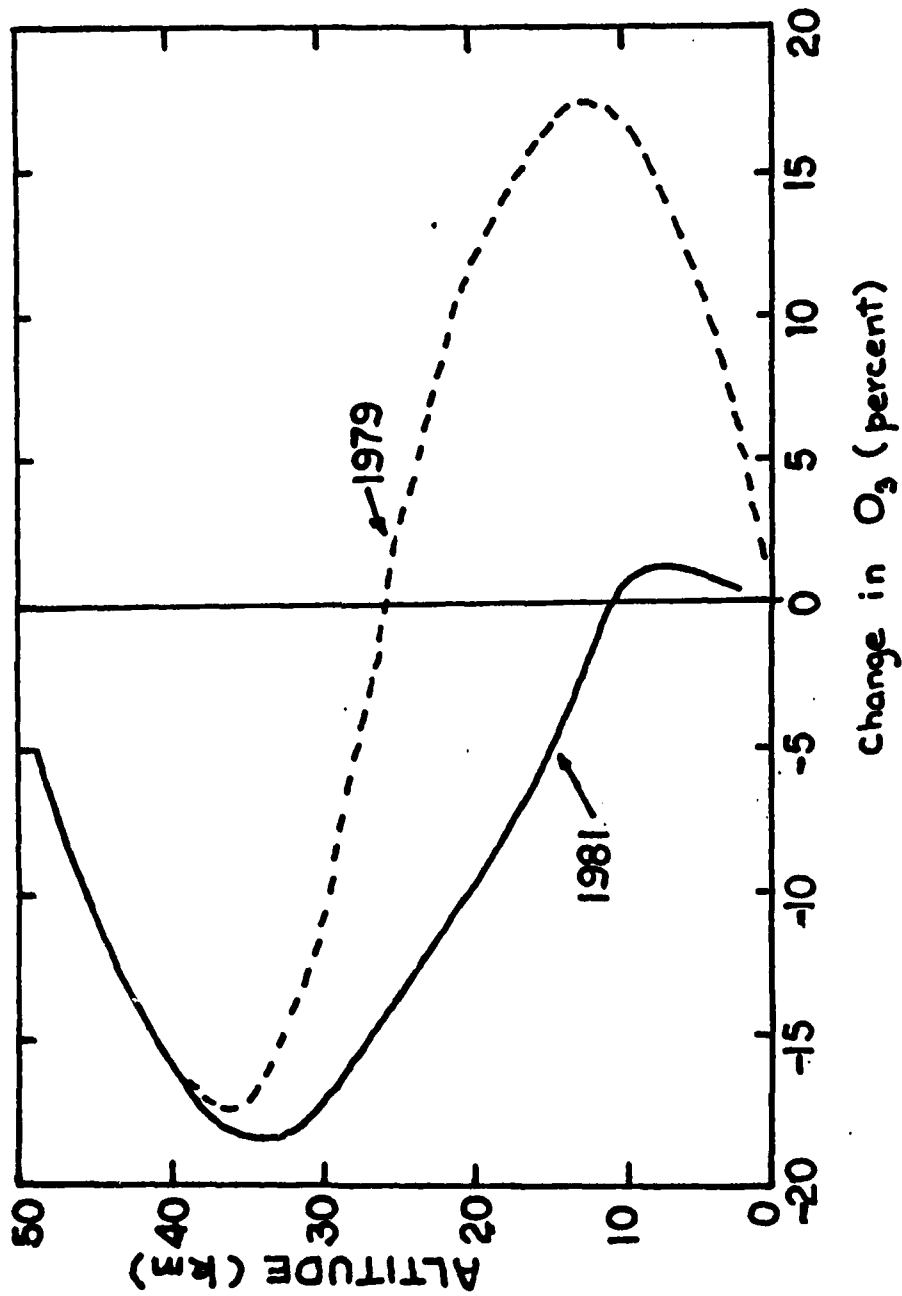


Figure 3-3

Comparison of 1-D model calculated changes in O₃ due to doubling of N₂O using reaction rate constants from NASA (1979) and NASA/WMO (1981).

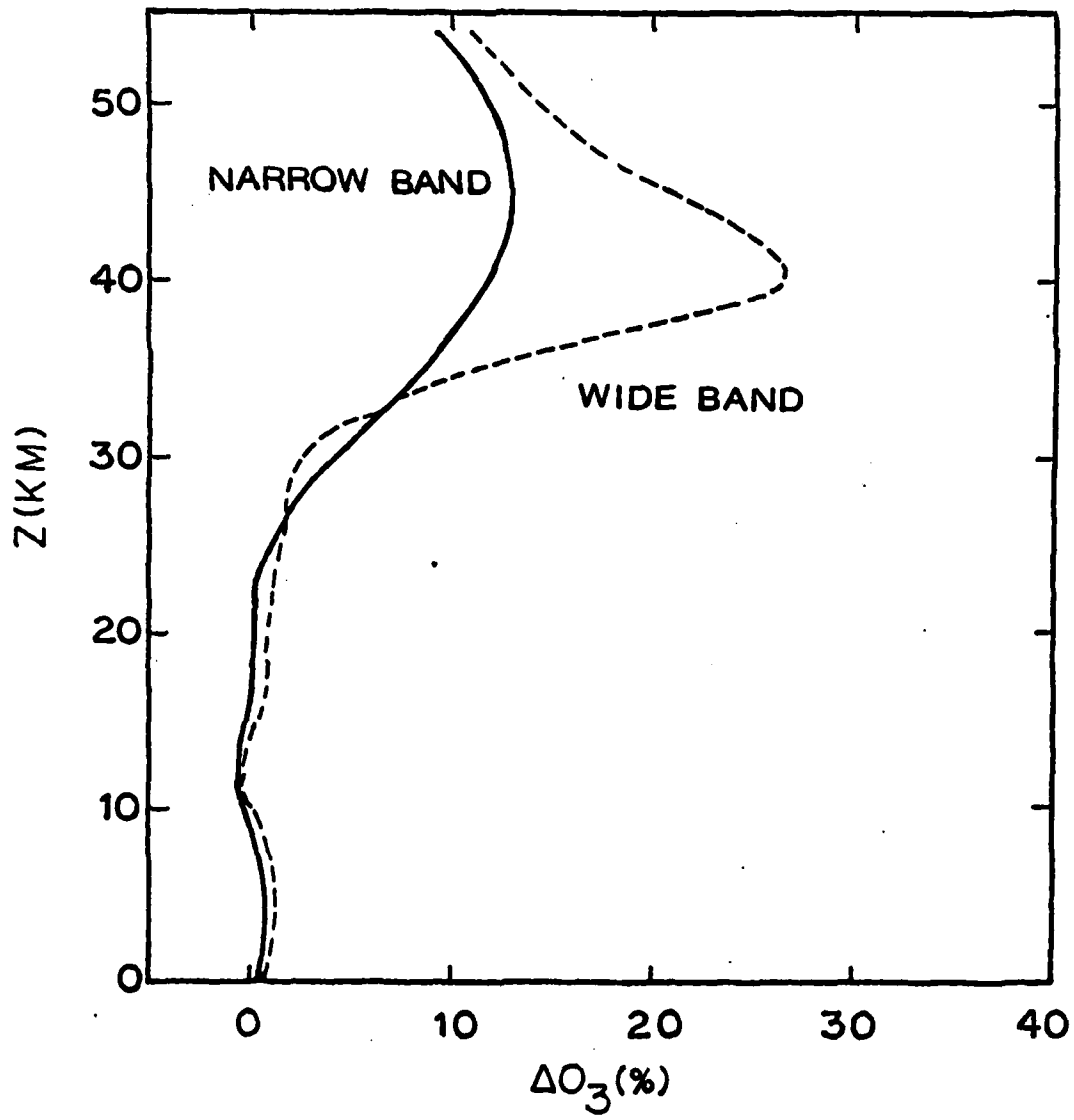
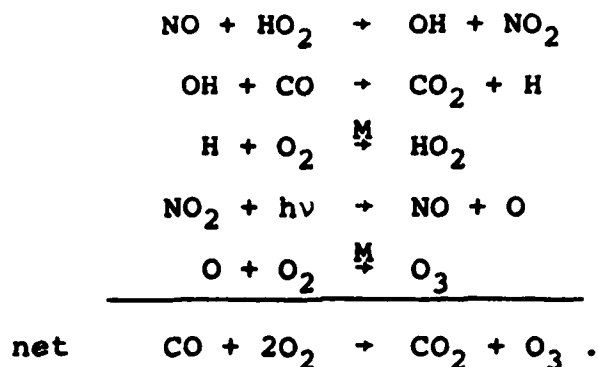


Figure 3-4

Effect of absorption band treatments on the one-dimensional radiative-convective-photochemical model calculated O_3 change due to CO_2 increase from 330 to 660 ppmv. The background ClX abundance is assumed to be 1 ppbv. The reaction rate constants are from NASA/WMO (1981).



Model calculations by the Lawrence Livermore National Laboratory (LLNL) indicates that the current operation of subsonic aircraft may contribute about 1% increase in column O_3 . Much of the calculated O_3 increase, however, occurs in the upper troposphere, a region where uncertainties in transport and photochemistry are particularly large.

Increases in atmospheric CH_4 might also perturb O_3 and stratospheric chemistry. Rasmussen and Khalil (1981), suggest an annual increase in CH_4 of about 2% per year on the basis of 22 months of almost continuous measurements of CH_4 at Cape Meares. Should this trend continue in the future, an O_3 increase on the order of a few percent is possible (Wang et al., 1980) since CH_4 oxidation is a source of O_3 (Johnston and Podolski, 1978) and its reaction with Cl plays a dominant role in the removal of stratospheric Cl.

3.2 Multiple Perturbation Studies

It is clear, from the above discussions, that human influences on global ozone are diverse and often complex. It seems, therefore, unrealistic to assess the anthropogenic effect on ozone based on a single perturbation. This is particularly true when the interaction of perturbations is nonlinear and sometimes even opposite in sign. Multiple perturbation studies have been initiated by Logan et al. (1978) and Sze et al. (1978). Their work focuses on the coupled effect of N_2O and CFCs on O_3 . They note that the effect of individual perturbations is not simply additive. For instance, the impact of CFCs on ozone strongly depends on the atmospheric level of N_2O . At an elevated N_2O level, the calculated response of O_3 to CFC releases diminishes significantly.

Table 3-3 illustrates some of the examples of multiple scenarios calculated by the AER one-dimensional model using NASA (1981) rates. In the joint scenario (A) involving simultaneous doubling of N_2O and constant emission rates of CFCs, the net total ozone reduction is 13%, only somewhat higher than the value of 10% predicted for doubling N_2O alone. It should be noted, however, that the evidence of an increasing trend in N_2O is mainly based on Weiss's (1981) observations. A long time series is needed to quantify the rate of N_2O increase in the atmosphere.

TABLE 3-3

Multiple Scenarios of O₃ Perturbations*

Model	Change in Column O ₃ (%)
A. CFCs (steady state) + 2 x N ₂ O	- 13.0
B. CFCs (steady State) + 2 x CO ₂	- 4.8**
C. CFCs (2010) + 1.5 x CO ₂	- 1.3**

* Refer to Table 3-1 for baseline calculations.

** Based on narrow band model in the CO₂ radiative cooling calculation.

Atmospheric CO₂, on the other hand, is observed to be increasing steadily since 1958 (Keeling et al., 1976a,b). A doubling in CO₂ could occur around the year 2025 to 2075 (CEQ, 1980), about 100-150 years before CFCs are projected to attain their steady state concentration. The joint effect of doubling CO₂ and constant emission rates of CFCs on total ozone is a 4.8% reduction, compared to 6.1% calculated with CFCs emission alone.

Scenario C represents a projection of coupled effect of CO₂ and CFCs on ozone on an intermediate time scale (~ year 2010). This scenario includes 500 ppm CO₂ and 4 ppb ClX [approximately 75% (i.e., 3 ppb) comes from CFCs] in the model. The net reduction in total ozone is 1.3%, almost a factor of two smaller than the value 2.3% calculated with no CO₂ increase (fix CO₂ at current level of 330 ppm).

3.3 2-D Perturbations

The results presented in Sections 3.1 and 3.2 refer to an average global perturbation to O₃ calculated by 1-D models. Earlier calculations by Pyle (1978) suggest that the maximum depletion of O₃ by CFCs occurs in winter at high latitudes, where the transmission of ultraviolet radiation is negligible. In contrast, the percentage of O₃ decrease is minimal in summer at low latitudes where the penetration of ultraviolet radiation is greatest. Since the exposure of human population and many plants to ultraviolet radiation is likely to be seasonal and latitudinal dependent, a global average O₃

reduction calculated by 1-D models (including those given in Sections 3.1 and 3.2) may not be very meaningful, particularly when 2-D model calculation suggests that O_3 depletion may vary significantly with latitudes and seasons.

Figure 3-5 shows the present day O_3 depletion by CFC's release calculated by the AER 2-D model with NASA/WMO 1981 rates. A detailed description of the model is given in Appendix A. The calculated latitudinal and seasonal dependence of O_3 depletion is qualitatively similar to the earlier calculation by Pyle (1978). The largest O_3 depletion is found in the winter at high latitudes. Our calculation, however, differs quantitatively from that of Pyle (1978), in one important aspect: that the ratio of polar to tropical O_3 depletion is about 1.8, a value significantly less than the corresponding ratio of 3.5 calculated by Pyle (1978). We believe the principal cause for the difference arises from the much faster rates for $OH + HNO_3$ and $OH + HNO_4$ used in our present model. Because of the higher stratospheric concentrations of HNO_3 and HNO_4 at high latitudes, these two reactions tend to suppress more OH at high latitudes than at the tropics. Reduced OH implies a less efficient chlorine cycle (I-2) as discussed in Section 2.

Figure 3-6 shows the possible effect of doubling N_2O on column ozone calculated by our 2-D model. The calculated column O_3 depletion shows large latitudinal gradients, ranging from about 5-7% reduction in the tropics to about 25% in

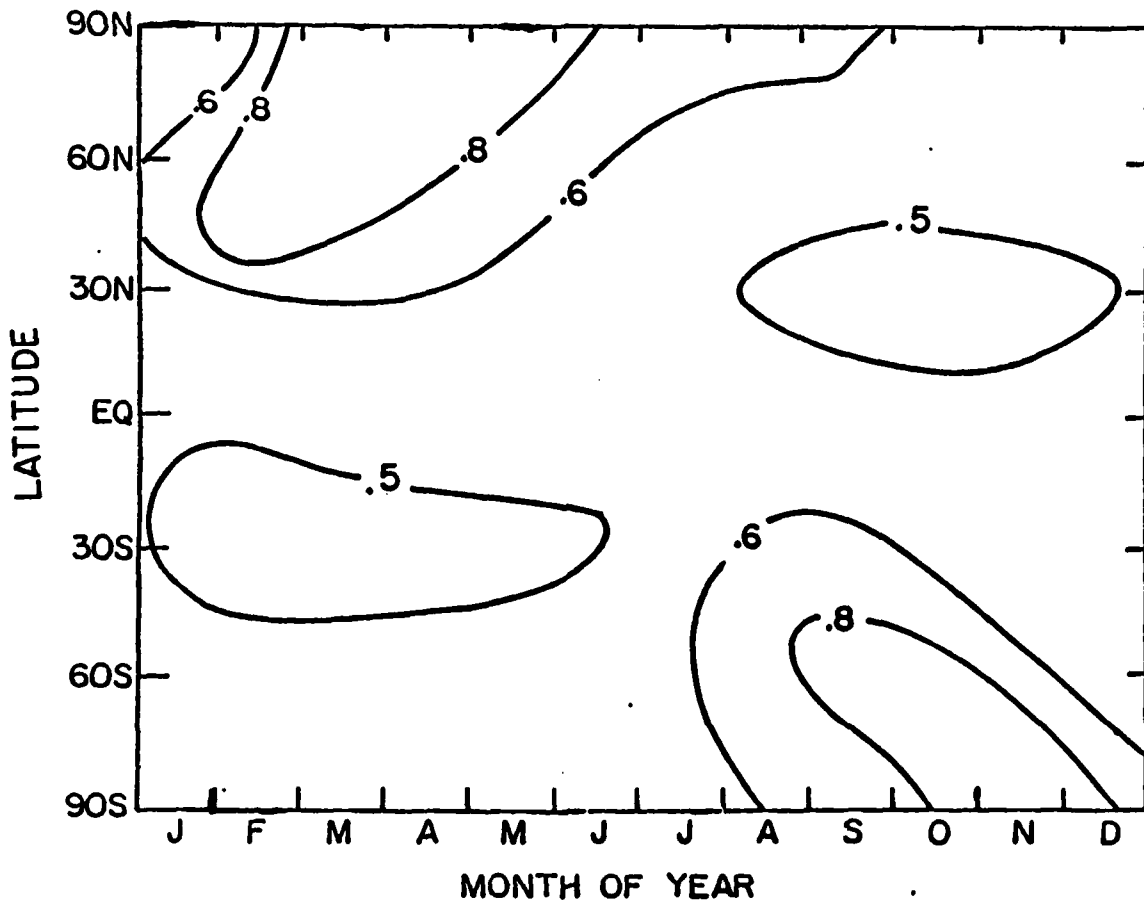


Figure 3-5

Calculated percentage depletion of column ozone by the year 1981 due to CFC-11 and CFC-12 releases.

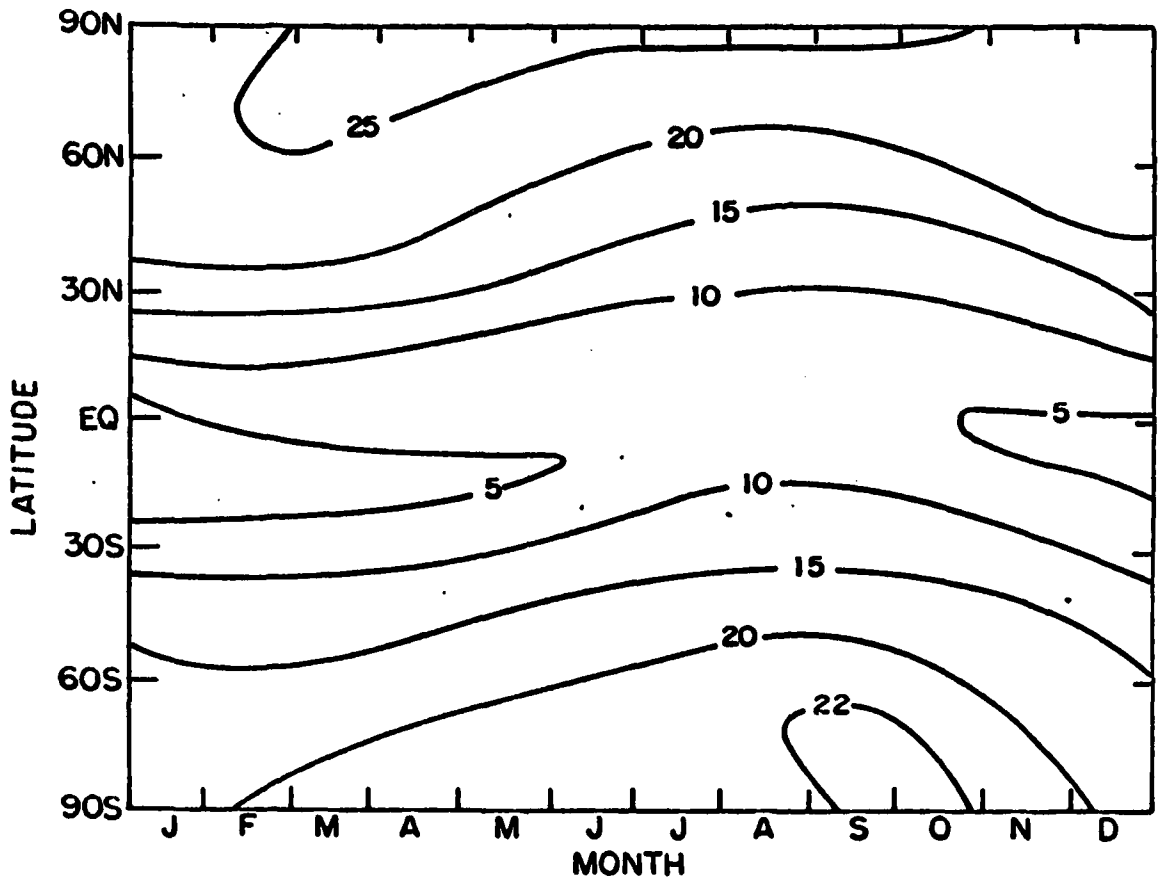


Figure 3-6

Calculated percentage depletion of column ozone due to doubling of N_2O .

the polar regions. The calculated seasonal gradient of O_3 depletion, however, is relatively small. It should, however, be pointed out that since our model calculates excessive NO_2 at high latitudes during winter season (possible due to the use of 24-hour average photolysis rates), it is likely that the ozone reduction by NO_x is somewhat overestimated above 30° latitude.

In summary, potential ozone perturbations by human activities may not be uniform in space and time. Some care is therefore needed in the interpretation of the O_3 depletion calculated by 1-D models, particularly in regards to the attempt of relating increase in UV-B dose with global O_3 depletion.

4. TWO-DIMENSIONAL MODEL STUDIES

4.1 Introduction

The AER zonal-mean model is designed to simulate the zonal-mean behavior of atmospheric trace gases. The domain of the model covers the globe from pole to pole and up to an altitude of 60 km. The horizontal and vertical resolutions are approximately 10^3 km and 3.5 km, respectively. The dynamic variables are governed by the system of equations obtained by taking the Eulerian zonal-mean of the simplified primitive equations which assumes geostrophic wind balance. Dynamic transport of trace gases is affected by advection from zonal-mean wind and eddy transport parameterized by a symmetric diffusion tensor. The photochemical scheme used in the 2-D model is based on the grouping techniques and calculates over 35 species affecting the O_3 balance. A 24-hour averaging of the photolysis rate is used to simulate diurnal average conditions. A more detailed description of the model is given in Appendix A. In Sections 4.2 and 4.3 the results of the calculation from this model are presented.

In addition to this basic model which was developed over the past 3 years, we have implemented additional features over the past contract year. These include a diurnal package for calculating the diurnal behavior of the short-lived species and a semi-implicit scheme for solving the trace-gas equation. These improvements together with some anticipated changes will be discussed in Section 4.4.

4.2 Comparison of 2-D Models with Observations

Considerable advances have occurred in the area of measurement of stratospheric trace gases. The developments have provided a wealth of new data on the concentration of many important stratospheric gases including the long-lived species (N_2O , CH_4 , CH_3Cl , C_2H_6 , $CFCl_3$, CF_2Cl_2) of tropospheric origin, the hydrogen radicals HO_x (OH , HO_2 , H_2O_2) derived from the photodecomposition of stratospheric H_2O , the nitrogen radicals NO_x (NO , NO_2 , HNO_3) from the decomposition of N_2O and the chlorine radicals (Cl , ClO , HCl , $ClNO_3$) from the photodecomposition of a variety of halocarbons.

In the area of stratospheric modeling, considerable progress has also been made in the development of a two-dimensional (2-D) model, although the assessment of potential environmental effects from human activities still relies mainly on one-dimensional (1-D) models (NASA, 1979; NAS, 1979). The major strength of 1-D models lies in their ability to include a detailed description of chemical processes without excessive demands on computer time. The problematic aspects of 1-D models concerns the interpretation of their simulated profiles which are considered to represent some sort of global (longitudinal and latitudinal) averages. Strictly speaking, 1-D model results should be compared with the observed global averages defined by a large set of spatial and temporal data. Acquisition of such a data set for any trace gas is clearly an enormous task - a task unlikely to be completed in the foreseeable future.

The main advantage of the 2-D model lies in its capability of simulating atmospheric latitudinal gradients and seasonal behavior by accounting for the important time-dependent meridional transport in the atmosphere, together with the seasonal and latitudinal variations of the solar zenith angle. The recent improvement in 2-D models involves the inclusion of detailed chemical processes. For instance, the chemical content of DuPont's (Miller et al., 1981) and AER's (Ko et al., 1980) 2-D model is now at par with that of the most advanced 1-D models.

On the other hand, one should recognize the fact that current 2-D models are not developed from first principles. Rather, the transport in the models is partly parameterized by eddy diffusion coefficients derived from observations. It is therefore essential to substantiate the models by comparison with observations. Specifically, observations complement model results in at least four general areas: i) boundary conditions, ii) atmospheric transport, iii) chemical system and iv) combined chemistry and transport.

First, observations often are used to define the necessary boundary conditions posed in the 2-D models. Second, because of the simplicity of chemistry for certain long-lived species such as N_2O , CH_4 and CFCs, data on these gases may be used to check on the appropriateness of transport parameterization. Third, data on radical species may be used to test our current understanding of various chemical cycles since the partition among the radical species is generally insen-

sitive to transport although transport may affect the absolute abundance of the radical calculated in the model. Finally, the observed spatial and temporal ozone distribution, which is believed to be controlled by both chemistry and transport, may be used to test our overall understanding of the stratospheric chemical and dynamical system. The last step obviously depends, to a large extent, on how well the model results agree with the observed long-lived and radical species.

This section is organized in the manner of discussing each of the above areas of interest. Theoretical results presented in this section are based on the AER 2-D model with NASA/WMO 1981 rates.

Our numerical experiment was carried out in two stages. We first performed the calculation solving for the annual periodic steady state distributions of N_2O , CH_4 , H_2 , CH_3Cl , CCl_4 , CH_3CCl_4 , CO , O_3 , Cl_x and NO_x using fixed mixing ratio conditions for the lower boundary as summarized in Table A-4 in Appendix A. The resulting concentrations can be interpreted as those of the "clean" atmosphere prior to introduction of CFC-11 and CFC-12. The model atmosphere is then integrated in time for 30 model years where CFC-11 and CFC-12 are introduced into the model atmosphere with time-dependent flux boundary conditions using the emission rates for the years 1950 to 1980 (CMA, 1980). The calculated values correspond to the gas concentration of the present day atmosphere.

4.2a Long-Lived Species

Among the long-lived species, the upward diffusing species - N_2O , CH_4 , CCl_4 , CH_3Cl , CH_3CCl_3 , CFC-11 and CFC-12 - are characterized by the fact that there is no in situ production in the atmosphere for these molecules. The gases enter the stratosphere by upward diffusion from the troposphere and are removed by photolysis, $O(^1D)$ and OH reactions in the stratosphere. An observed feature common among the upward diffusing species is that at each altitude above the tropopause, higher concentrations are always found in the tropical stratosphere. This is to be expected from the known meteorological patterns through which upward transport occurs, preferentially in the tropical latitudes, followed by poleward transport within the stratosphere. This important feature is present in our model calculation for the aforementioned gases and is illustrated by a latitude-altitude plot of the mixing ratio for N_2O in Figure 4-1. The figure shown corresponds to winter conditions in the northern hemisphere (December). It is interesting to note that there is a poleward rise in the stratospheric concentration in the winter hemisphere at high latitudes reflecting the lack of chemical removal. This model feature, of course, remains to be verified by future observations.

Among the upward diffusing species, sufficient data from different latitudes are available for N_2O , CFC-11 and CFC-12. The bulk of these data was collected by four research groups:

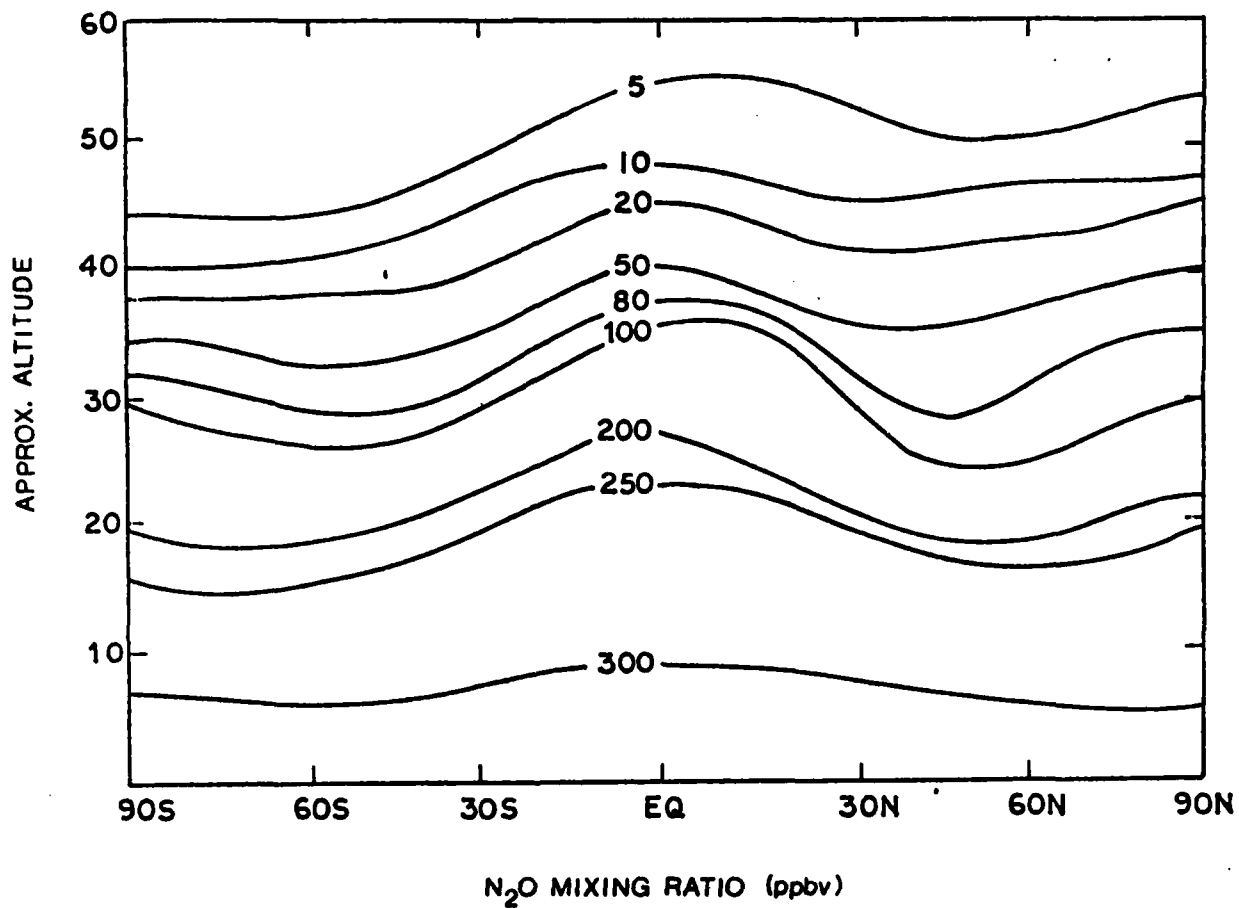


Figure 4-1

Latitude-altitude cross-sections for the calculated mixing ratio of N₂O for the month of December.

NOAA Goldan et al. (1980, 1981). Balloon-borne evacuated grab samples.

NCAR Heidt et al. (1975). Balloon-borne cryosampler.

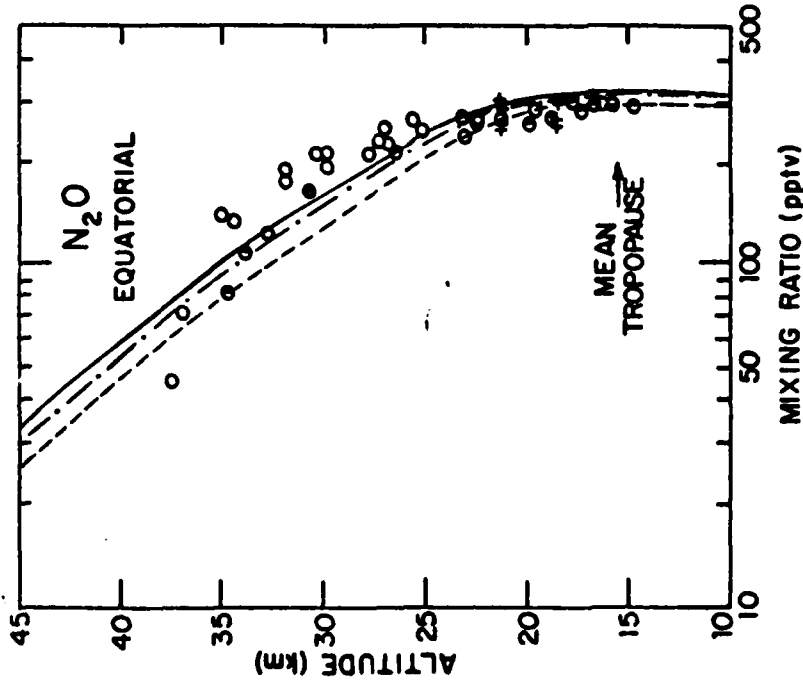
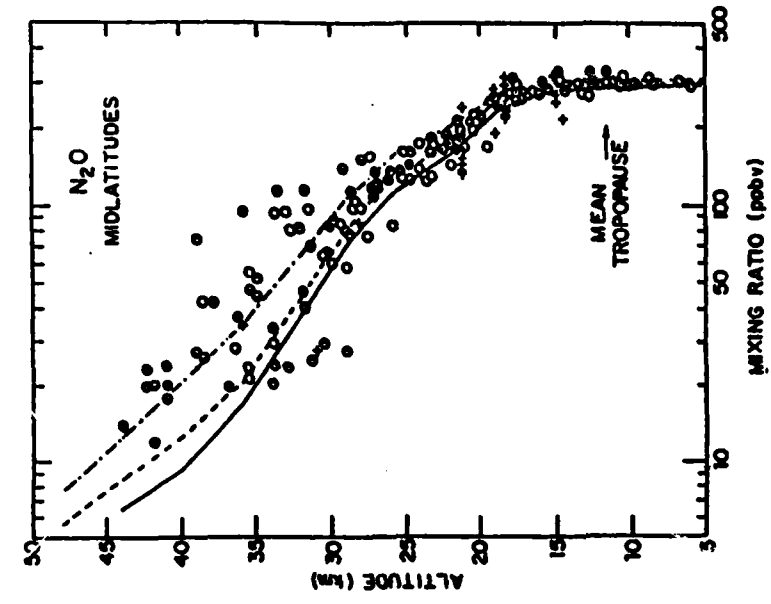
KFA Schmidt et al. (1981). Balloon-borne cryosampler.

Ames Tyson et al. (1978); Vedder et al. (1978); Vedder et al. (1981). Balloon- and aircraft-borne cryosampler.

N₂O

Figures 4-2a and b show the calculated N₂O profiles together with observations for the equatorial and mid-latitude regions respectively. Note that the data are collected over a number of flights and this may account for the scatter in the data at high altitudes. The data show that, at any latitude, the mixing ratios of N₂O decrease with altitude above the tropopause; a feature reflecting that these gases are removed in the stratosphere. Another interesting feature concerns the latitudinal variations of these species at constant pressure (altitude) levels. Specifically, the data show that the mixing ratios at a given altitude (above tropopause) decrease towards the high latitude regions.

The agreement between the 2-D model calculations and observations for N₂O is good. The model successfully simulates the observed vertical gradients as well as the latitudinal gradients of N₂O. As discussed in Appendix A, the dynamic transport in the AER model uses the advection wind-fields calculated by Harwood and Pyle (1977) and the eddy diffusion coefficients from Luther (1973). No attempt was



(a)

- - - 10° S
- · - · - EQ
- 10° N

(b)

- - - 30° N
- · - · - 40° N
- 50° N

Figure 4-2

Comparison of calculated N₂O profiles with observations. The data are from the measurement programs of NOAA, NCAR and NASA Ames as compiled for the 1981 NASA Workshop publication.

made to adjust any of the parameters. Thus, the favorable agreement between observation and calculation should perhaps be viewed as a partial validation of the dynamic parameters used.

CFC-11 and CFC-12

Since 1975, a large number of measurements of CFC-11 and CFC-12 have been reported. Most measurements involve laboratory analysis by gas chromatography of air samples collected by balloon-borne samples. The research groups which have produced large numbers of data points are the four groups mentioned earlier in the section, viz. NOAA, NCAR, KFA and NASA Ames. The NASA Workshop (June, 1981) has recommended that some of the NCAR data be excluded because of problems associated with the sampling procedure. In the mid-latitude region, only those from NOAA and KFA will be considered.

The data were collected over a period of time between 1975 and 1979. The concentrations of CFC-11 and CFC-12 change with time since the gases are introduced with time-dependent input rates. Figure 4-3 shows the normalized concentrations for CFC-11 and CFC-12 as functions of time for different altitudes. Note that the concentrations at 25 km increase by about a factor of 1.6 from 1975 to 1979. Thus, the data should be compared with the calculations for the appropriate time.

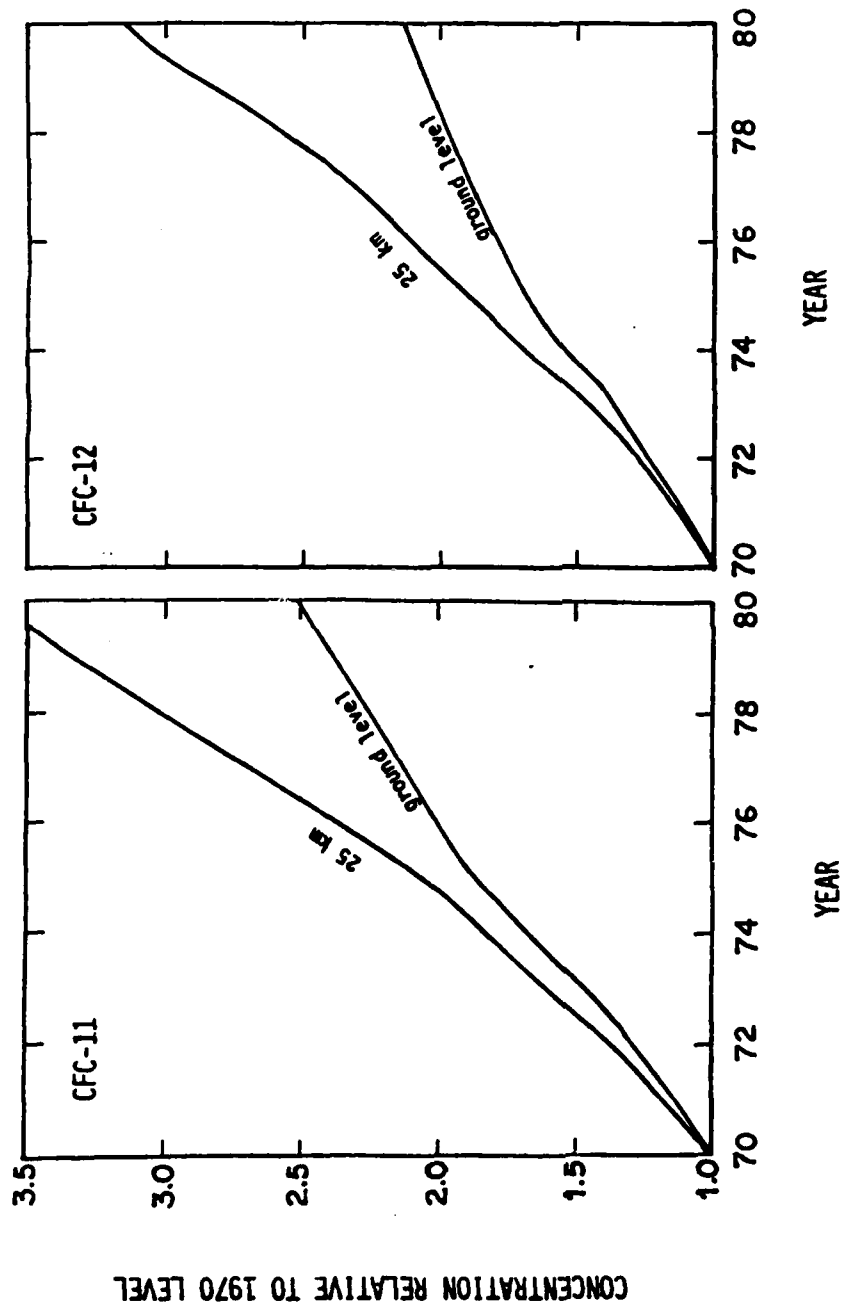


Figure 4-3

Model calculation concentrations for CFC-11 and CFC-12 as a function of time. The concentrations for 2 levels are plotted; each of them are normalized with the 1970 concentrations equal to 1. The values are taken from the 2-D model calculation at 40° N.

Data for CFC-11 and CFC-12 are plotted in Figures 4-4 through 4-7 together with the calculated profiles. The altitude profiles are from the time-dependent calculation corresponding to the years 1975 and 1979 as indicated. Agreement is reasonably good for CFC-11 at the equator but poor at mid-latitude. The calculated mid-latitude CFC-11 mixing ratios above 25 km lie significantly above NOAA's data. Although the overall agreement is somewhat better for CFC-12, the calculated mid-latitude CFC-12 mixing ratios above 25 km are higher than observations. In sum, the model seems to have underestimated the latitudinal gradients for CFC-12 and more so for CFC-11.

There are several possible explanations for the poor agreement between model and observation. First, the photolytic destruction rates for CFC-11 and CFC-12 may be underestimated in the model because of the errors in the treatment of the Schumann Runge bands. Second, the transport rates may be in error. Specifically, the diffusion coefficient K_{yy} which controls the latitudinal gradients of the mixing ratios may be too fast. A slower K_{yy} may increase the magnitude of the latitudinal gradient.

Since CFC-12 and N_2O are chemically more inert than CFC-11 in the stratosphere, we therefore expect that the calculated stratospheric distribution of CFC-11 is more sensitive to the adjustment of diffusion coefficients. In other words, it is possible to tune diffusion coefficients for better agreement between calculated and observed CFC-11,

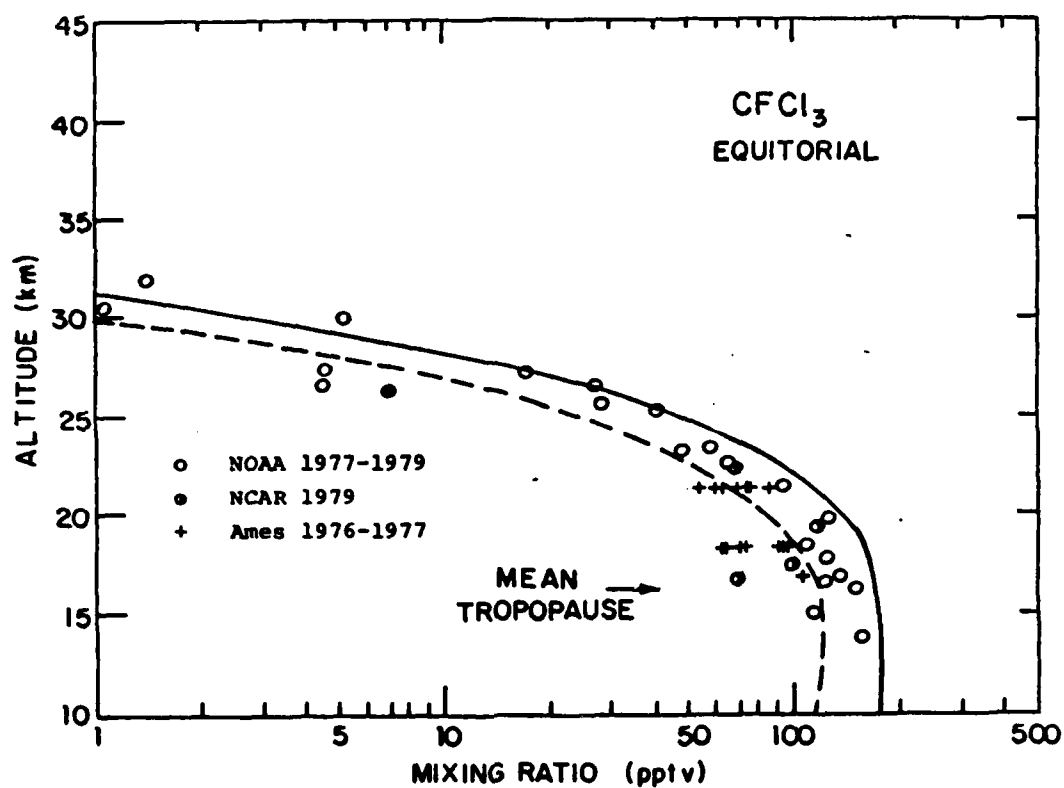


Figure 4-4

Comparison of the calculated CFC₁₃ profiles with observations. The data are from the measurement programs of NOAA, NCAR and NASA Ames as compiled for the 1981 NASA Workshop publication.

— Equator - corresponding to 1979 concentration
 - - - Equator - corresponding to 1975 concentration

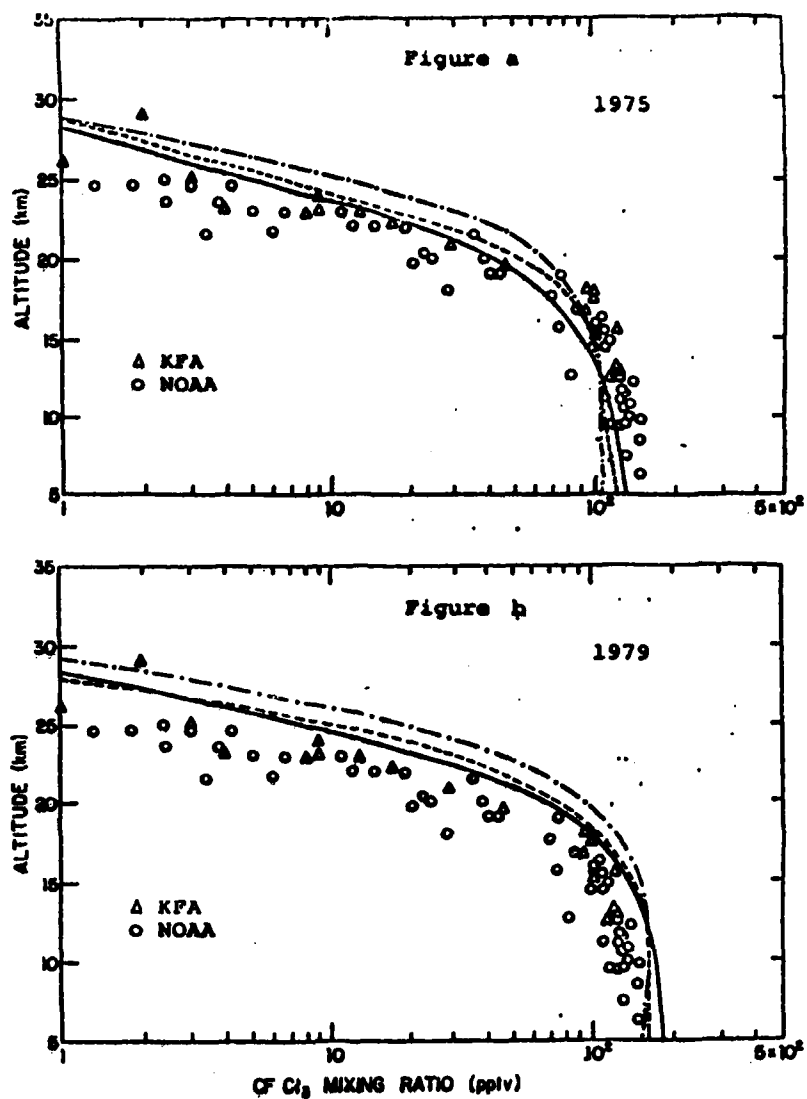


Figure 4-5

Comparison of the calculated CFCl_3 profiles with observation. The data are from the measurement programs of KFA and NOAA as compiled for the 1981 NASA Workshop publication. The profiles correspond to 1975 and 1979 concentrations in Figures a and b respectively.

- · - · - 30° N
 - - - 40° N
 ——— 50° N

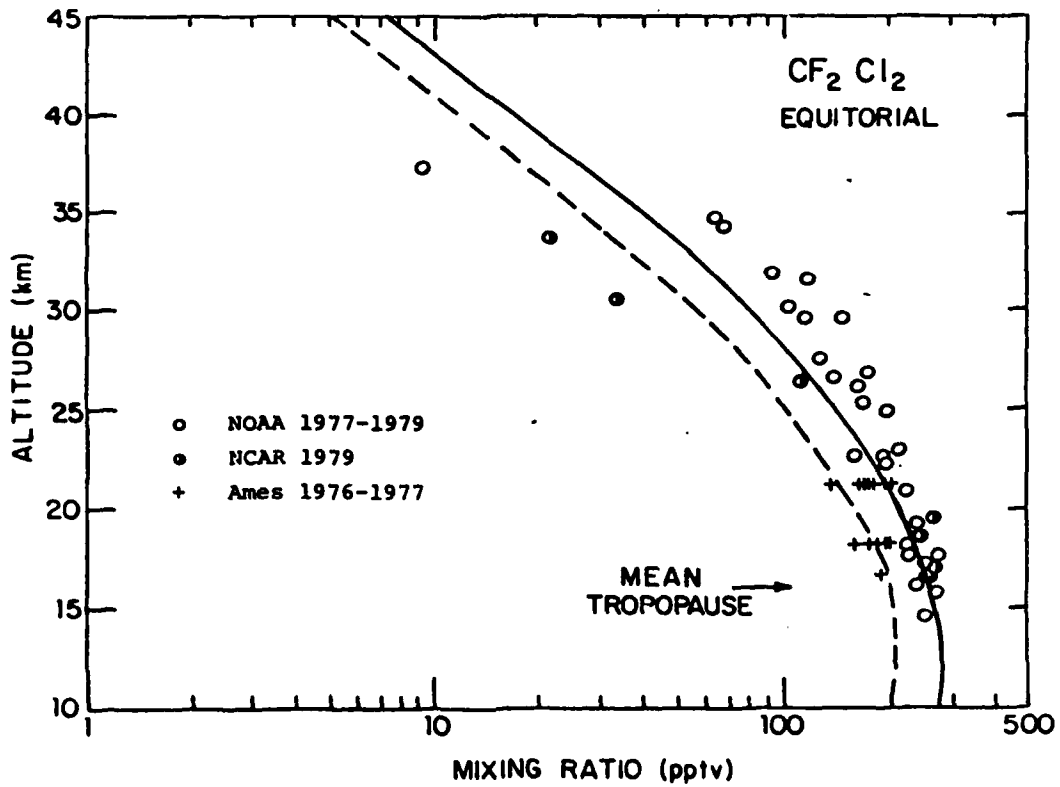


Figure 4-6

Comparison of the calculated CF_2Cl_2 profiles with observations. The data are from the measurement programs of NOAA, NCAR and NASA Ames as compiled for the 1981 NASA Workshop publication.

— Equator - corresponding to 1979 concentration
 - - - Equator - corresponding to 1975 concentration

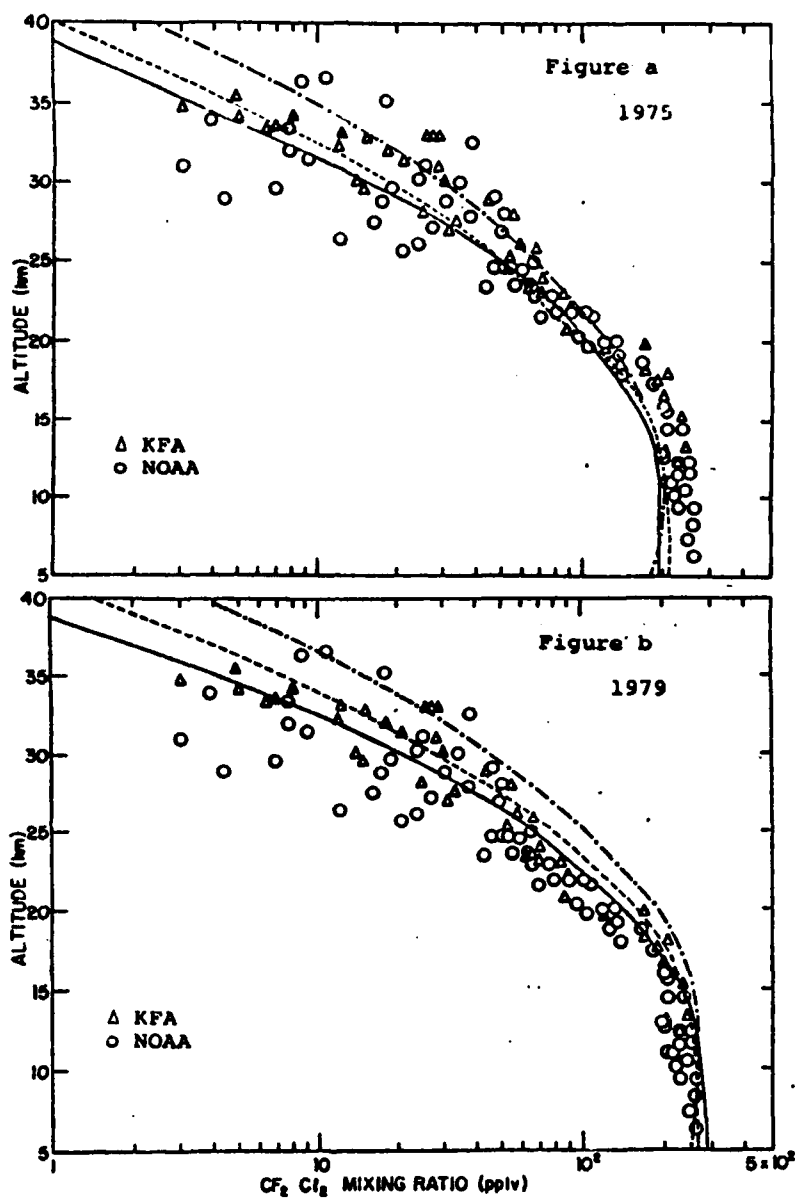


Figure 4-7

Comparison of the calculation of CF₂Cl₂ profiles with observations. The profiles correspond to 1975 and 1979 concentrations in Figures a and b respectively.

- · - · - 30° N
 - - - 40° N
 ——— 50° N

with only relatively small changes in the calculated profiles of N_2O and CFC-12.

CH₄ and CH₃Cl

Both CH₄ and CH₃Cl differ from the species discussed previously in that they are removed in the troposphere by reaction with OH. Reactions with O(¹D) and Cl also play a role in the stratospheric removal of CH₄.

The agreement between the calculated CH₄ distribution (Fig. 4-8) and observation is fairly good, although the calculated mixing ratio lies somewhat below the observations in the equatorial region. It should be noted that the data are based on a single observation profile. A smaller stratospheric OH abundance or a more efficient upwelling, via a faster K_{zz} , for example, could bring the model into closer agreement with observations.

The calculated mid-latitude profiles for CH₃Cl (Fig. 4-9) lie above the observations. It must be pointed out that there are less data available for CH₃Cl than for CFC-11 and CFC-12. Nevertheless, the behavior of the model calculated CH₃Cl appears to be consistent with those of CFC-11 and CFC-12 pointing to the possibility that a slower K_{yy} may increase the latitudinal gradient and improve the agreement with observations.

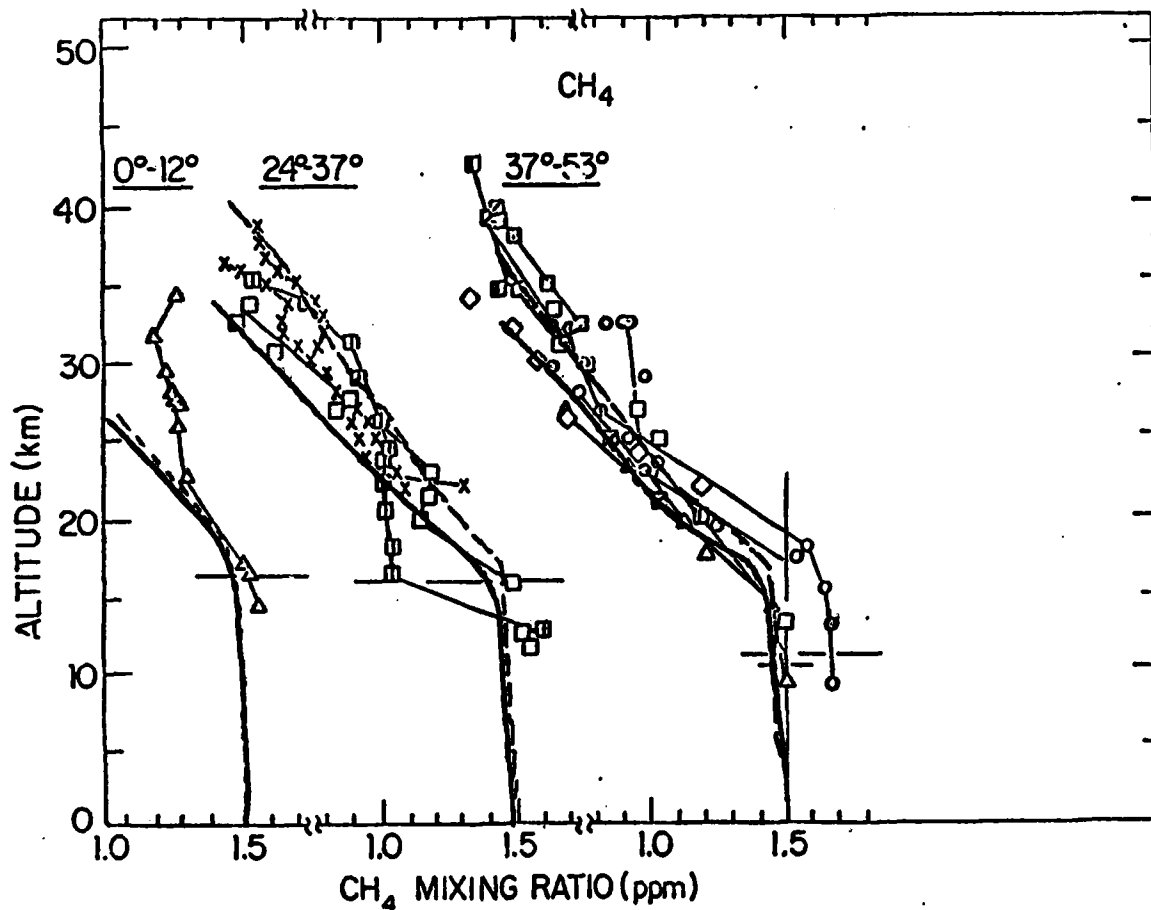


Figure 4-8

Comparison of the calculated CH₄ profiles with observations for different latitudes. The data are from Bush et al. (1979), Heidt and Krasnec (1978), Ehhalt (1978) and Fabian et al. (1979) as compiled in NASA 1049. The curves (---, —) correspond to (Equator, 10° N), (20° N, 40° N) and (40° N, 60° N) respectively in the three panels.

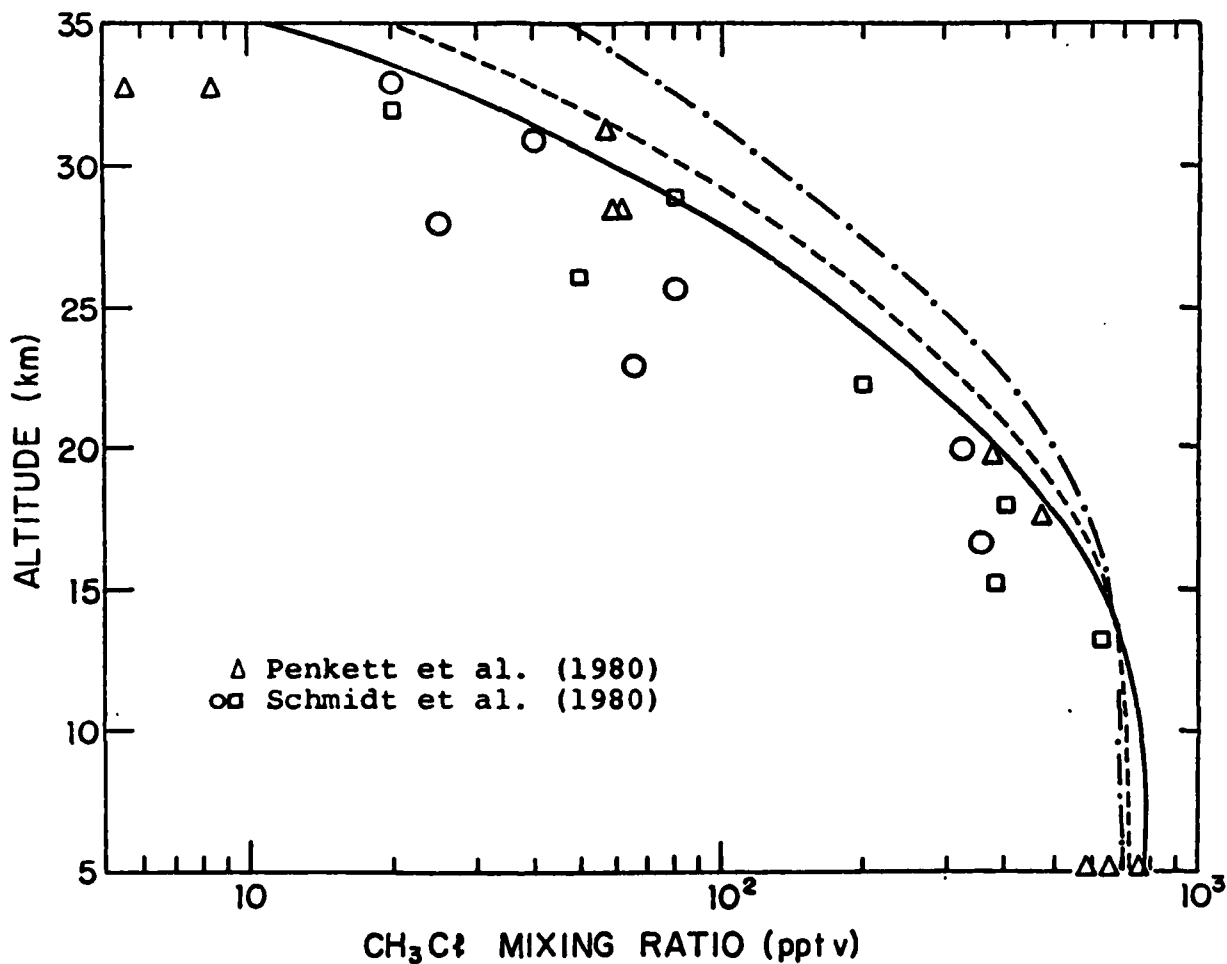


Figure 4-9

Comparison of the calculated CH_3Cl profiles with observations for different latitudes. The data from Penkett et al. (1980) and Schmidt et al. (1980) are compiled for the 1981 NASA Workshop. The curves (---) 30° N , (- - -) 40° N and (—) 50° N .

H₂ and CO

The other long-lived species for which there are available data are H₂ and CO. The interpretation of the comparison between calculations and observations is less straightforward because these species are also produced in the atmosphere via photochemical reactions.

For H₂, the agreement between observation and calculation is good below 30 km (Fig. 4-10). Above 30 km, the calculated profiles lie below the observations. It should be noted that the observations show less of a latitudinal gradient than the upward diffusive species, possibly indicating that the effect of in situ chemical production may be comparable to dynamic transport in determining local concentrations.

The amount of CO data is rather limited. Figure 4-11 shows the calculation together with data. The agreement is good except for the data above 30 km which are based on column measurements of Zander et al. (1981).

4.2b Radical Species

The radical species are usually characterized by chemical lifetimes much shorter than the transport time scale. The partition among various radical species is therefore mainly controlled by photochemistry, although their absolute concentrations still may be affected by the stratospheric distribution of the long-lived (precursor) species discussed in the earlier section. Nevertheless, a comparison between

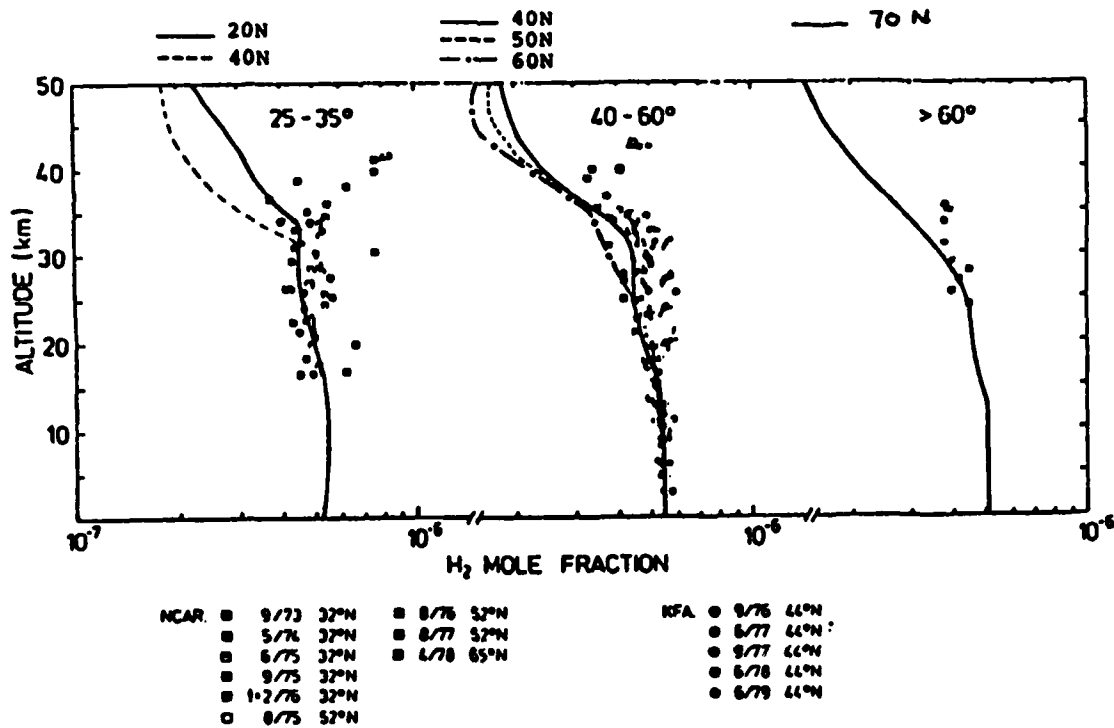


Figure 4-10

Comparison of the calculated H₂ profiles with observations. The data are compiled for the 1981 NASA Workshop publication.

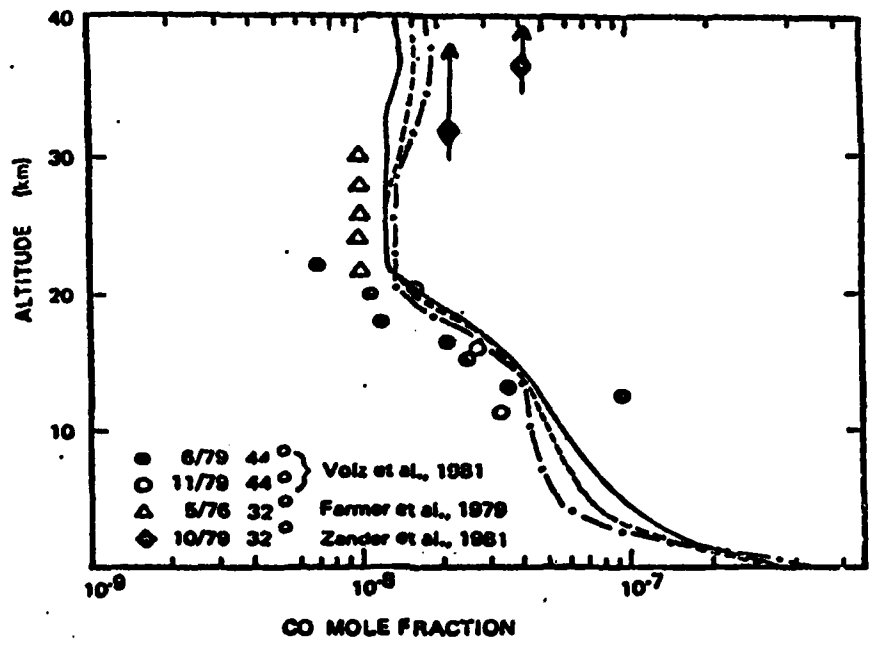


Figure 4-11

Comparison of the calculated CO profiles with observation.

- 30° N
- 40° N
- 50° N

the observed and calculated radicals at different altitudes, latitudes and seasons should provide useful insights into the stratospheric chemical system, particularly when the distribution of the long-lived species is simulated well in the model.

The vertical profiles for different latitudes and seasons presented here correspond to the daytime condition. Quantitative comparison of the calculated radical concentrations with observation remains difficult for the following reasons. First, the concentrations are often very sensitive to the detailed diurnal variation of solar zenith angle. A full diurnal treatment is not included in our 2-D calculation because of the enormous computing requirement. Second, observations may be subject to local variabilities influenced by factors not included by current models. The calculated latitude and altitude cross-section of the radical species are given in Appendix B. Note that those calculations were performed using 24-hour average conditions. The result presented in Appendix B is useful in giving a perspective on the latitudinal variation of the species. For comparison with data, it is more convenient to use altitude profiles. A common feature among the calculated profiles is that the summer profiles for different latitudes are much closer together than the corresponding set of winter profiles in the northern hemisphere. This feature appears to reflect the smaller differences in the solar zenith angle among the different latitudes in the summer hemisphere.

O³(P), OH, HO₂

Figures 4-12, 4-13 and 4-14 show the calculated profiles for O³(P), OH and HO₂ respectively together with the measurements. The agreement for O³(P) is good. The OH and HO₂ profiles are calculated using a uniform concentration of 5 ppmv for stratospheric water vapor. The agreement for OH is good. In the case of HO₂, the calculated profiles are somewhat lower than the observations. Note that the data for OH and HO₂ below 30 km are still non-existent.

NO, NO₂, HNO₃

The calculated behavior of the nitrogen radicals is affected by NO_x distribution. Figure 4-15 shows the calculated NO_x profiles for different latitudes corresponding to summer condition.

Our calculations show that in the upper stratosphere, the bulk of the NO_x is in the form of NO. Note that the latitudinal variation of NO (Fig. 4-16) closely mimics that of NO_x in that region. In the lower stratosphere, most of the NO_x is in the form of NO₂ and HNO₃. The behavior of the NO₂ profile for 50° N in winter (Fig. 4-17) seems contrary to the recent seasonal data reported by Noxon (1979) and Coffey et al. (1981) which showed that there should be less NO₂ in the winter hemisphere at high latitudes. Our preliminary investigation shows that this may have resulted from the diurnal treatment being used. A more realistic treat-

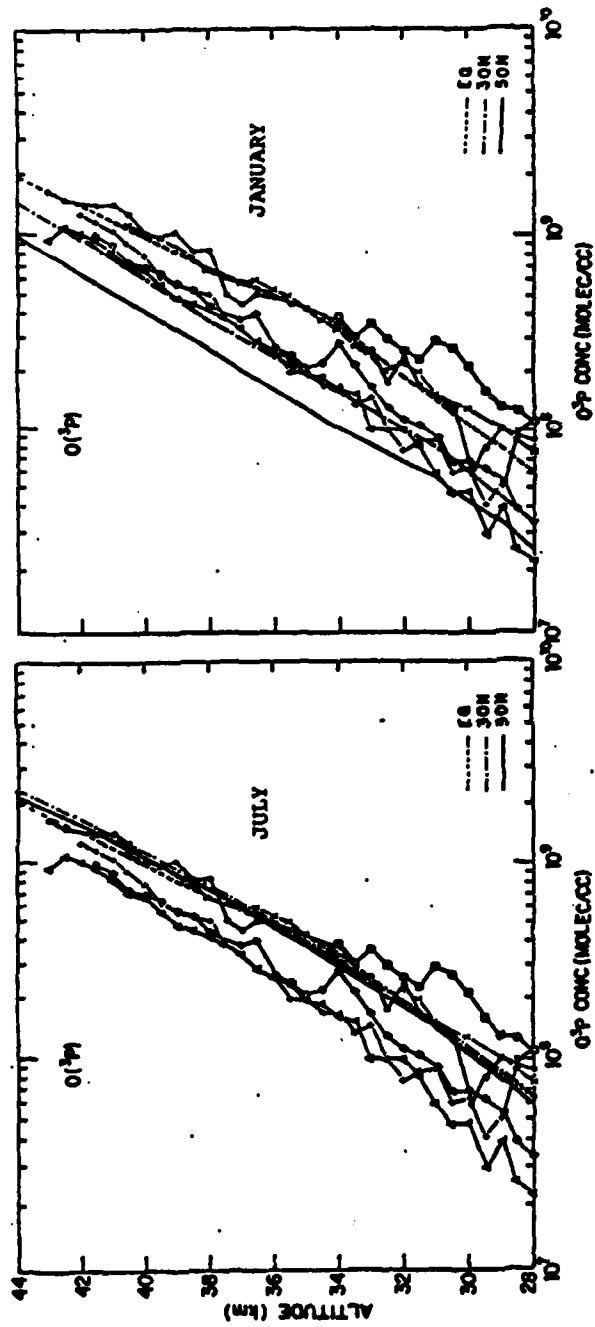


Figure 4-12

Calculated daytime concentrations of O(³p) in the northern hemisphere for different seasons. The data are from Anderson and co-workers (1975, 1980). The dates and zenith angles at time of observation are:

DATE	X
11/25/74	56°
2/7/75	51°
10/25/77	45°
12/2/77	50°
11/17/78	45°
6/15/78	24°

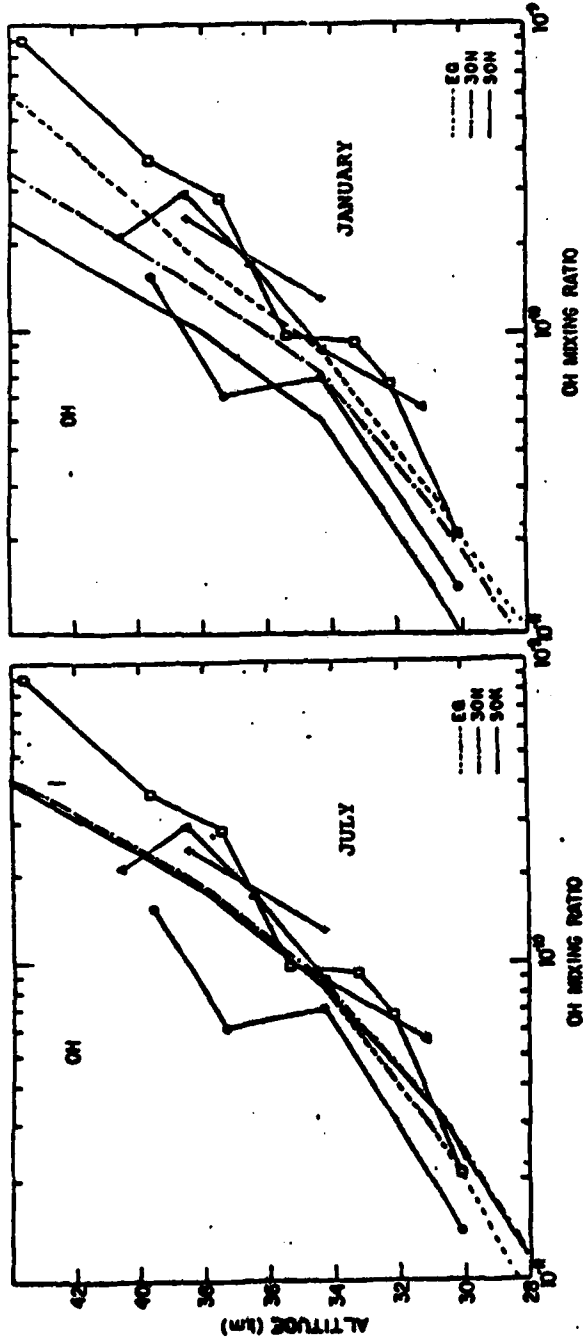


Figure 4-13

Calculated daytime concentrations of OH in the northern hemisphere for different seasons. The data are from Anderson et al. (1976, 1980). The dates and the solar zenith angles at time of observation are given. The scaling factor which is used to adjust for observations made at low zenith angles is also included.

DATE	X	Scale Factor
1/12/76	80°	2
4/26/77	80°	2
7/14/77	41°	1
9/29/77	41°	1

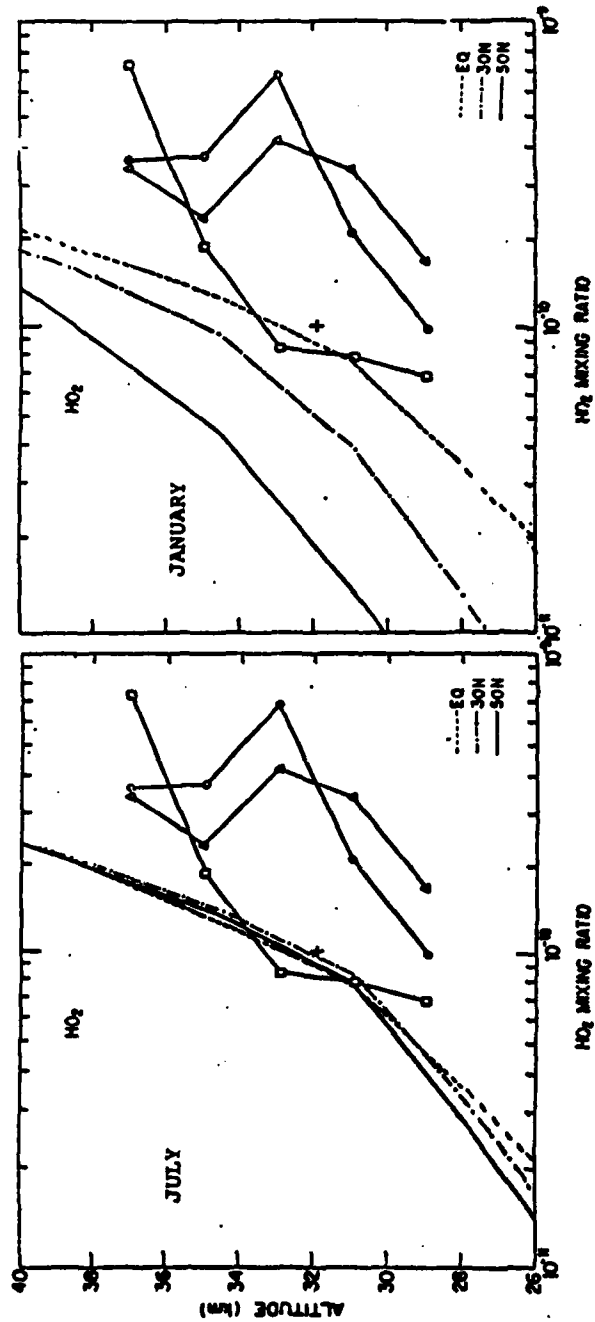


Figure 4-14

Calculated daytime concentrations of HO₂ in the northern hemisphere for different seasons. The observed profiles are from Anderson et al. (1981) while the single point (+) is from Mihelcic et al. (1978). The dates and the solar zenith angles at time of observation are given.

DATE	X	LATITUDE
9/20/77	41°	32°N
10/25/77	45°	32°N
12/2/77	50°	32°N
8/8/76	-	53°N

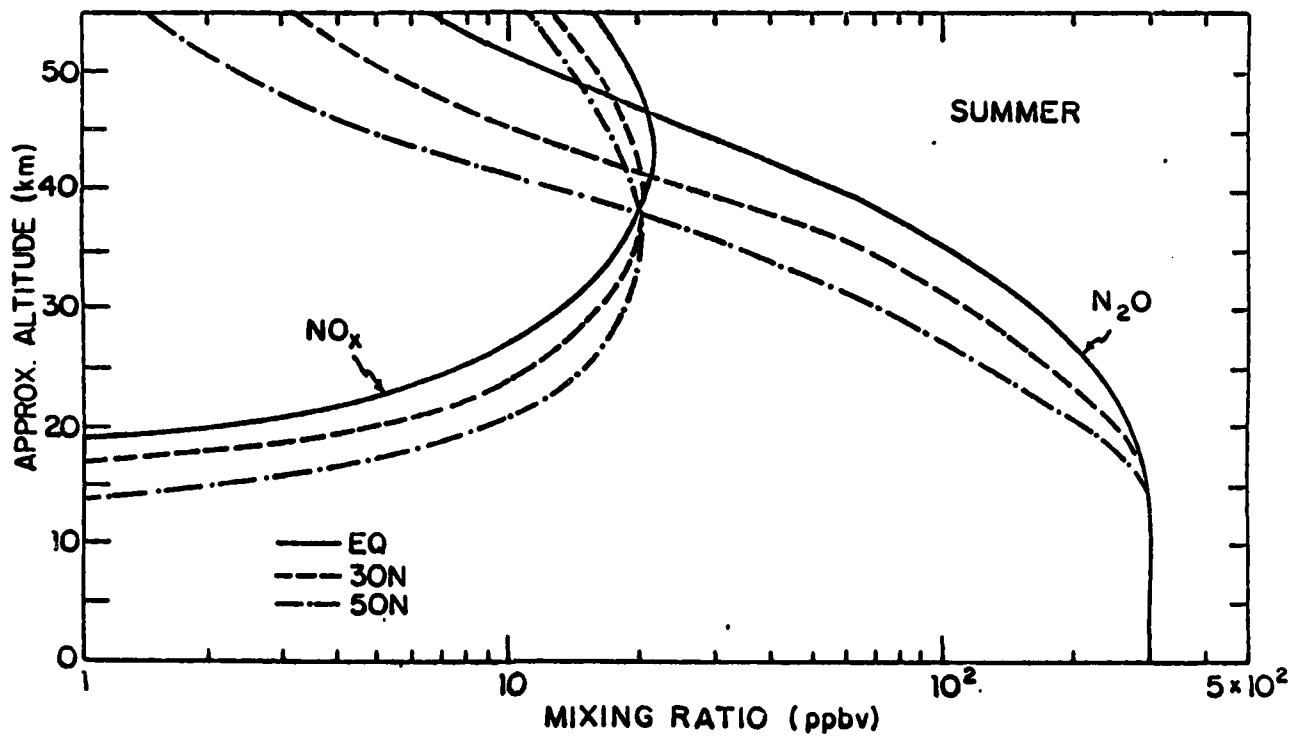


Figure 4-15

Calculated altitude profiles for NO_x and N₂O for different latitudes corresponding to summer in the northern hemisphere.

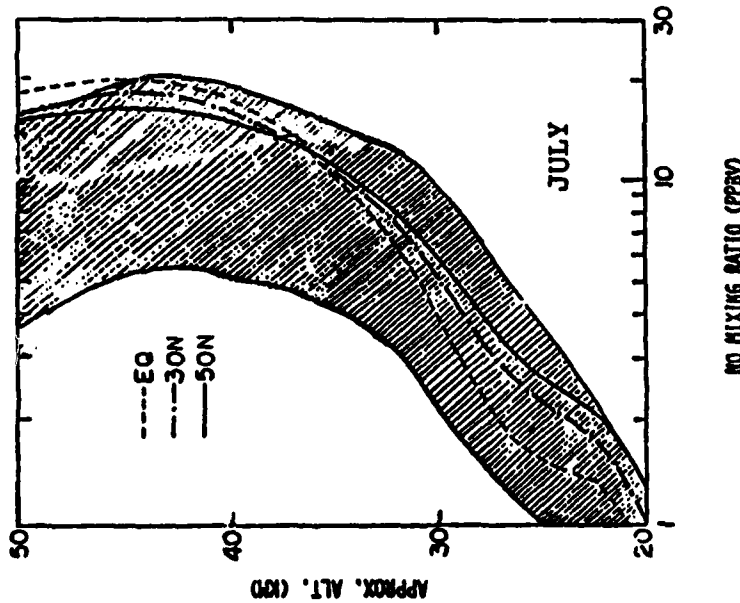
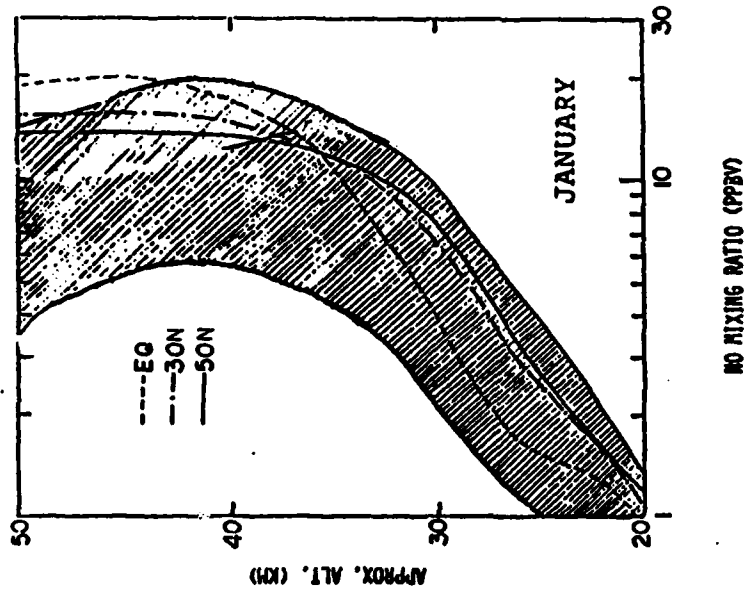


Figure 4-16

Calculated day time concentrations of NO in the northern hemisphere for different seasons. The shaded areas correspond to observations reported by Ridley and Howlett (1974), Ridley et al. (1977), Ridley and Hastie (1981), Ridley and Schiff (1981), Mason and Horvath (1976), Horvath and Mason (1978), Loewenstein and Savage (1975), Loewenstein et al. (1975, 1978a,b) and Patel et al. (1974).

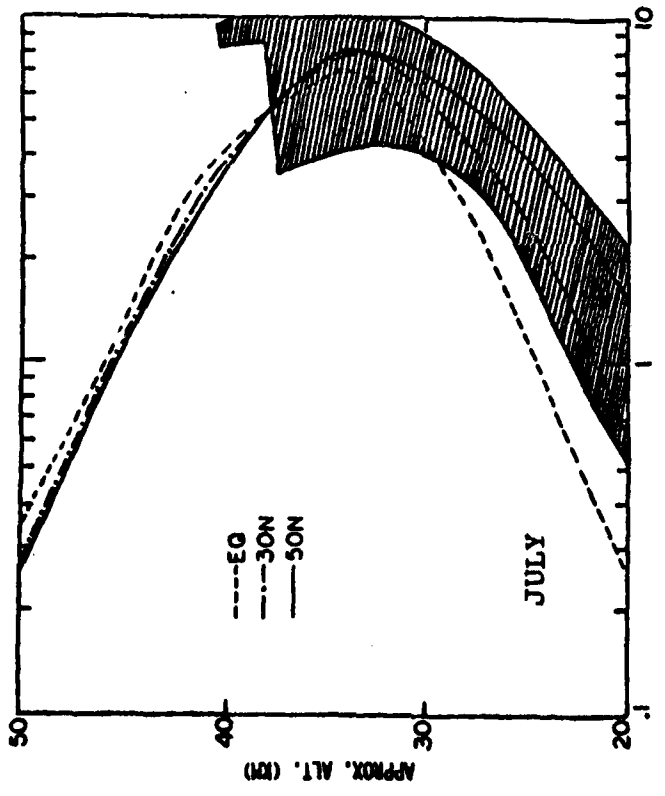
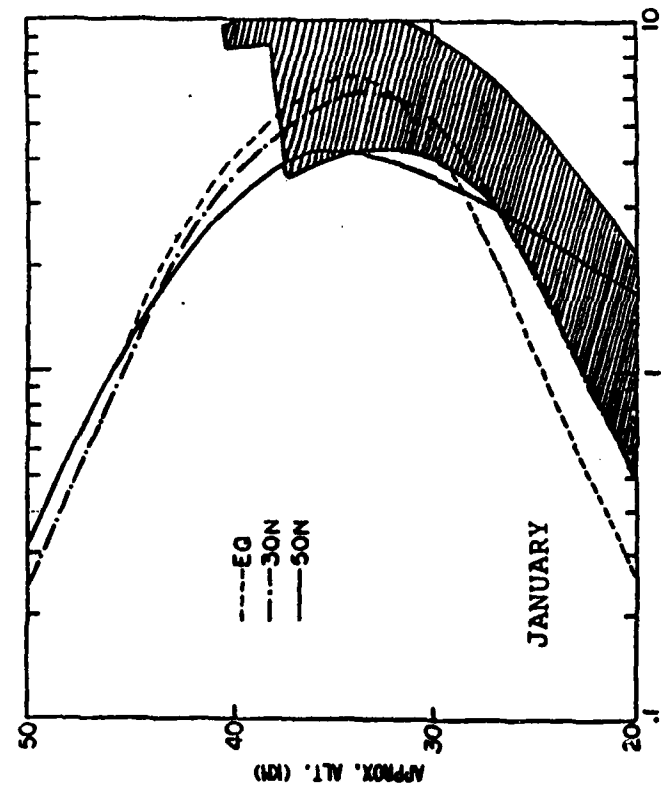


Figure 4-17

Calculated day time concentrations of NO₂ in northern hemisphere for different seasons. The shaded areas correspond to data reported by Ackerman and Muller (1973), Murcray et al. (1974), Ackerman et al. (1975), Fontanella et al. (1975), Kerr and McElroy (1976), Evans et al. (1978), Goldman et al. (1978) and Blatherwick et al. (1980).

ment of the diurnal behavior may be required to simulate the high latitude NO_2 during winter conditions.

The calculated profiles of HNO_3 agree well with observation in the lower stratosphere but lie above observations in the upper stratosphere, as shown in Figure 4-18. Observations of HNO_3 column as a function of latitude are also available and show a minimum at the equator. Figure 4-19 shows the calculated HNO_3 column abundance together with the observations. Both calculations and observations indicate that the minimum HNO_3 column occurs around the equator. The behavior of column HNO_3 in Figure 4-19 is consistent with the latitudinal variation of NO_x in Figure 4-15.

On balance, the calculated concentrations agree reasonably well with the observations except for NO and HNO_3 in the upper stratosphere, where the model tends to overestimate the species abundance.

ClO , HCl , ClNO_3 , Cl

Figure 4-20 shows the ClX profiles for different latitudes corresponding to summer conditions. In contrast to NO_x , ClX is well mixed in the upper stratosphere (no vertical gradient) because of the absence of a stratospheric sink.

Figure 4-21a and b show the altitude profiles for HCl which is the major stratospheric chlorine reservoir. The calculated HCl appears to lie within a factor of 2 of the observations, although in the upper stratosphere (~ 40 km), the model results lie in the lower range of observations.

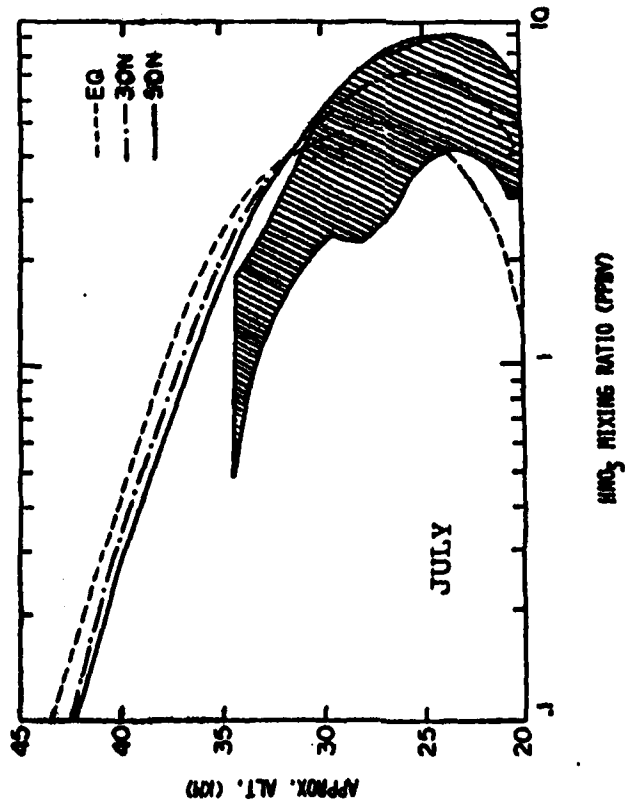
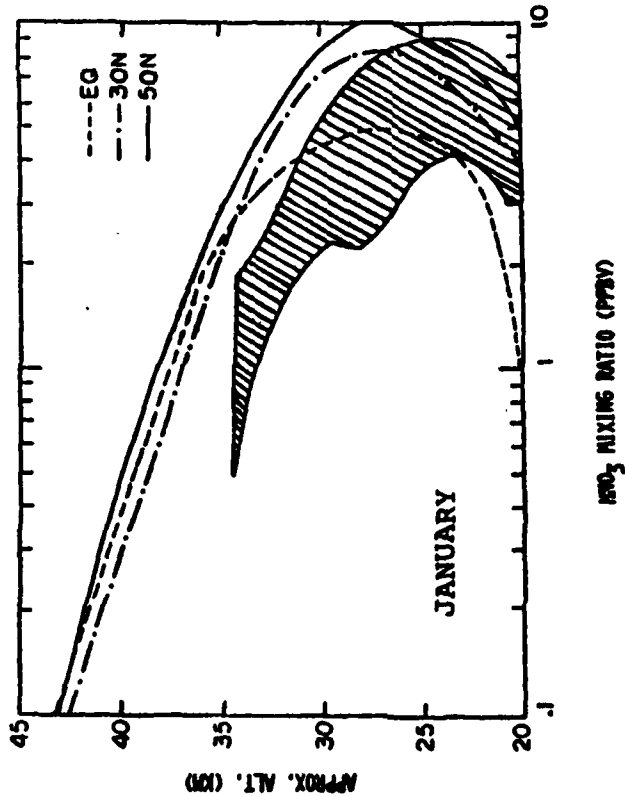


Figure 4-18

Calculated day time concentration of HNO₃ in the northern hemisphere for different seasons. The shaded areas correspond to data reported by Lazarus and Gandrud (1974), Fontanella et al. (1975), Harries et al. (1976), Evans et al. (1978) and Arnold et al. (1980).

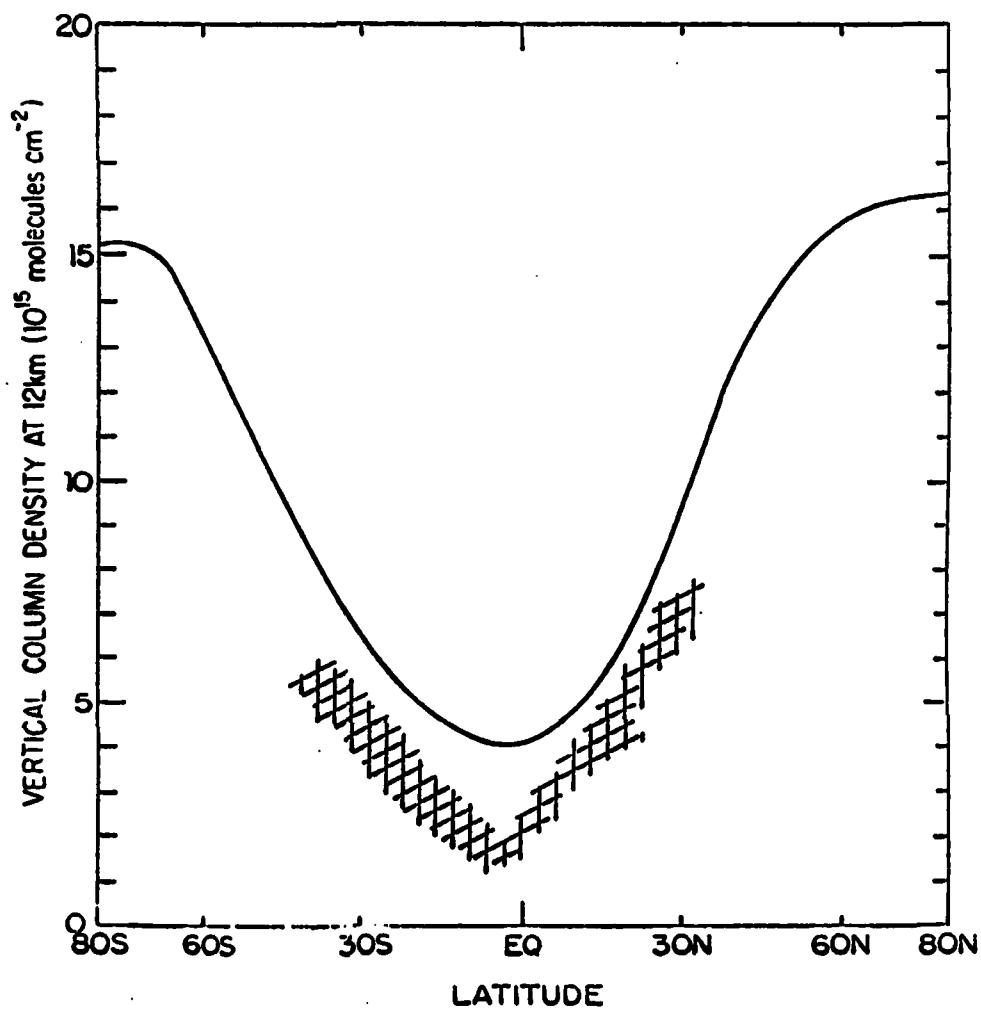


Figure 4-19

Calculated column abundance of HNO₃ corresponding to spring time condition. Shaded area corresponds to the data reported by Murcray et al. (1975).

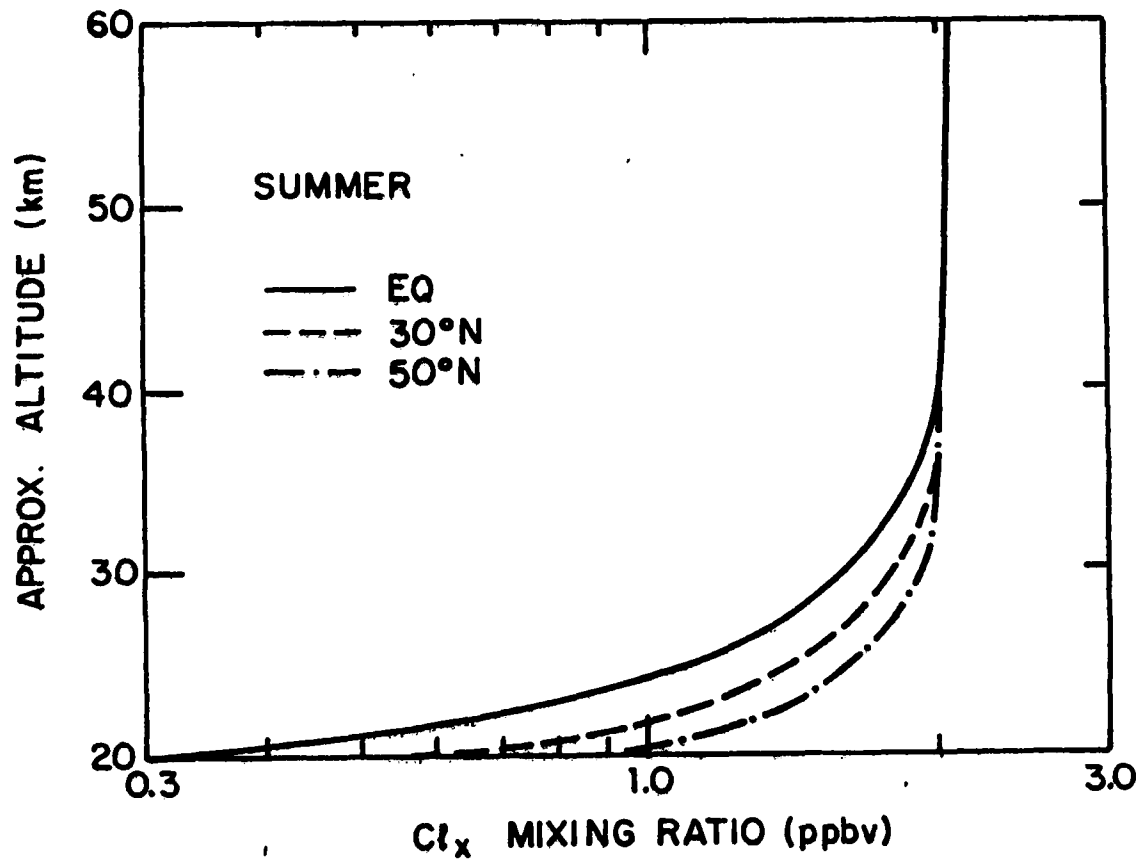
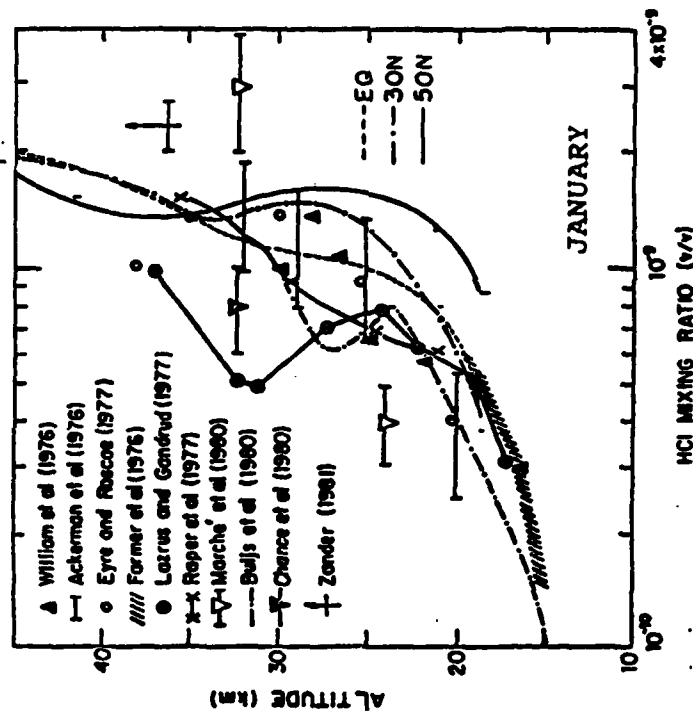
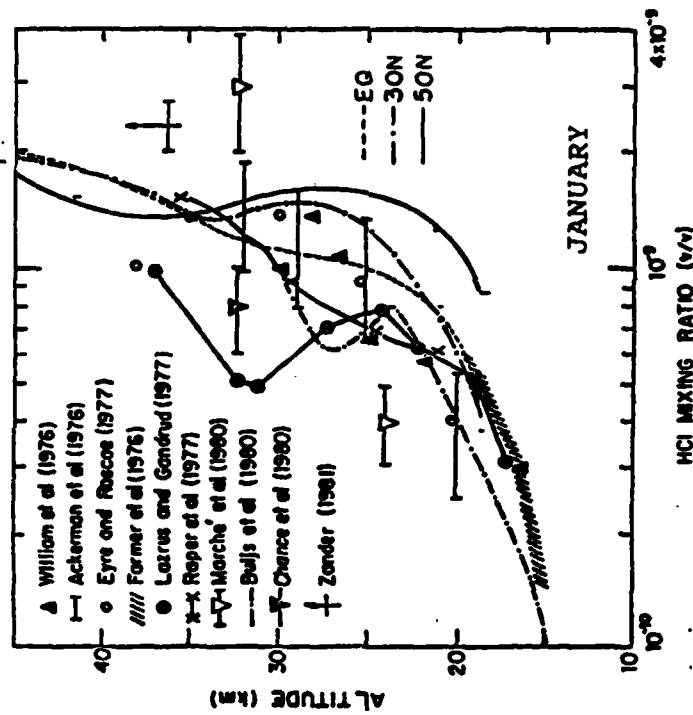


Figure 4-20

Calculated ClX concentrations for different latitudes for summer condition.



(a)



(b)

Figure 4-21

Calculated day time concentrations of HCl in the northern hemisphere for different seasons. The data are as indicated in the figure.

A higher stratospheric chlorine content would improve the agreement.

Figure 4-22 shows the calculated profiles of ClO together with the observations. With the recent revision in the reaction rates as discussed in Section 2, the agreement in the lower stratosphere is much better than before (prior to 1980). However, the observed mixing ratios appear to peak at higher altitudes than our model does. Furthermore, the model tends to underestimate the ClO abundance by about a factor of 2 above 35 km. The situation is somewhat disturbing, since the discrepancy occurs in the region where the CFCs-induced ozone depletion is predicted to be the greatest. This apparent discrepancy may be caused by a combination of factors, such as underestimation of upper stratospheric OH or total chlorine content by the model. If the upper stratospheric OH were underestimated by the model, then it is possible that current models might have understated the impact of CFCs on ozone. This interpretation may be invalid if the discrepancy is actually due to the underestimate of the stratospheric chlorine content by the models. It is therefore difficult to relate the present ClO data with CFC's impact without knowing the cause for the discrepancy between observation and model. A simultaneous measurement of OH, CH₄, ClO and HCl around 38 km will help to resolve this issue.

The calculated profiles for ClNO₃ are given in Figure 4-23. The concentrations calculated with the slow ClNO₃ formation rate as recommended by NASA/WMO (1981) are signif-

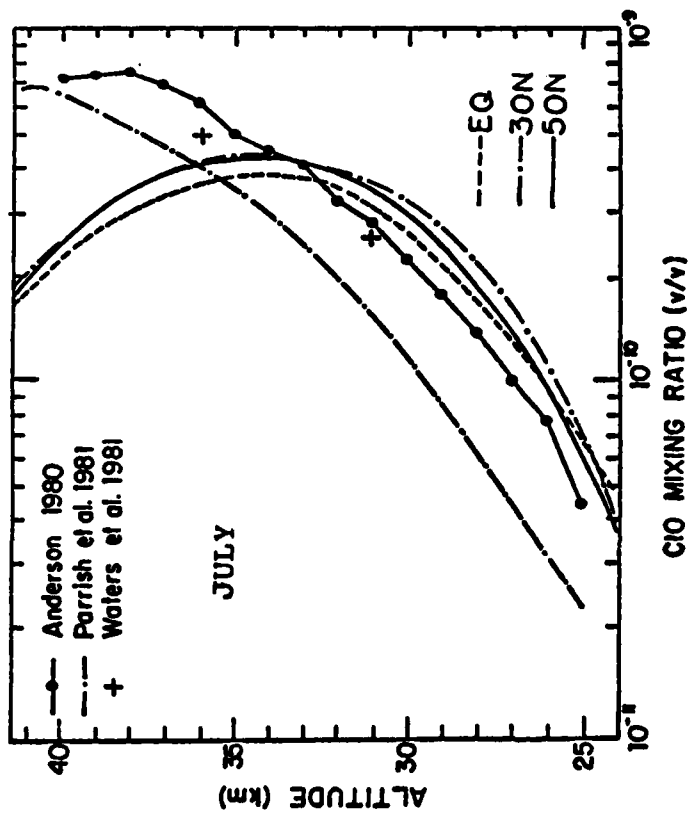
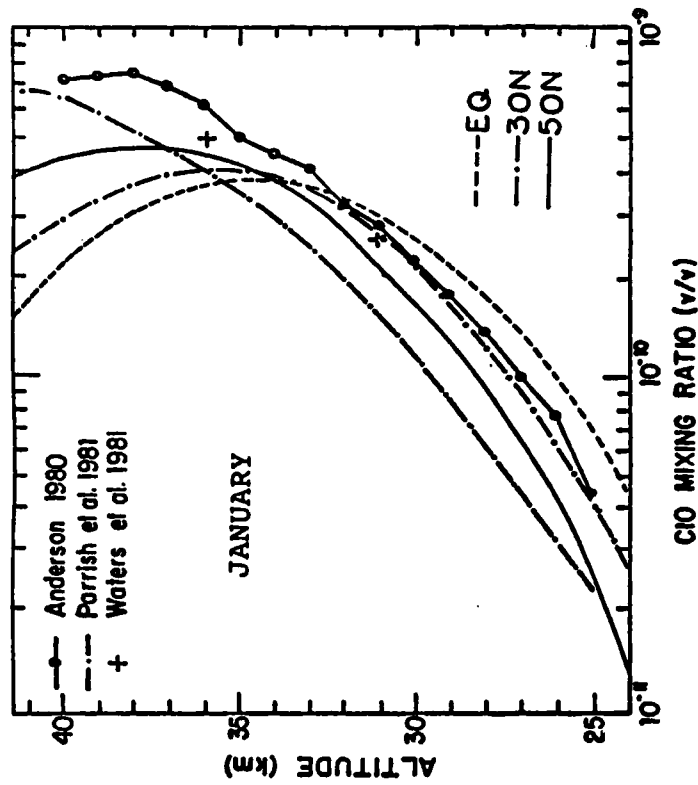


Figure 4-22

Calculated day time concentrations of ClO in the northern hemisphere for different seasons. The curve labeled Anderson 1980 compared to the data of Anderson excluding the July 14 measurement.

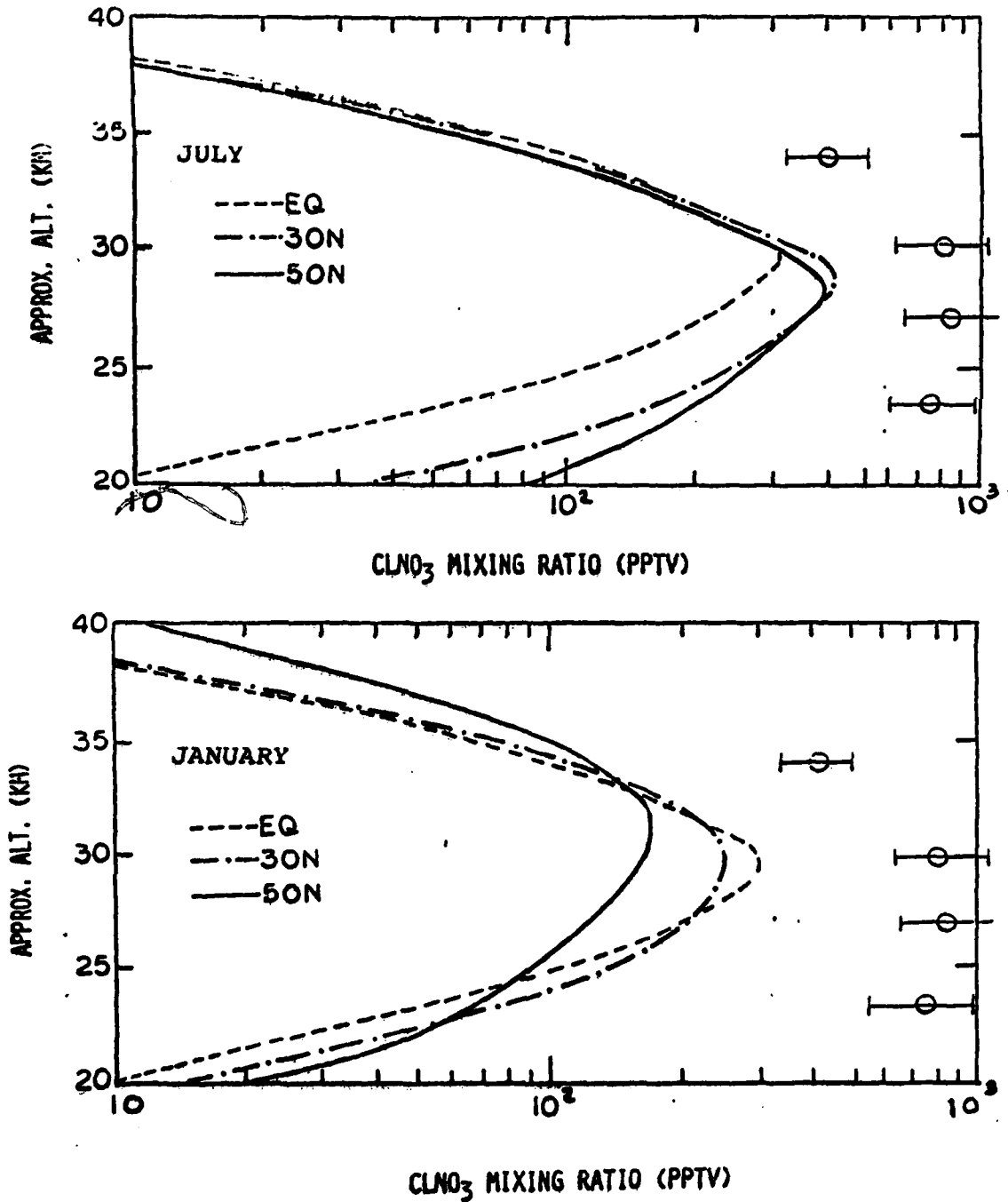


Figure 4-23

Calculated day time concentrations of ClNO₃ in the northern hemisphere for different seasons. The data are from Murcray et al. (1979).

icantly lower than the observations of Murcray et al. (1979). Measurement of this species may provide some insights as to which formation rate of ClNO_3 under stratospheric conditions is more appropriate.

The calculated profiles for Cl are given in Figure 4-24. Again, as in the case of ClO , the model seems to have underestimated the Cl abundance at around the 38-40 km region. The possible causes for the difference between calculated and observed Cl at 40 km may be similar to that for ClO as discussed earlier.

4.2c Ozone

Figures 4-25a and b show the photochemical lifetime of ozone calculated via the expression

$$\tau_{\text{O}_3} = \frac{[\text{O}_3]}{2 \times J_2[\text{O}_2]} \quad (4.1)$$

as a function of latitude and altitude for two seasons. Since the stratospheric dynamic time scale is typically a few weeks, the figure also delineates regions where photochemistry or dynamic transport dominate. Typically, in the tropics above 30 km, O_3 concentration is determined by local chemical sources and sinks, whereas in the lower stratosphere ($z < 30$ km) O_3 is mainly controlled by transport. Since much of the total ozone resides below 30 km, the behavior of column O_3 must be strongly influenced by atmospheric transport.

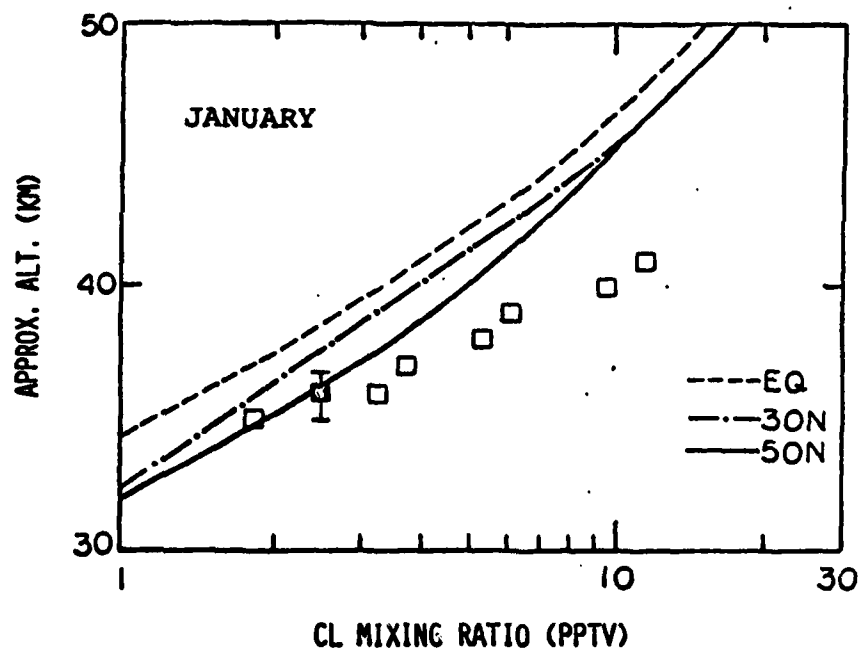
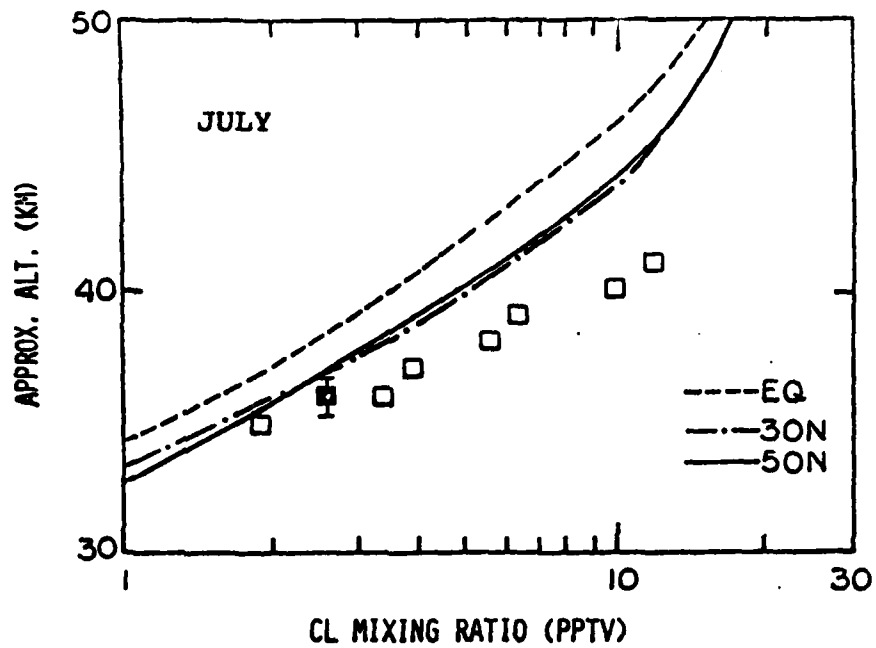
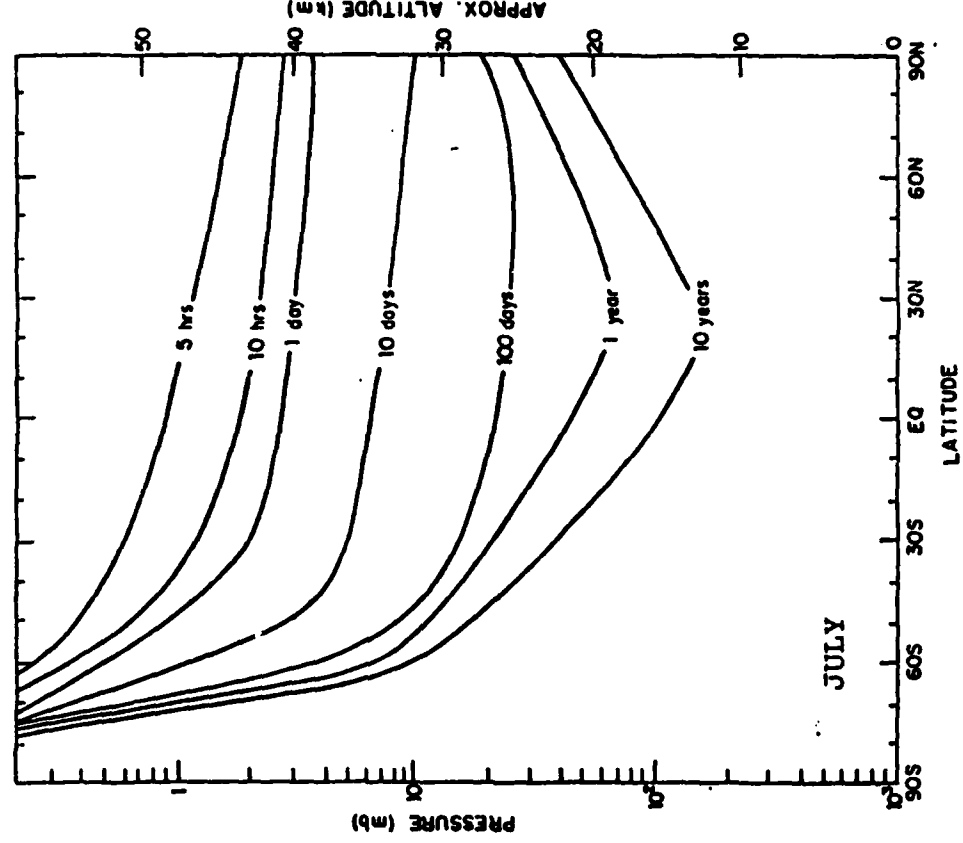
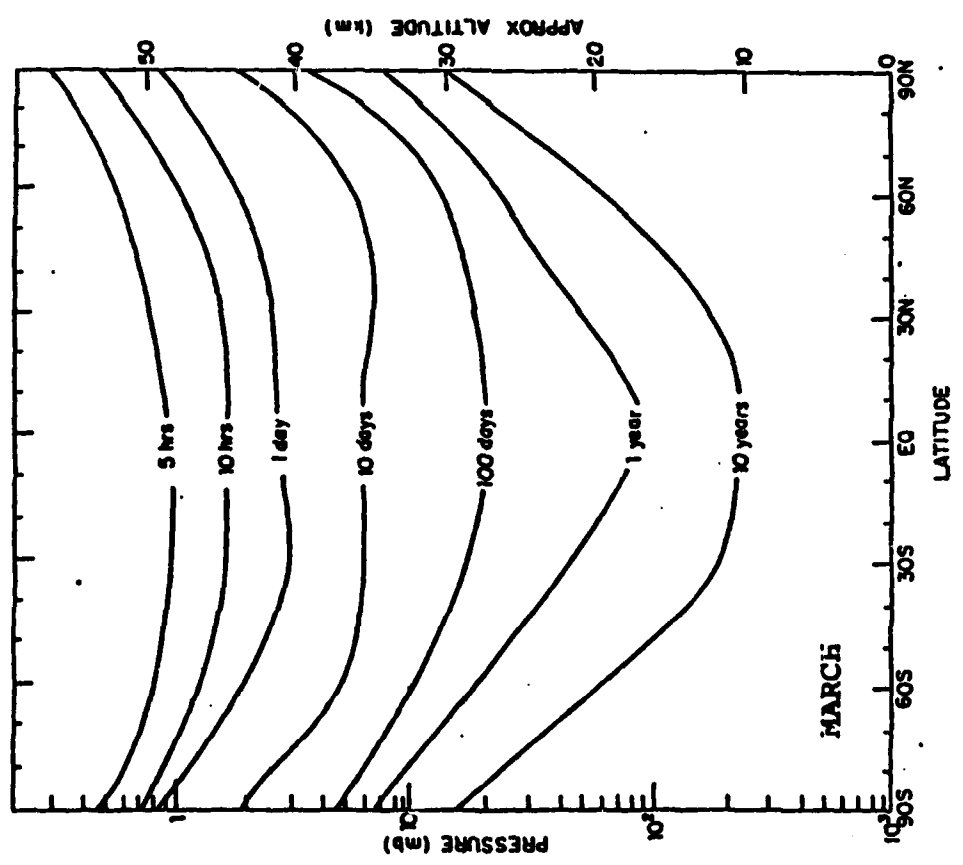


Figure 4-24

Calculated day time concentrations of Cl in the northern hemisphere for different seasons. The data are from Anderson et al. (1977, 1980).



(a)



(b)

Figure 4-25

Calculated photochemical lifetime of ozone as a function of latitude and altitude for different seasons. The lifetime is given by the ratio $[O_3]/2J_2[O_2]$.

Figure 4-26 shows the observed behavior of column O_3 as a function of latitude and season as compiled by Deutsch (1971) from ozone measurements obtained from the Dobson network. The essential features are the relatively low values (~ 260 Dobson units) around the equatorial region and the occurrence of the spring time maxima (April and November) at high latitudes in each hemisphere.

Figure 4-27 shows the calculated O_3 distribution of the present day atmosphere from our 2-D model. Though the calculated features are qualitatively correct, the calculated latitudinal gradient of column ozone is somewhat smaller than the observed values. In addition, the northern hemispheric spring time maximum occurs at a later time (May instead of late March).

It is well known that transport is mainly responsible for the latitudinal and seasonal behavior of column O_3 . We therefore performed a numerical experiment to see if adjustment of the eddy diffusion coefficient would lead to better agreement. In the formulation of Reed and German (1965), the value $\alpha = K_{yx}/K_{yy}$ gives the slope of the mixing path. A higher value for α would imply a larger counter gradient transport from the equatorial to the high latitude region. In the experiment, we double the value of K_{yz} in the model calculation. In order to preserve numerical stability, the value of K_{zz} has to be multiplied by 4 at the same time. The resulting O_3 column distribution is shown in Figure 4-28 which shows a larger contrast between the equatorial minima

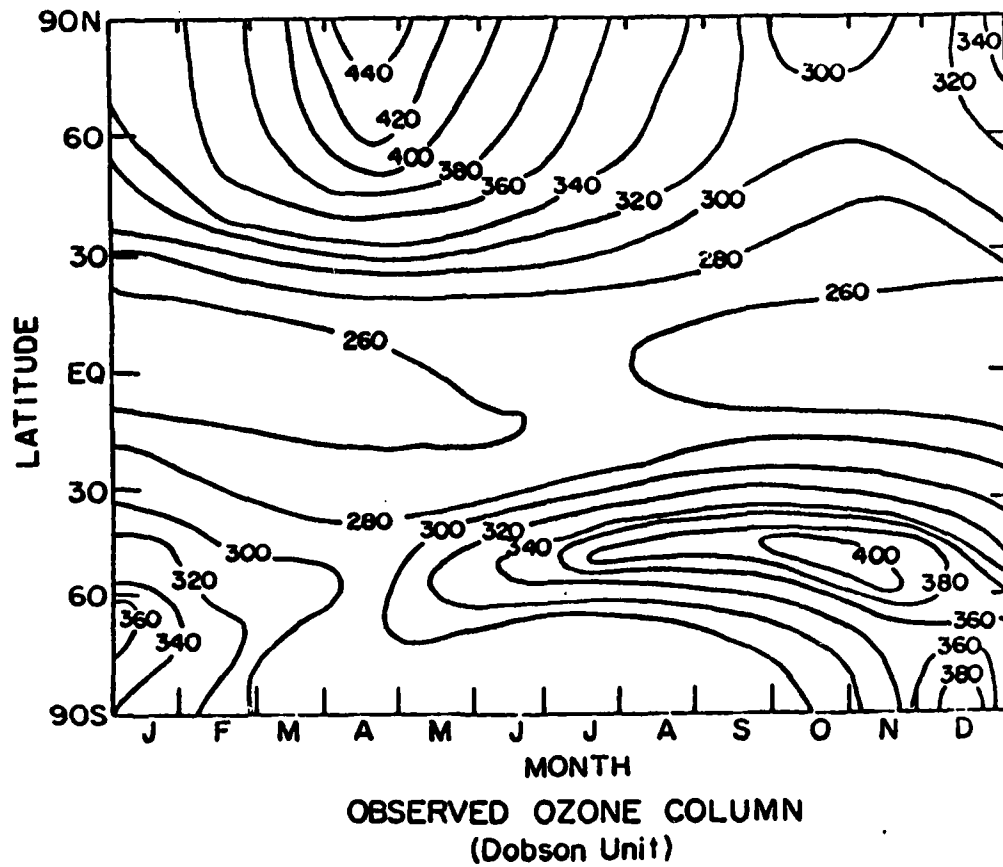


Figure 4-26

Observed ozone column as a function of latitude and season as compiled by Deutsch (1971).

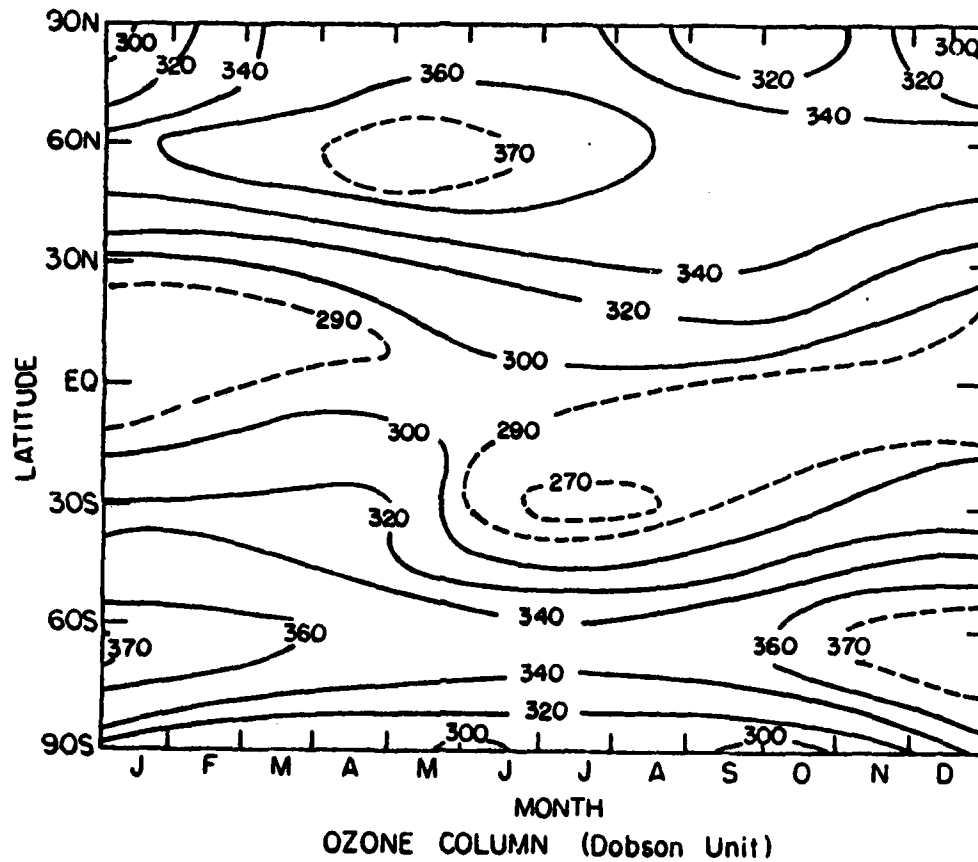


Figure 4-27

Calculated column ozone as a function of latitude and season. The reaction rate constants are from NASA/WMO (1981).

and the spring time maxima. A similar result has been obtained by Harwood and Pyle (1980).

We next performed several numerical experiments to examine the effect of chemistry on the calculated O_3 . Figure 4-29 shows the result from a model run that incorporates only oxygen and hydrogen chemistry. As expected, the magnitude of the calculated O_3 column is higher than the observation. However, the ratio of the spring time maximum to the equatorial value of column O_3 is much closer to the observed value. Note that the spring time maximum also occurs at approximately the right time.

Figure 4-30 shows the calculated O_3 column when nitrogen chemistry is added. From the comparison of Figure 4-29 with Figure 4-30, it is evident that NO_x has relatively little impact on equatorial column O_3 but very large impact on high latitude column O_3 . This observation leads us to explore the possibility that the present model with a 24-hour average scheme might have overestimated the O_3 removal at high latitudes due to the reaction of $NO_2 + O$. We are currently incorporating detailed diurnal treatment in our 2-D model as a possible means to reconcile model results with observations.

Figure 4-31 shows the calculated mixing ratio of O_3 as a function of latitude and altitude for different seasons. The maximum occurs at an altitude of 35 km, and at a latitude corresponding roughly to the position of the overhead sun for each season.

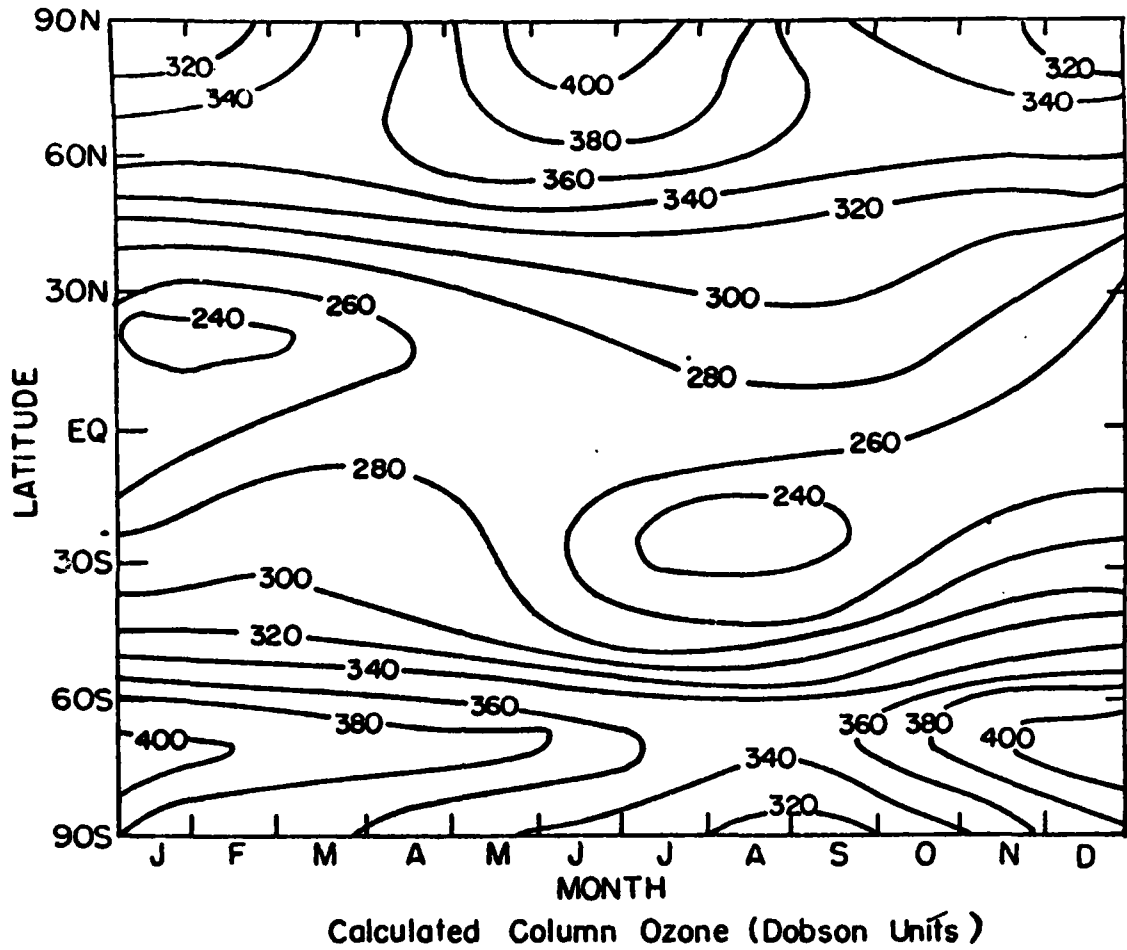


Figure 4-28

Calculated column ozone from the numerical experiment testing the sensitivity of column ozone to changes in the eddy diffusion coefficient. In the experiment, K_{yz} and K_{zz} increased by a factor of 2 and 4 respectively.

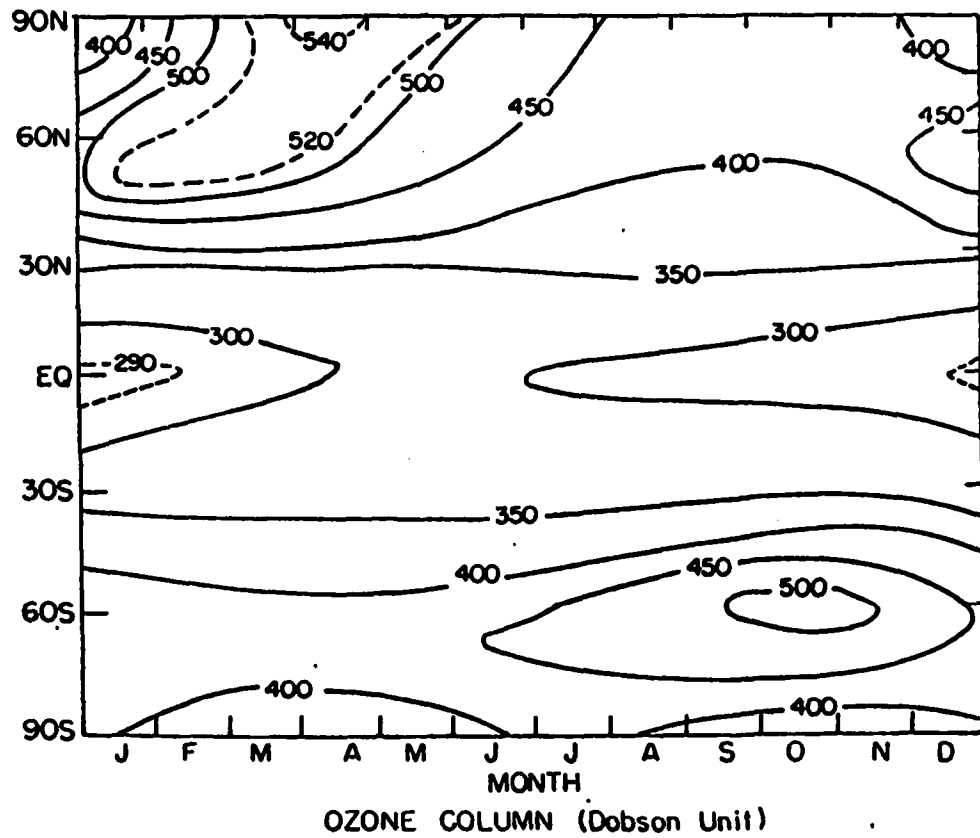


Figure 4-29

Calculated column ozone using oxygen-hydrogen chemistry only.

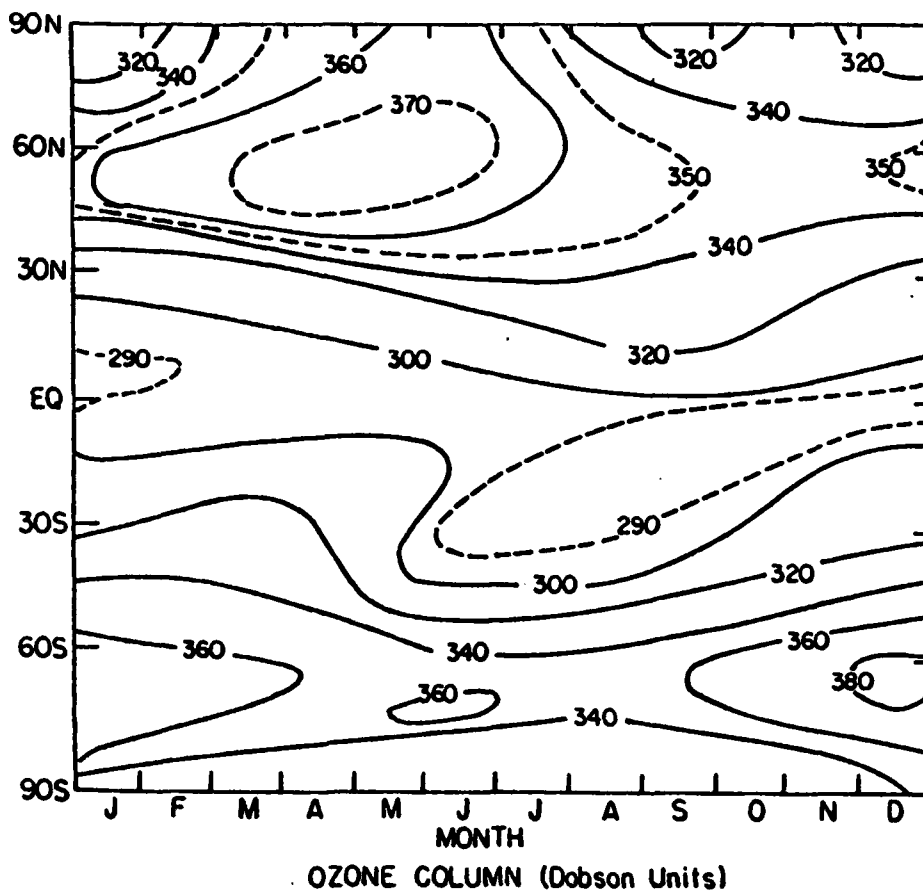
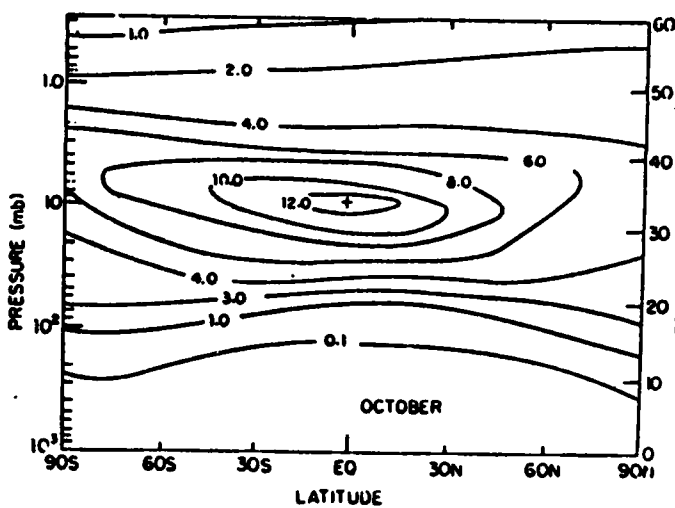
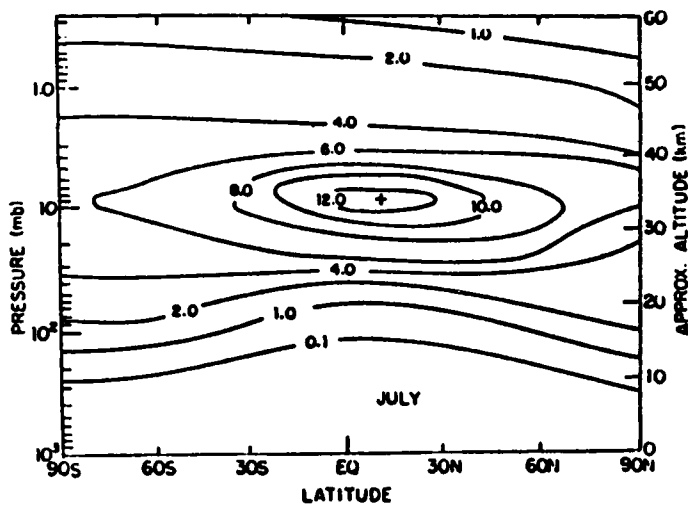
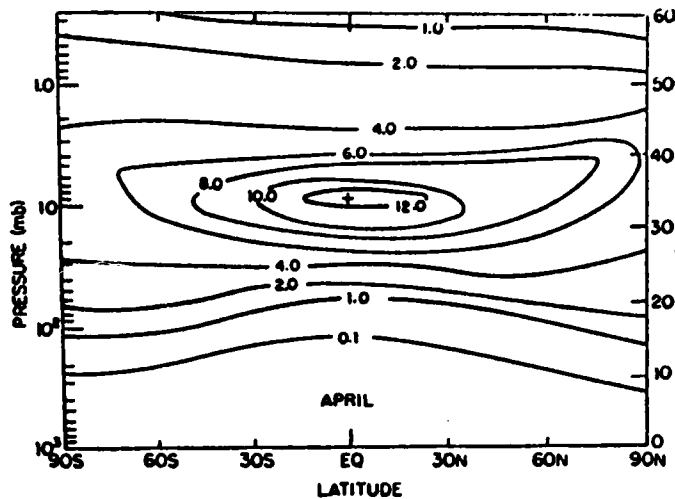
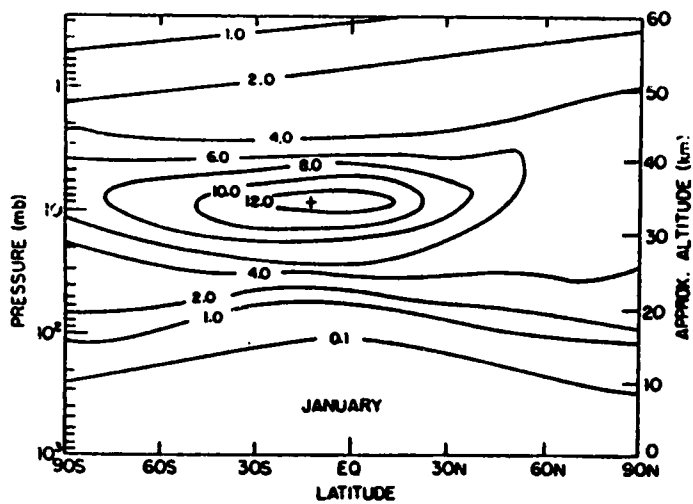


Figure 4-30

Calculated column ozone using oxygen-hydrogen-nitrogen chemistry.



MIXING RATIO
(ppmv)

Figure 4-31
Calculated mixing ratio of O_3 for different seasons.

Figure 4-32 shows the observed cross-sections of O_3 for different seasons as compiled by Deutsch (1978). The overall feature of our calculated distribution is similar to the observation. The calculated maximum mixing ratio of 12 ppmv appears to be somewhat higher than the observations which shows a broad maximum of >8 ppmv.

4.2d Summary of Comparisons

We have compared the AER 2-D model results with observations of important stratospheric gases. In our previous studies (Sze et al., 1978, 1980), we have pointed to several discrepancies between the observed and the calculated concentrations of ClO, C_2H_6 and ratios of $HNO_3:NO_2$ and HF:HCl in the lower stratosphere (20-30 km). We suggested that these discrepancies might be attributed to a common cause - that models have overestimated the OH concentration in the 20-30 km region where data for OH are lacking. Recent revisions in the rate constants for several key HO_x reactions have significantly lowered the calculated stratospheric OH abundance and thereby greatly improved the agreement between model and observations except for C_2H_6 which still lies significantly above observations.

Several important discrepancies, however, still remain. The discrepancy concerning the calculated and observed ClO at around 40 km has actually been amplified when the new rate data were adopted. The discrepancy in ClO is particularly disturbing since it occurs at a region (~ 40 km)

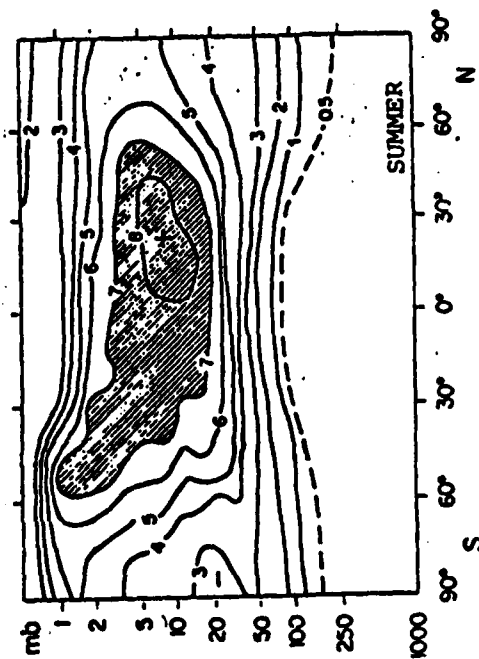
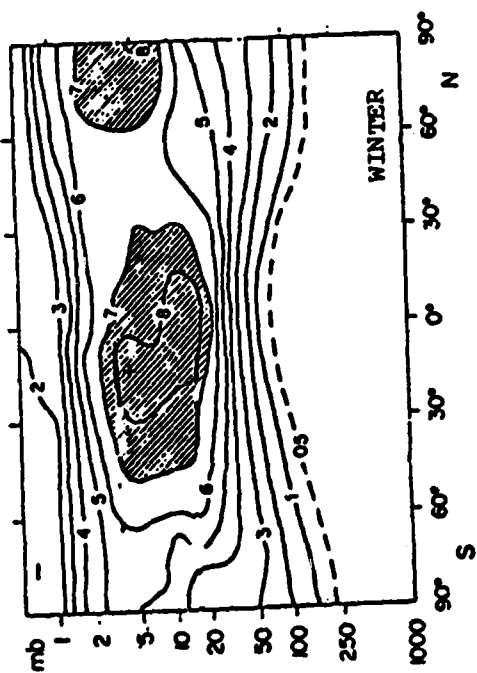
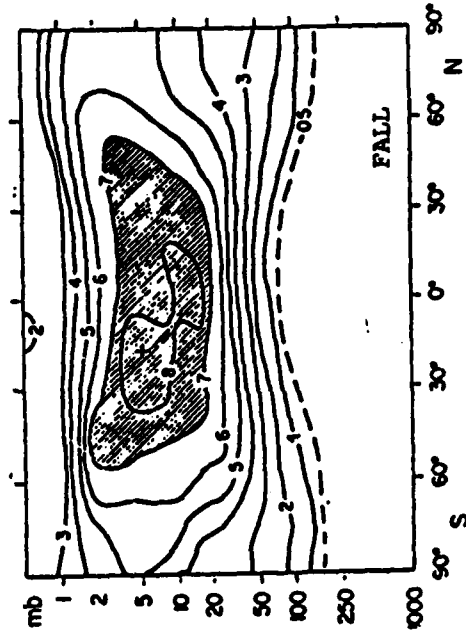
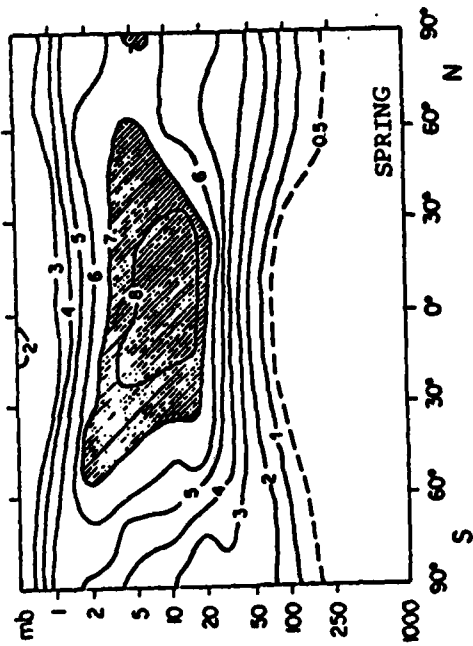


Figure 4-32

Observed latitude-altitude cross-sections of O₃ for different seasons as compiled by Deutsch (1978). The labels refer to the season in the Northern Hemisphere.

where catalysis of O_3 removal by ClO is predicted to be the greatest. The precise cause for this discrepancy is currently unknown.

Another important discrepancy concerns the excessive amount of stratospheric (25-30 km) CFCs (particularly CFC-11) calculated by the models. Again, the cause for this discrepancy is unknown, although it has been suggested that photolysis rates of CFCs in the lower stratosphere might have been underestimated by models. Resolution of this discrepancy could have important implications for CFCs' lifetime estimates.

Agreement between the calculated and observed vertical profiles of NO_x species at mid-latitudes is reasonably good, except for HNO_3 above 30 km, a region where the model calculates significantly more HNO_3 than observation. On the other hand, our 2-D model did relatively poorly in the simulation of the latitudinal and seasonal behaviors of NO_2 and NO , particularly in winter time at high latitudes. This discrepancy, however, remains to be investigated with a 2-D model with full diurnal treatment in stratospheric chemistry before one can isolate the causes of such a discrepancy.

Finally, the calculated column ozone distributions are qualitatively consistent with observations, although the model seems to have underestimated the latitudinal and seasonal gradients of column ozone. In view of the several discrepancies between the calculated and observed trace gases discussed above, it is perhaps unrealistic to expect excellent agreement

between the calculated and observed column ozone. However, if the above discrepancies in the trace gases were resolved, then any remaining discrepancy in column ozone should be considered very serious.

4.3 Model Predictions of Atmospheric Lifetimes for N_2O , CFC-11 and CFC-12

As evident from observation as well as from our model results (Cf. Fig. 4-2, 4-4, 4-5, 4-6, 4-7), the spatial distribution of N_2O , CFC-11 and CFC-12 varies significantly with latitude as well as altitude. A prominent feature common to each of the three species is that higher concentrations are always found in the tropical stratosphere. This behavior is expected from the known meteorological patterns through which upward transport occurs, preferentially in tropical latitudes, followed by poleward transport within the stratosphere itself.

It is also evident that the uv solar radiation which dissociates the above gases is significantly more intense in the tropical stratosphere than in the mid-latitude stratosphere. Given the strong latitudinal variations in both the mixing ratios and the photolysis rates, it seems natural to inquire (1) whether the lifetimes predicted by current 1-D (vertical only) models are realistic, and (2) whether the 2-D model together with the field data can be used in future studies to improve the lifetime estimates?

Using our 2-D models, we calculated the atmospheric lifetimes of these gases and examined the effect of the latitudinal variations of the mixing ratios and photolysis rates. The

results have been published (Ko and Sze, 1982). A brief discussion will be given below.

The atmospheric lifetime (τ) of a trace gas that has attained a steady state concentration in the atmosphere can be defined as

$$\tau = \left\langle \frac{\text{global burden}}{\text{global removal}} \right\rangle = \left\langle \frac{\int fNdV}{\int LNfdv} \right\rangle \quad (4.2)$$

where N is the air number density, f and L are the volume mixing ratio and loss frequency of the trace gas respectively, and the bracket represents an annual average over time. Formally, a knowledge of the spatial and temporal behavior of f and L are required for calculating τ .

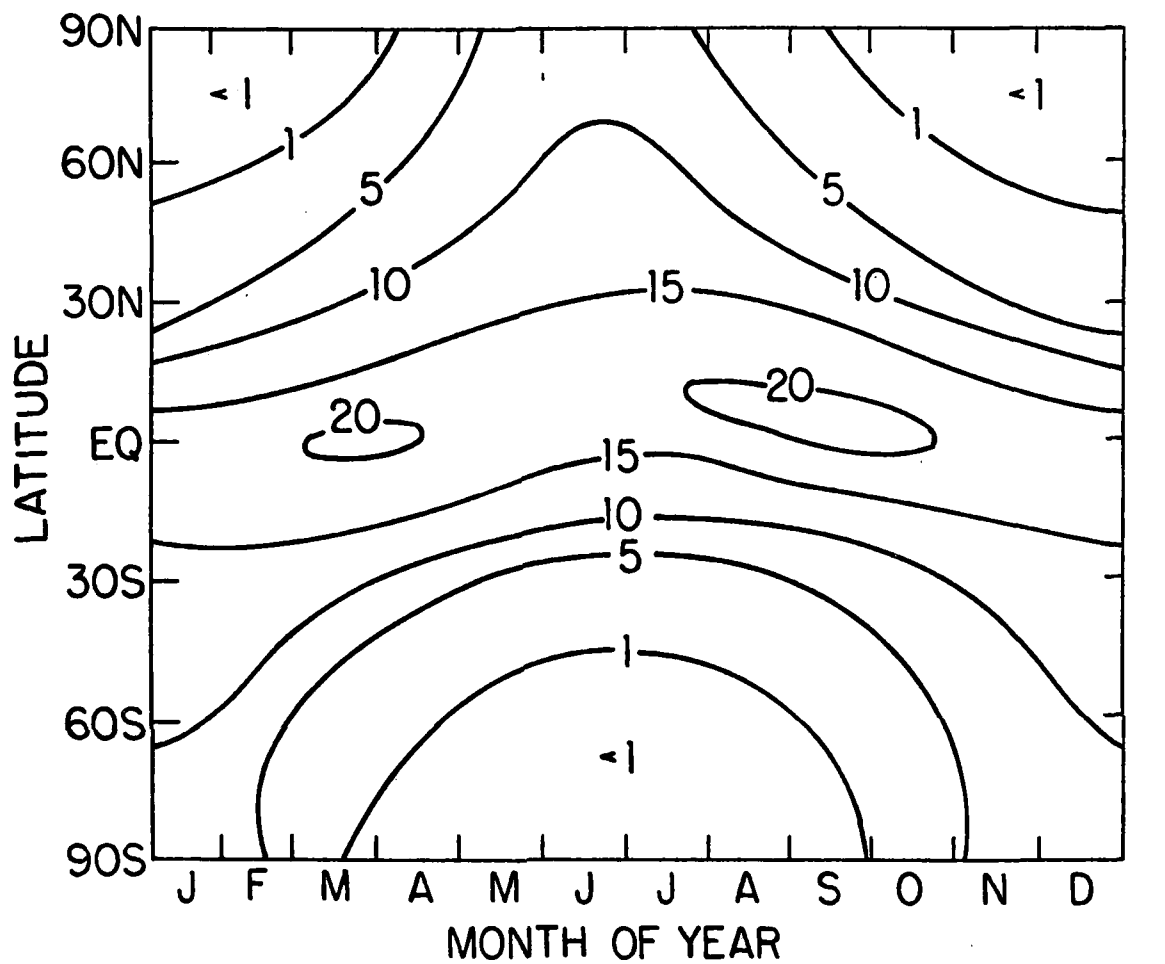
The global burden of N_2O , CFC-11 and CFC-12 may often be estimated from the observed concentrations at a few ground stations since the bulk of these gases resides in the troposphere where they are well mixed. The calculation of the global removal rate is, however, less straight forward as it involves the integral of the product of f , L and N . The major contribution to the integral arises from the stratospheric region where the quantities f , L and N vary significantly with altitudes and latitudes. A common approach is to approximate the integral (which may be interpreted as a spatial and temporal average of the product) by the product of the corresponding averaged quantities. This approach clearly ignores the correlation between the quantities f , L and N and hence its contribution to the integral. We

shall show in what follows that the global removal rate depends not only on the vertical structure of f , L and N in the stratosphere, but also on their latitudinal distributions and correlations as well.

The distribution of f calculated from the two-dimensional zonal-mean model is representative of the zonal average concentrations. If one assumes that the zonal deviation of f is small, the global removal rate can accurately be approximated by integrating the product of the zonal-mean f and zonal-mean L .

Figure 4-33 shows the calculated column removal rate of N_2O as a function of time and latitude from our 2-D model. Note the strong latitudinal gradient, a feature reflecting the important effect of the latitudinal variations in local concentration and local solar flux. During Spring and Fall seasons, the maxima occur around the equator, whereas during Summer and Winter seasons, the maxima occur about 15° above and below the equator respectively. Our calculation shows that the net contribution to the global removal rate from the covariance of f and L is positive. The annual average column removal rate for N_2O is 1.2×10^9 molecules $cm^{-2} s^{-1}$. With a calculated column abundance of 6×10^{18} molecules cm^{-2} , a lifetime of 159 years is derived. This value may be compared with values of 175 and 150 years calculated by Johnston et al. (1979) and Levy et al. (1979) respectively.

The column removal rate of CFC-12 has features very similar to that of N_2O . For CFC-11, the latitudinal gradient



N₂O COLUMN REMOVAL RATE (10⁸ MOLECULES CM⁻²S⁻¹)

Figure 4-33

Calculated N₂O column removal rate as a function of latitude and time of the year.

of the removal rate is somewhat stronger as shown in Figure 4-34. The calculated lifetimes are 65 and 135 years for CFC-11 and CFC-12 respectively. The corresponding 2-D model calculated lifetimes reported by Hinds (1979) are 81 and 102 years and those from the Oxford University models (DOE, 1979) are 78 and 133 years respectively.

The question of whether these calculated values truly represent the actual atmospheric lifetimes can be answered only following further validation of the corresponding calculated distributions using more observational data and improvement in transport and chemical data. However, we believe that the latitudinal behavior of the column removal rate simulated by the 2-D model is qualitatively correct and that the positive correlation between the latitudinal variation of f and L should not be ignored.

Our analysis points to two limitations of 1-D models in regards to their lifetime predictions. First is their inability to incorporate the covariance effects discussed here. Second, and more problematic, is the inherent difficulty in validating their lifetime predictions using field data. Our discussion points to the fact that, even for a fully validated 1-D model in which the calculated profiles are in agreement with global average observations, the model may still underestimate the global removal rate and, therefore, overestimate the lifetime because of its inability to account for the positive contribution from the covariance of f and L . With a modest increase in computer time, 2-D models, on

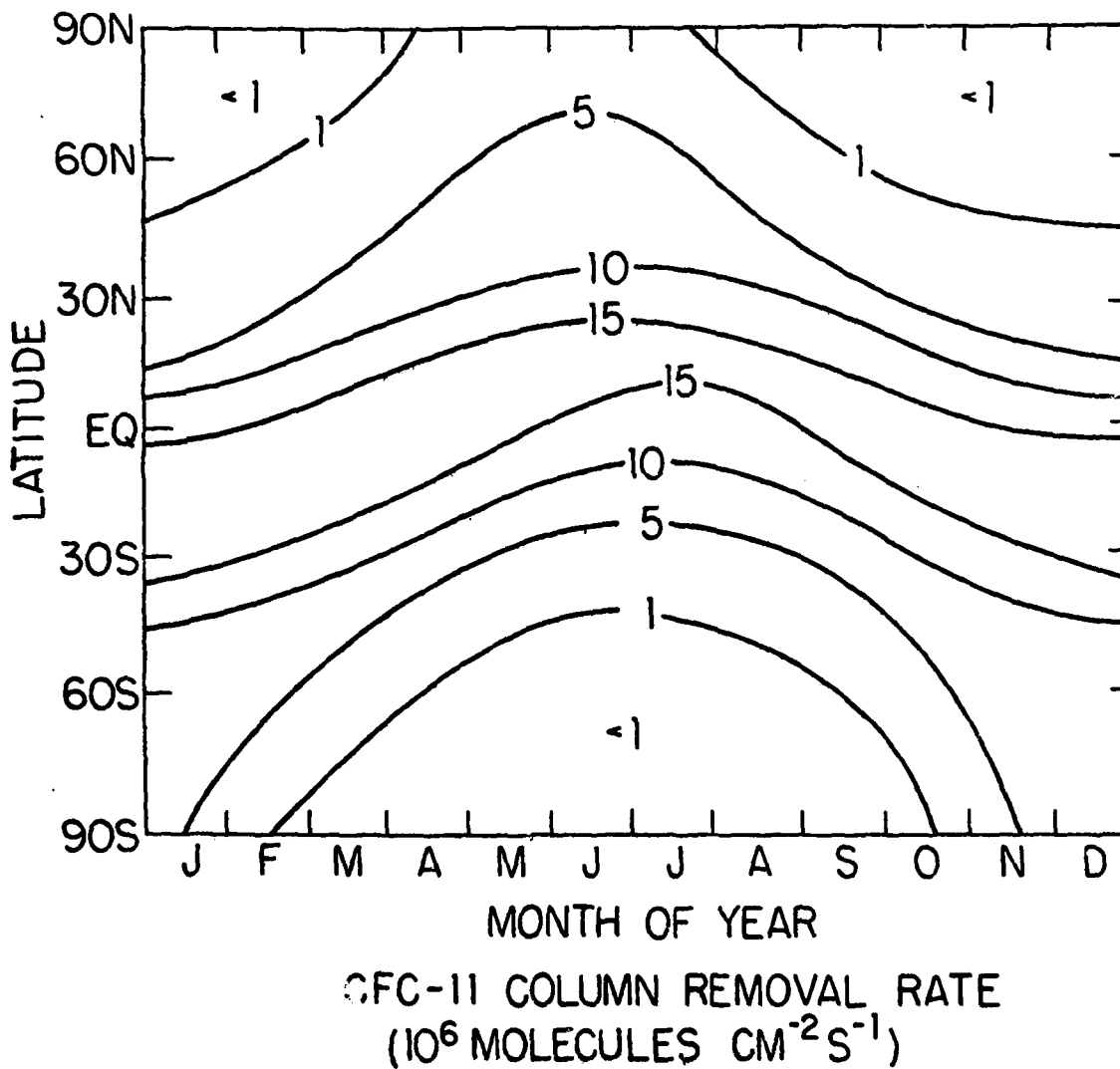


Figure 4-34

Calculated CFC-11 column removal rate as a function of latitude and time of the year. The model simulation was performed using a boundary value of p bbv at the ground.

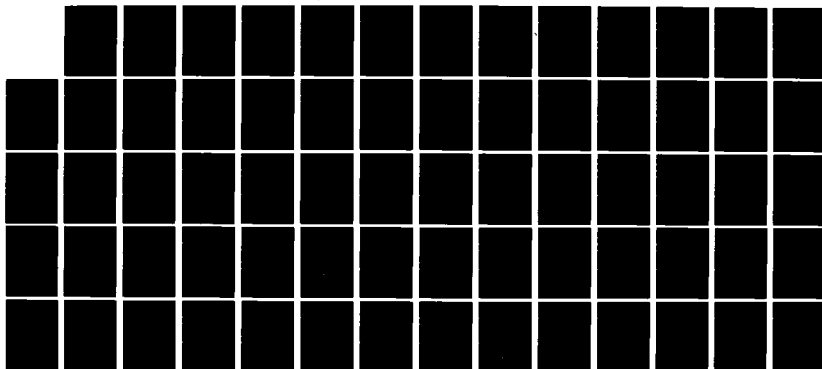
AD-A120 407

A RESEARCH PROGRAM FOR ATMOSPHERIC CHEMISTRY RADIATION
AND DYNAMICS(U) ATMOSPHERIC AND ENVIRONMENTAL RESEARCH
INC CAMBRIDGE MA N D SZE ET AL. JUL 82 AFGL-TR-82-0207
F19628-81-C-0016 F/G 7/2

2/2

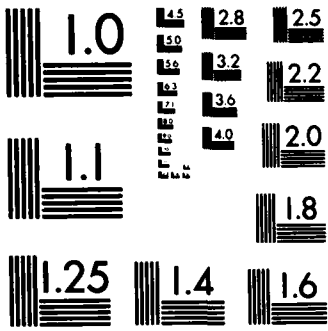
UNCLASSIFIED

NL

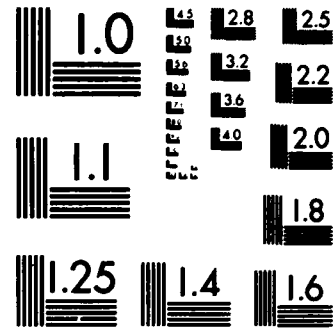


END

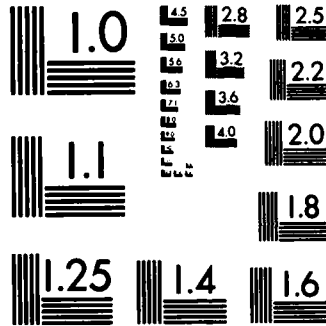
FORMED
1/1
011C



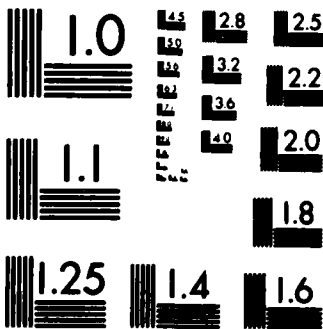
MICROCOPY RESOLUTION TEST CHART
NATIONAL BUREAU OF STANDARDS-1963-A



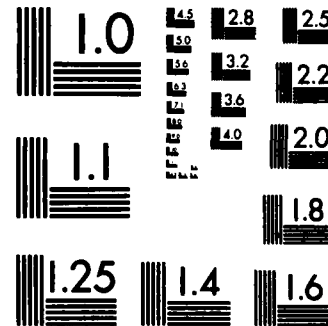
MICROCOPY RESOLUTION TEST CHART
NATIONAL BUREAU OF STANDARDS-1963-A



MICROCOPY RESOLUTION TEST CHART
NATIONAL BUREAU OF STANDARDS-1963-A



MICROCOPY RESOLUTION TEST CHART
NATIONAL BUREAU OF STANDARDS-1963-A



MICROCOPY RESOLUTION TEST CHART
NATIONAL BUREAU OF STANDARDS-1963-A

the other hand, can simulate the latitudinal and seasonal variations of atmospheric species as well as the solar insolation and may therefore be useful in refining the lifetime estimates calculated by 1-D models.

4.4 Summary of Model Developments

In addition to the features described in Appendix A, the following additional capabilities were implemented in our model during this past year.

In the previous contract year, a diurnal code was developed for the 1-D model (Sze et al., 1980) for calculating the radical species concentration. With the grouping technique, the partition of the radical species is determined by local photochemical reactions independent of transport. Thus, the same code can be adopted for the 2-D model with minor modification. The 2-D model has the capability of calculating the diurnal behavior of all the short-lived species once the concentrations of the long-lived species are specified. The results of the calculations are being prepared for publication. In addition, in the past month, we have explored ways to include diurnal effects in the O_3 equation.

The present 2-D model uses an explicit time scheme to solve the trace gas equation. To ensure numerical stability, a 4-hour time step has to be used to propagate the solutions in time. We have succeeded in devising a semi-implicit scheme using the alternative direction method. With the new scheme,

the time step can be taken to be 1 day. Further work, however, is required to apply the method to the full model.

Finally, in the past year, we have been assessing alternate methods of treating the dynamic transports in the model so as to include the coupling between radiation-dynamics and chemistry. The Eulerian formalism used in the present models required values for eddy diffusion coefficients which are parameterized from observations of the present day atmosphere. Among the recently suggested alternate methods, we found the formalism of residual circulation to be most attractive (Holten, 1981; Tung, 1982). We are at present exploring ways to test some of these alternative approaches.

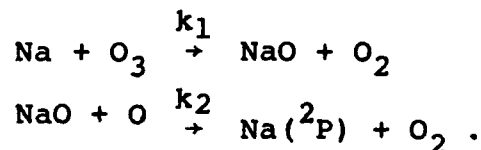
Although our 2-D model is performing to our expectations, we still feel some of these improvements will add to the capability of the model. We will be looking for alternate sources of funding for this work.

5. EFFECT OF TRACE METAL ON STRATOSPHERIC CHEMISTRY

5.1 Background

It is now believed that trace metals are introduced into the earth's atmosphere via ablation of meteors. The metal diffuses downward and is found in neutral form around and below 90 km. Meteors contain various metals including about 10% by weight each of Fe and Mg, with Na, Ca, Al and Ni each constituting about 1-2% by weight. Among the metals, Na is most studied because of the observation of the Na layer around 90 km as deduced from spectroscopic (Cf. see Hunten, 1967) and laser radar measurements (Sanford and Gibson, 1970; Blamont et al., 1972; Megie and Blamont, 1977, Simonich et al., 1979).

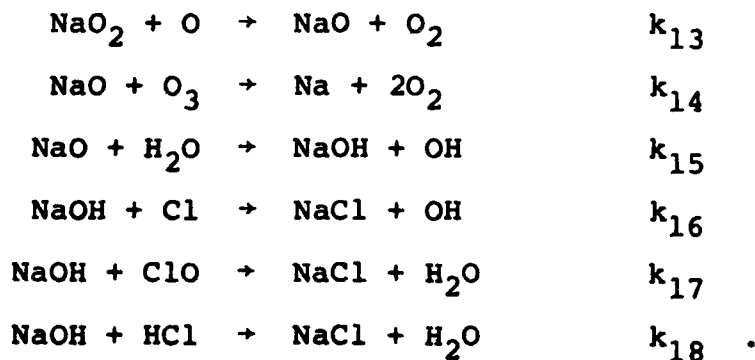
The basic sequence of reactions responsible for maintaining the neutral sodium concentration was first suggested by Chapman (1939) to be



However, since there is no laboratory measurement of the kinetic reaction rates, it can only be demonstrated that with reasonable assumed rates for k_1 and k_2 and observed O and O_3 concentrations, one can deduce distributions for Na that are consistent with observations.

Recently, Ferguson (1978) argued that the mass spectro-metric measurement of positive ions in the stratosphere (Arnold et al., 1977, 1978) can be interpreted as NaOH clusters. Furthermore, he estimated the NaOH concentrations to be $\sim 10^5 \text{ cm}^{-3}$ at 40 km. The modeling work of Liu and Reid (1979) was one of the more recent studies that extended the calculation of the sodium species down to the stratosphere. Using the reaction scheme summarized in Table 5-1, they succeeded in simulating the neutral sodium layer at 90 km with a concentration of $3 \times 10^3 \text{ cm}^{-3}$ and found NaOH to be the most abundant sodium species below 80 km. In addition, the NaOH concentration at 40 km is calculated to be $\sim 3 \times 10^5 \text{ cm}^{-3}$, in agreement with Ferguson's estimates.

Murad and Swider (1979) re-examined the thermodynamic data on the sodium species and pointed out the following reactions are estimated to be exothermic and therefore might have to be considered in the sodium chemistry scheme.



In addition, the reaction of NaOH with HNO_3 and CO_2 ,

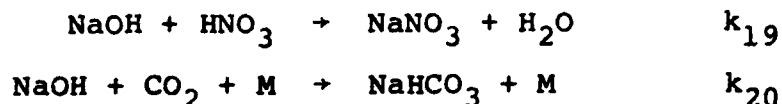
Table 5-1

Reactions		Rate Constants (a)
K ₁	Na + O ₃ → NaO + O ₂	3.3 × 10 ⁻¹⁰ (b)
K ₂	NaO + O → Na + O ₂	1.6 × 10 ⁻¹⁰ (b)
K ₃	Na + O ₂ + M → NaO ₂ + M	8.4 × 10 ⁻³⁴ exp($\frac{290}{T}$) (c)
K ₄	NaO + O ₃ → NaO ₂ + O ₂	5 × 10 ⁻¹¹
K ₅	NaO + HO ₂ → NaOH + O ₂	1 × 10 ⁻¹¹
K ₆	NaO ₂ + H → NaOH + O	7 × 10 ⁻¹²
K ₇	NaO ₂ + OH → NaOH + O ₂	1 × 10 ⁻¹¹
K _{8a}	Na + HO ₂ → NaOH + O	7 × 10 ⁻¹²
K _{8b}	Na + HO ₂ → NaH + O ₂	1 × 10 ⁻¹¹
K _{8c}	Na + HO ₂ → NaO + OH	8 × 10 ⁻¹²
K ₉	NaOH + hν → Na + OH	same as photolysis of water
K ₁₀	NaOH + O(¹ D) → NaO + OH	2.3 × 10 ⁻¹⁰
K ₁₂	NaOH + H → Na + H ₂ O	2 × 10 ⁻¹¹ exp($-\frac{800}{T}$)

(a) Units are cm³ s⁻¹ for two-body reactions and cm⁶ s⁻¹ for three-body reactions. All rates are assumed except as noted below.

(b) Estimated by Kolb and Elgin (1976).

(c) Estimated using high T measurement of Carabetta and Kashan (1968).



could conceivably be important, although there is a lack of data for NaNO_3 and NaHCO_3 to estimate the energetics for the reactions.

Of the reactions suggested, reactions 16 through 20 are of particular interest if NaOH is the dominant sodium species in the stratosphere. In a subsequent paper, Murad et al. (1981) argued that other metals from meteors may proceed via analogous reactions to combine with chlorine species to form metal chlorides which may then be incorporated in aerosols and removed via depositions. It was further suggested that high flying aircrafts may be another source of trace metals through combustion of jet fuel and engine erosion. Our study reported here was initiated to assess the impact of the reaction of the trace metals as a sink for chlorine species in the stratosphere with particular attention to the possible influence on the chlorine-catalyzed destruction of O_3 .

5.2 Model Study

We first used our 1-D model to estimate the steady state concentrations of total metal in the atmosphere. The trace metals are either injected at the mesopause to simulate downward diffusion of meteoric metal from the mesosphere or injected in the lower stratosphere to simulate aircraft emission.

In all cases, a tropospheric sink with a lifetime of 10 days is used to simulate rainout and deposition.

Figure 5-1 shows the calculated total metal concentrations as a function of altitude for several cases with different injection parameters:

- (i) top injection of 2×10^6 metal molecules $\text{cm}^{-2} \text{s}^{-1}$ (2×10^4 ton/yr) at 71 km to simulate the effect of ablation from meteor (curve marked Mx)
- (ii) injection of 2×10^3 ton/yr of metal spread uniformly over a 1 km thick band at 16 km and 20 km respectively to simulate effect of aircraft engine emissions for different modes of operation (curve marked I_{16} and I_{20})

Studies (CIAP, 1975a,b) indicated that the emissions of metals from engine erosion is much higher than those associated with fuel combustion. The metal content in jet fuel is estimated to be in the ppb level while metals component of exhaust from engine erosion could be in the ppm level. Using the CIAP reported estimate of 3×10^9 ton/yr for the total exhaust associated with aircraft operations, we arrived at the value of 2×10^3 ton/yr by assuming that the exhaust contains ~ 1 ppm of metal.

The value of $2 \times 10^6 \text{ cm}^{-2} \text{ s}^{-1}$ for meteoric input is based on Gadsden's (1976) estimate of 9×10^4 ton/yr for total meteor flux and that about 20% of the meteor flux is ablated to produce metal atoms. The estimates for total meteoric flux range from 10^2 to 10^7 tons/yr (Hughes, 1972)

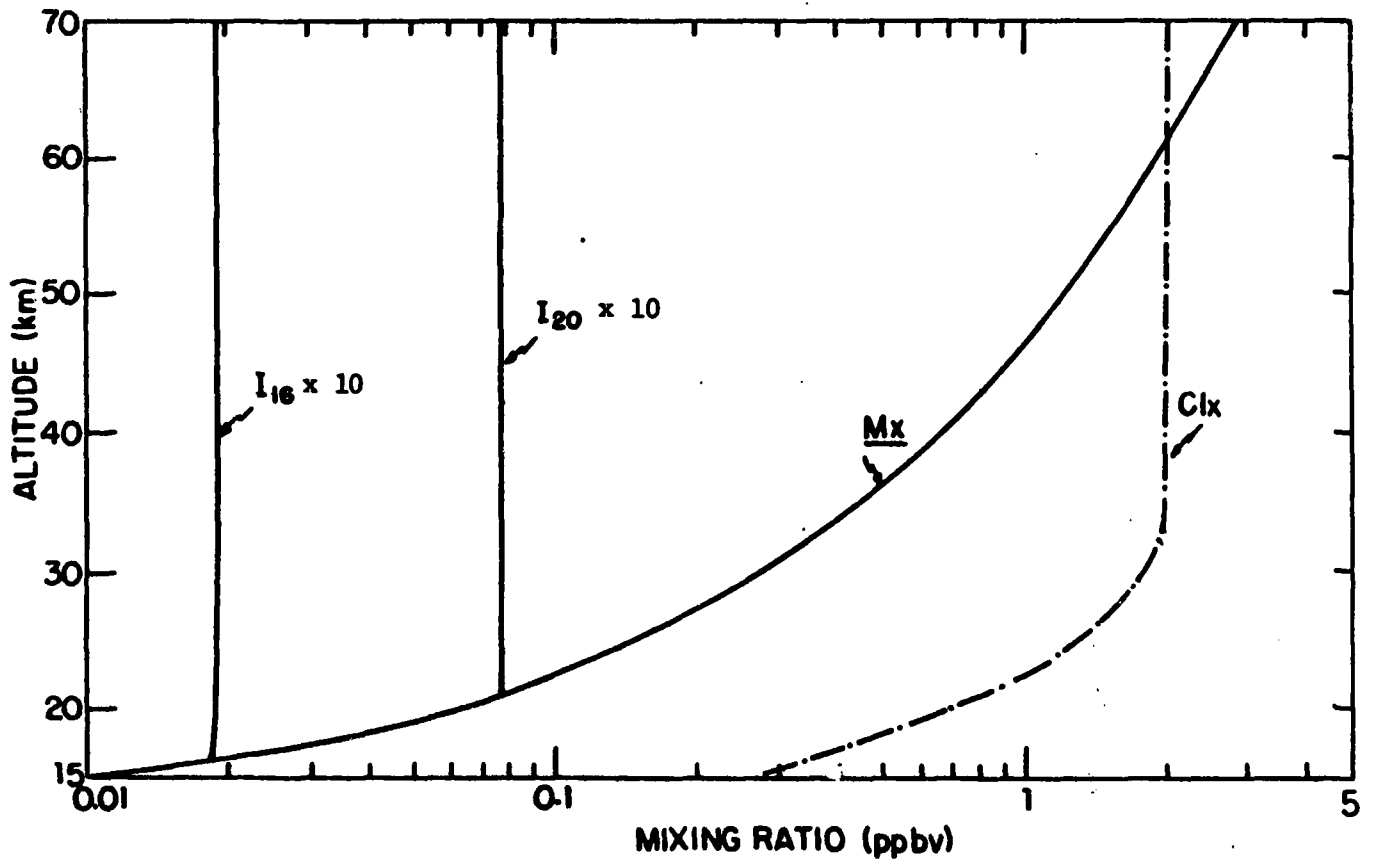


Figure 5-1

Calculated total metal profiles for different injection rates. See text for injection parameters. The Cl_x profile is included for comparison.

although values of order 10^4 ton/yr are most often used. It should be noted that the value of $2 \times 10^6 \text{ cm}^{-2} \text{ s}^{-1}$ is about a factor of 10^2 larger than the values of Na-flux used by Liu and Reid (1979). Given the fact that about a few percent of the metal flux is in the form of Na, our assumed input rate seems reasonable. We will now restrict our discussion to meteor input case since the total metal concentration resulting from aircraft emissions are much smaller.

In this study, following Murad et al. (1981), we assumed that once the metal chloride (MCl) is formed, it will be removed via heterogeneous processes and that there is no pathway to recycle MCl back to free metal and chlorine. The calculated total chlorine (ClX) in the present day atmosphere is also plotted in Figure 5-1. In the case of no recycling, each metal atom can only react with the chlorine species once. Since there is a comparable amount of ClX and MX above 50 km, most of the ClX can be converted to MCl if the reaction is sufficiently fast. In contrast, the MX concentration is about 1/3 of the ClX concentration around 40 km. The reaction between metal and chlorine species can at most reduce the free chlorine concentration by 1/3 even if conversion is complete.

The amount of free metal ($MY \equiv MX - MCl$) in the atmosphere will clearly depend on whether the rate of conversion is slow enough for the free metal to diffuse downward. Since HCl is the most abundant chlorine species, the conversion

rate for MX to MCl can be estimated using the reaction

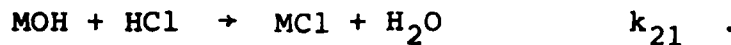


Figure 5-2 shows the mixing ratio for MY for different assumed rates of k_{21} . Murad et al. (1981) estimated that reaction 21 can proceed as fast as $10^{-9} \text{ cm}^3 \text{ s}^{-1}$. Thus, there should be very little free metal in the atmosphere.

Figure 5-3 shows the distribution of the chlorine species for the case with $k_{21} = 10^{-11} \text{ cm}^3 \text{ s}^{-1}$. Note that although the free chlorine concentration is reduced significantly above 50 km, there is little impact below 40 km because of lack of metal atoms. The chlorine catalytic destruction of ozone is most effective around 35 km. Thus, the overall impact of metal on the chlorine-ozone cycle is small unless we have grossly underestimated the amount of metal in the stratosphere.

5.3 Recent Developments

Since our study, there have been several new reports on the kinetic data on several of the reactions. Recent work by Husain and Plain (1982) indicates a rate of $10^{-30} \text{ cm}^6 \text{ s}^{-1}$ for k_3 . Most recently, Rowland and Makide (1982) found NaOH absorbs strongly in the ultraviolet region and has a photolysis rate of about a factor of 10^3 faster than those assumed in Table 5-1. With these new data, NaO_2

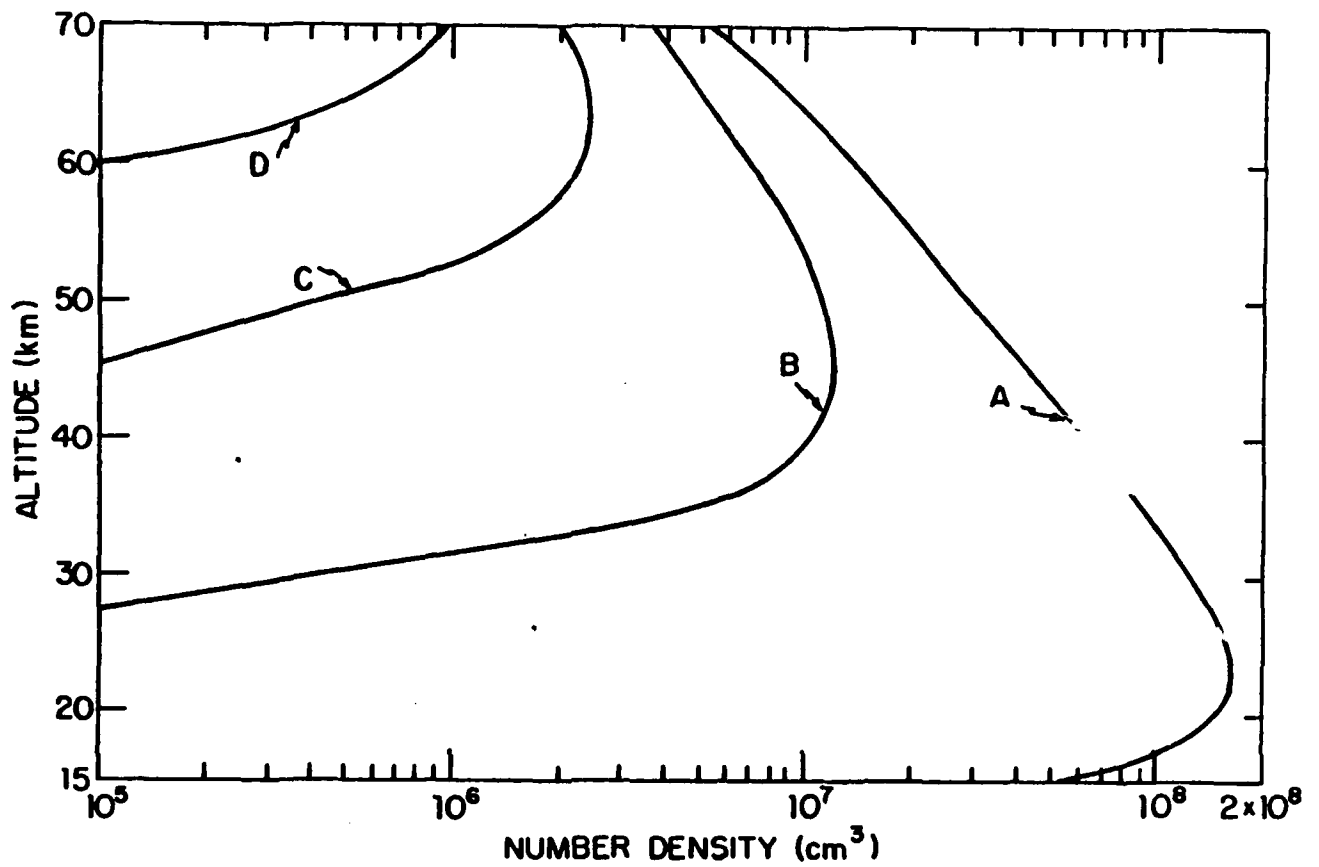


Figure 5-2

Calculated mixing ratio profiles for free metal
($MY = MX - MCl$) for different assumed values of
reaction rate k_{21} .

Case A: $k_{21} = 0$
 Case B: $k_{21} = 10^{-15} \text{ cm}^3 \text{ s}^{-1}$
 Case C: $k_{21} = 10^{-13} \text{ cm}^3 \text{ s}^{-1}$
 Case D: $k_{21} = 10^{-11} \text{ cm}^3 \text{ s}^{-1}$

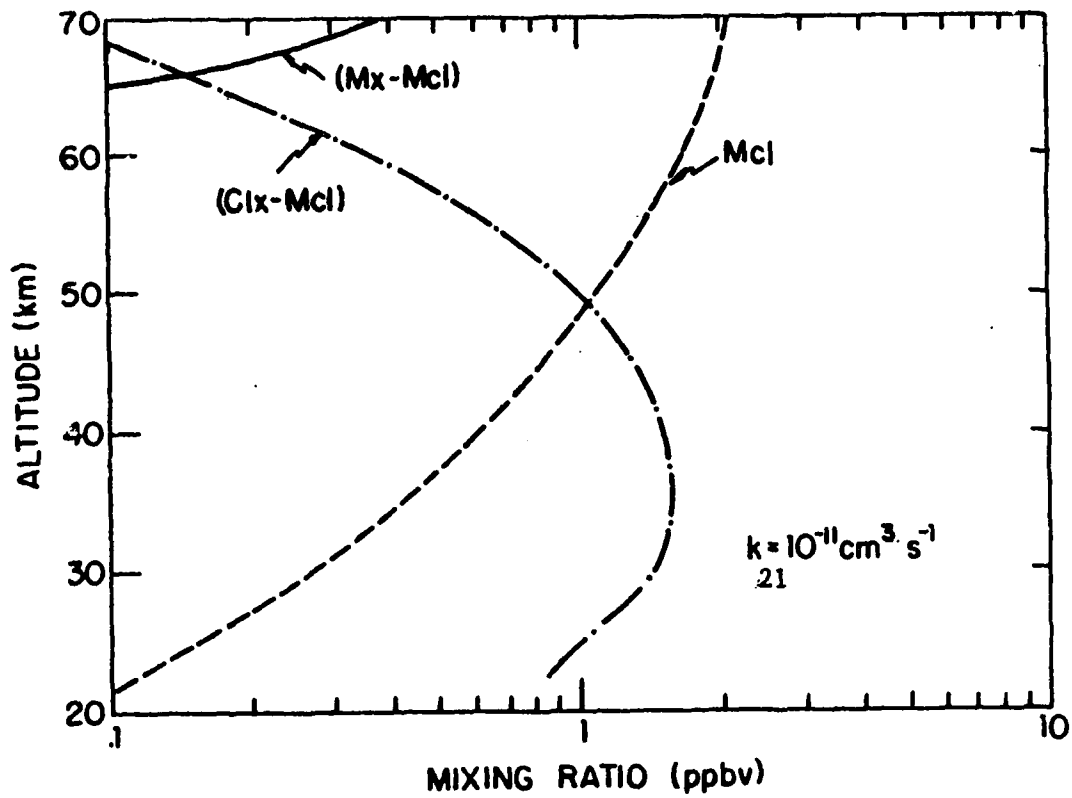


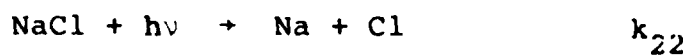
Figure 5-3

Calculated mixing ratio profiles for various metal and chlorine species when $k_{21} = 10^{-11} \text{ cm}^3 \text{ s}^{-1}$.

became the dominant species below 80 km with NaOH playing a secondary role.

With regard to the positive ion clusters data, Arnold and Henschen (1981) reported that they failed to detect any Na^+ thus negating Ferguson's (1978) estimates of NaOH concentration.

Another recent development concerns the atmospheric fate of NaCl. Recent work by Rowland and Rogers (1982) indicates that NaCl photolyzes rapidly and has stratospheric lifetimes of about a few minutes. Reaction k_{18} followed by photolysis



is equivalent to



and may lead to a potential catalytic pathway for converting HCl to Cl. Once the catalytic cycle is introduced, the impact of metal is no longer limited by its concentrations. It seems prudent to re-examine the role of metal chemistry in regard to other chemical cycles in view of the new reports on kinetic data.

REFERENCES

- Ackerman, M. and C. Muller (1973) Stratospheric Methane and Nitrogen Dioxide from Infrared Spectra. Pure Appl. Geophys., 106-108, 1325-1335.
- Ackerman, M., J.C. Fontanella, D. Frimout, A. Girard, N. Louisnard and C. Muller (1975) Simultaneous Measurements of NO and NO₂ in the Stratosphere. Planet. Space Sci., 23, 651-660.
- Ackerman, M., D. Frimout, A. Girard, M. Gottingnier and C. Muller (1976) Stratospheric HCl from Infrared Spectra. Geophys. Res. Lett., 3, 81-83.
- Anderson, J.G. (1975) The Absolute Concentration of O(³P) in the Earth's Stratosphere. Geophys. Res. Lett., 2, 321-328.
- Anderson, J.G. (1976) The Absolute Concentration of OH(X²) in the Earth's Stratosphere. Geophys. Res. Lett., 3, 165-168.
- Anderson, J.G. (1980) Free Radicals in the Earth's Stratosphere: A Review of Recent Results. Proceedings of NATO Advanced Study Institute of Atmospheric Ozone: Its Variations and Human Influences. A.C. Aiken (ed.).
- Anderson, J.G., J.J. Margitan and D.H. Stedman (1977) Atomic Chlorine and the Chlorine Monoxide Radical in the Stratosphere: Three in situ Observations. Science, 198, 501-503.
- Anderson, J.G., H.J. Grassl, R.E. Shetter and J.J. Margitan (1980) Stratospheric Free Chlorine Measured by Balloon-Borne in situ Resonance Fluorescence. J. Geophys. Res., 85, 2869-2887.
- Anderson, J.G., H.J. Grassl, R.E. Shetter and J.J. Margitan (1981) HO₂ in the Stratosphere: Three in situ Observations. Geophys. Res. Lett., 8, 289.
- Arnold, F., H. Boehringer and G. Henschen (1978) Composition Measurements of Stratospheric Positive Ions. Geophys. Res. Lett., 5, 653-656.
- Arnold, F., R. Fabian, G. Henschen and W. Joos (1980) Stratospheric Trace Gas Analysis from Ions: H₂O and HNO₃. Planet. Space Sci., 28, 681-685.

- Arnold, F. and G. Henschen (1982) Positive Ion Composition Measurements in the Upper Stratosphere - Evidence for an Unknown Aerosol Component. Planet. Space Sci., 30, 101-108.
- Arnold, F., D. Krankosky and K.H. Marien (1977) First Mass Spectrometric Measurements of Positive ions in the Stratosphere. Nature, 267, 30-32.
- Blatherwick, R.D., A. Goldman, D.G. Murcray, F.J. Murcray, G.R. Cook and J.W. Van Allen (1980) Simultaneous Mixing Ratio Profiles of Stratospheric NO and NO₂ as Derived from Balloon-Borne Infrared Solar Spectra. Geophys. Res. Lett., 7, 471-473.
- Blamont, J.E., M.L. Chanin and G. Megie (1972) Vertical Distribution and Temperature Profile of the Night Time Atmospheric Sodium Layer Obtained by Laser Back Scatter. Ann. Geophys., 28, 833-838.
- Boughner, R.E. (1978) The Effects of Increased Carbon Dioxide Concentrations on Stratospheric Ozone. J. Geophys. Res., 83, 1326.
- Buijs, H.L., G.L. Vail, G. Tremblay and D.J.W. Kendall (1980) Simultaneous Measurement of the Volume Mixing Ratios of HCl and HF in the Stratosphere. Geophys. Res. Lett., 7, 205-208.
- Bush, Y.A., A.L. Schmeltekopf, F.C. Fehsenfeld, D.L. Albritton, J.R. McAfee, P.D. Goldan and E.E. Ferguson (1978) Stratospheric Measurements of Methane at Several Latitudes. Geophys. Res. Lett., 5, 1027-1029.
- CEQ (1981) Global Energy Futures and the Carbon Dioxide Problem. Council on Environmental Quality. Executive Office of the President. Washington, DC.
- Chance, K.V., J.C. Brasunas and W.A. Traub (1980) Far Infrared Measurement of Stratospheric HCl. Geophys. Res. Lett., 7, 704-706.
- Chapman, S. (1930) Notes on Atmospheric Sodium. Ap. J., 90, 309-316.
- Chemical Manufacturers Association (1980) World Production and Release of Chlorofluorocarbon 11 and 12 Through 1979.
- CIAP (1975a) Propulsion Effluents in the Stratosphere. CIAP Monogr. 2, DOT-TST-75-52.
- CIAP (1975b) The Stratosphere Perturbed by Propulsion Effluents. CIAP Monogr. 3, DOT-TST-75-53.

- Clarke, R.H. (1970) Recommended Methods for the Treatment of the Boundary Layer in Numerical Models. Am. Met. Mag., 18, 51-71.
- Coffey, M.T., W.G. Mankin and A. Goldman (1981) Simultaneous Spectroscopic Determination of the Latitudinal, Seasonal and Diurnal Variability of Stratospheric N₂O, NO, NO₂ and HNO₃. J. Geophys. Res., 86, 7331.
- Department of the Environment (1979) Chlorofluorocarbons and Their Effect on Stratospheric Ozone. U.K. Department of the Environment, Paper #5.
- Dunkerton, T. (1978) On the Mean Meridional Mass Motions of the Stratosphere and Mesosphere. J. Atmos. Sci., 35, 2325.
- Dütsch, H.U. (1971) Photochemistry of Atmospheric Ozone. Adv. in Geophys., 15, 219.
- Dütsch, H.U. (1978) Vertical Ozone Distribution on a Global Scale. Pure Appl. Geophys., 116, 514.
- Ehhalt, D.H. (1978) In situ Measurements of Stratospheric Trace Constituents. Rev. Geophys. Space Phys., 16, 217-224.
- Ehhalt, D.H., L.E. Heidt, R.H. Lueb and W. Pollock (1975) Vertical Distribution of Trace Gases in the Stratosphere. Pure Appl. Geophys., 113, 389-402.
- Evans, W.F.J., H. Fast, J.B. Kerr, C.T. McElroy, R.S. O'Brien, D.I. Wardle, J.C. McConnell and B.A. Ridley (1978) Stratospheric Constituent Measurements from Project Stratosphere. Proceedings WMO Symposium on the Geophysical Aspects and Consequences of Change in the Composition of the Stratosphere. WMO Publ. 511, World Meteorological Organization, Toronto, June.
- Eyre, J.R. and H.K. Roscoe (1977) Radiometric Measurement of Stratospheric HCl. Nature, 266, 243-244.
- Fabian, P., R. Borchers, K.H. Weiler, U. Schmidt, A. Volz, D.H. Ehhalt, W. Seiler, F. Muller (1979) Simultaneously Measured Vertical Profiles of H₂, CH₄, CO, N₂O, CFC1₃, and CF₂Cl₂ in the Mid-Latitude of Stratosphere and Troposphere. J. Geophys. Res., 84, 3149-3154.
- Farmer, C.B., O.F. Raper and R.H. Norton (1976) Spectroscopic Detection and Vertical Distribution of HCl in the Troposphere and Stratosphere. Geophys. Res. Lett., 3, 13-16.

- Farmer, C.B., O.F. Raper, B.D. Robbins, R.A. Toth and C. Muller (1980) Simultaneous Spectroscopic Measurements of Stratospheric Species: O_3 , CH_4 , CO , CO_2 , N_2O , H_2O , HCl and HF at Northern and Southern Mid-Latitudes. J. Geophys. Res., 85, 1621-1632.
- Ferguson, E.E. (1978) Sodium Hydroxide Ions in the Stratosphere. Geophys. Res. Lett., 5, 1035-1038.
- Fontanella, J.-C., A. Girard, L. Gramont and N. Louisnard (1975) Vertical Distribution of NO , NO_2 and HNO_3 as Derived from Stratospheric Absorption Infrared Spectra. Appl. Optics, 14, 825-839.
- Gadsden, M. (1970) Ann. Geophys., 26, 141-150.
- Goldan, P.D., W.C. Kuster, D.L. Albritton and A.L. Schmeltekopf (1980) Stratospheric $CFCl_3$, CF_2Cl_2 and N_2O Height-Profile Measurements at Several Latitudes. J. Geophys. Res., 85, 413-423.
- Goldan, P.D., W.C. Kuster, A.L. Schmeltekopf, F.C. Fehsenfeld and D.L. Albritton (1981) Correction of Atmospheric N_2O Mixing Ratio Data. J. Geophys. Res., 86, 5385.
- Goldman, A., F.G. Fernald, W.J. Williams and D.G. Murcray (1978) Vertical Distribution of NO_2 in the Stratosphere as Determined from Balloon Measurements of Solar Spectra in the 4500 Å Region. Geophys. Res. Lett., 5, 257-260.
- Groves, K.S., S.R. Mattingly and A.F. Tuck (1978) Increased Atmospheric Carbon Dioxide and Atmospheric Ozone. Nature, 273, 711.
- Harries, J.E., D.G. Moss, N.R.W. Swann, G.F. Neill and P. Gildward (1976) Simultaneous Measurements of H_2O , NO_2 and HNO_3 in the Daytime Stratosphere from 15 to 35 km. Nature, 259, 300-301.
- Harwood, R.S. and J.A. Pyle (1975) A Two-Dimensional Mean Circulation Model for the Atmosphere Below 80 km. Quart. J. Roy. Meteorol. Soc., 101, 723.
- Harwood, R.S. and J.A. Pyle (1977) Studies of the Ozone Budget Using a Zonal Mean Circulation Model and Linearized Photochemistry. Quart. J. Roy. Meteorol. Soc., 103, 219-343.
- Harwood, R.S. and J.A. Pyle (1980) The Dynamical Behavior of a Two-Dimensional Model of the Stratosphere. Quart. J. Roy. Meteorol. Soc., 106, 395-420.
- Heidt, L.E., R. Lueb, N. Pollack and D.H. Ehhalt (1975) Stratospheric Profiles of $CFCl_3$, CF_2Cl_2 . Geophys. Res. Lett., 6, 191.

- Heidt, L.E. and J.P. Krasnec (1978) Tropospheric Distributions of CO, CH₄, CO₂ and N₂O in the Northern and Southern Hemispheres (abstract), EOS, Trans. AGU, 59, 1077.
- Hinds, M.K. (1979) Studies of Residence Times of Chlorofluorocarbons Using a Two-Dimensional Model. Met. Mag., 108, 221-240.
- Holton, J.R. (1975) The Dynamic Meteorology of the Stratosphere and Mesosphere. Meteor. Monogr., 37, 216.
- Holton, J.R. (1981) An Advective Model for Two-Dimensional Transport of Stratospheric Trace Species. J. Geophys. Res., 86, 11989.
- Horvath, J.J. and C.J. Mason (1978) Nitric Oxide Mixing Ratios near the Stratosphere Measured by a Rocket-Borne Chemiluminescent Detector. Geophys. Res. Lett., 5, 1023-1026.
- Hughes, D.W. (1972) Planet. Space Sci., 20, 1949-1959.
- Hunten, D.M. (1967) Spectroscopic Studies of the Twilight Airglow. Space Sci. Rev., 6, 493-576.
- Husain, D. and J.M.C. Plain (1982) Kinetic Investigation of the Reaction between Na + O₂ + M by Time-Resolved Atomic Resonance Absorption Spectroscopy. J. Chem. Soc. Faraday Trans. 2, 78, 163-178.
- ISE Publ. 81-3. Chemical Kinetic and Photochemical Data for Use in Stratospheric Modelling. NASA Panel for Data Evaluation, 1981.
- Johnston, H.S. and J. Podolski (1978) Interpretation of Stratospheric Photochemistry. Rev. Geophys. Space Phys., 15, 491-519.
- Johnston, H.S., O. Serange and J. Podolski (1979) Instantaneous Global Nitrous Oxide Photochemical Rates. J. Geophys. Res., 84, 5077-5082.
- Keeling, C.D., R.B. Bacastow, A.E. Bainbridge, C.A. Ekdahl, Jr., P.R. Guenther and L.S. Waterman (1976a) Atmospheric Carbon Dioxide Variations at Mauna Loa Observatory, Hawaii. Tellus, 28, 538.
- Keeling, C.D., J.A. Addams, Jr., C.A. Ekdahl, Jr. and P.R. Guenther (1976b) Atmospheric Carbon Dioxide Variations at the South Pole. Tellus, 28, 552.
- Kennedy, J.S. (1964) Energy Equation through Radiative Processes in the Lower Stratosphere. MIT Report No. 11, December 1964.

- Kerr, J.B. and C.T. McElroy (1976) Measurement of Stratospheric Nitrogen Dioxide from the AES Stratospheric Balloon Program. Atmosphere, 14, 166-171.
- Ko, M.K.W., M. Livshits and N.D. Sze (1980) Atmospheric Ozone: Comparison of Observations with One- and Two-Dimensional Model Calculations. Quadrennial International Ozone Symposium, Boulder, CO.
- Ko, M.K.W. and N.D. Sze (1982) A 2-D Model Calculation of Atmospheric Lifetimes for N_2O , FCF-11 and CFC-12. Nature, 297, 317-319.
- Lazarus, A.L. and B.W. Gandrud (1974) Distribution of Stratospheric Nitric Acid Vapor. J. Atmos. Sci., 31, 1102-1108.
- Lazarus, A.L., B.W. Gandrud, J. Greenberg, J. Bonelli, E. Mroz and W.H. Sedlacek (1977) Mid-Latitude Seasonal Measurement of Stratospheric Chlorine Vapour. Geophys. Res. Lett., 4, 587.
- Levy, H., J.D. Mahlman and W.J. Moxim (1979) A Preliminary Report on the Numerical Simulation of the Three-Dimensional Structures and Variability of Atmospheric N_2O . Geophys. Res. Lett., 6, 155-158.
- Liu, S.C. and G.C. Reid (1979) Sodium and Other Minor Constituents of Meteoric Origin in the Atmosphere. Geophys. Res. Lett., 6, 283-286.
- Logan, J.A., M.J. Prather, S.C. Wofsy and M.B. McElroy (1978) Atmospheric Chemistry: Response to Human Influence. Phil. Trans. Roy. Soc., 290, 187.
- Lorentz, E.N. (1967) The Nature and Theory of the General Circulation of the Atmosphere. World Meteorological Organization, Geneva.
- Loewenstein, M. and H. Savage (1975) Latitudinal Measurements of NO and O_3 in the Lower Stratosphere from 5° to 82° North. Geophys. Res. Lett., 2, 448-450.
- Loewenstein, M., H.F. Savage and R.C. Whitten (1975) Seasonal Variation of NO and O_3 at Altitudes of 18.3 and 21.3 km. J. Atmos. Sci., 32, 2185-2190.
- Loewenstein, M., W.L. Starr and D.G. Murcay (1978a) Stratospheric NO and HNO_3 Observations in the Northern Hemisphere for Three Seasons. Geophys. Res. Lett., 5, 531-534.
- Loewenstein, M., W.J. Borucki, H.F. Savage, J.G. Borucki and R.C. Whitten (1978b) Geographical Variations of NO and O_3 in the Lower Stratosphere. J. Geophys. Res., 83, 1875-1882.

- Luther, F.M. (1973) Monthly Mean Values of Eddy Diffusion Coefficients in the Lower Stratosphere. AIAA paper 73-498, AIAA/AMS Conference, Denver, CO.
- Luther, F.M., D.J. Wuebbles and J.S. Chang (1977) Temperature Feedback in a Stratospheric Model. J. Geophys. Res., 82, 4935-4942.
- Marche, P., A. Barbe, C. Secroun, J. Corr and P. Jouve (1980) Ground Based Spectroscopic Measurements of HCl. Geophys. Res. Lett., 11, 869-872.
- Mason, C.J. and J.J. Horvath (1976) The Direct Measurement of Nitric Oxide Concentration in the Upper Atmosphere by a Rocket-Borne Chemiluminescent Detector. Geophys. Res. Lett., 3, 391-394.
- McConnell, J.C. and W.F.J. Evans (1978) Implications of Low Stratospheric Hydroxyl Concentrations for CFM and SST Scenario Calculations of Ozone Depletion. EOS Trans. AGU, 59.
- Megie, G. and J.E. Blamont (1977) Laser Sounding of Atmospheric Sodium, Interpretation in Terms of Global Atmospheric Parameters. Planet. Space Sci., 25, 1093-1109.
- Mihelcic, D., D.H. Ehhalt, G.F. Kulesa, J. Klomfass, M. Trainer, U. Schmidt and H. Rohrs (1978) Measurement of Free Radicals in the Atmosphere by Matrix Isolation and Electron Paramagnetic Resonance. Appl. Geophys., 116, 530.
- Miller, C., D.L. Filkin, A.J. Owens, J.M. Steed and J.P. Jesson (1981) A Two-Dimensional Model of Stratospheric Chemistry and Transport. J. Geophys. Res., 86, 12039.
- Murad, E., W. Swider and S.W. Benson (1981) Possible Role for Metals in Stratospheric Chlorine Chemistry. Nature, 289, 273-274.
- Murad, E. and W. Swider (1979) Chemistry of Meteor Metals in the Stratosphere. Geophys. Res. Lett., 6, 929-932.
- Murcray, D.G., A. Goldman, W.J. Williams, F.H. Murcray, J.N. Brooks, J. Van Allen, R.N. Stocker, J.J. Kusters, D.B. Barker and D.E. Snider (1974) Recent Results of Stratospheric Trace-Gas Measurements from Balloon-Borne Spectrometers. Proceedings of Third CIAP Conference DOT-TSC-OST-74-15, 184-192. U.S. Dept. of Transportation, Washington, DC.

- Murcray, D.G., A. Goldman, F.H. Murcray, F.T. Murcray and W.J. Williams (1979) Stratospheric Distribution of ClONO_2 . Geophys. Res. Lett., 6, 857-859.
- Murgatroyd, R.J. and F. Singleton (1961) Possible Meridional Circulations in the Stratosphere and Mesosphere. Wuart. J. Roy. Meteorol. Soc., 87, 125.
- NASA (1979) The Stratosphere: Present and Future. R.D. Hudson and E.I. Reed (eds.) NASA Ref. Publ. 1049. NASA Goddard Space Flight Center.
- Newell, R.A., T.M. Wallace and T.R. Mahaney (1966) The General Circulation of the Atmosphere and Its Effect on the Movement of Trace Substances, II. Tellus, 18, 363.
- Noxon, J.F. (1979) Stratospheric NO_2 , 2, Global Behavior. J. Geophys. Res., 84, 5067-5076.
- Oort, A.H. and E.M. Rasmussen (1971) Atmospheric Circulation Statistics. NOAA Prof. Paper #5. U.S. Government Printing Office. National Oceanic and Atmospheric Administration.
- Parrish, A., R.L. deZafra, P.M. Solomon, J.W. Barrett and B.R. Carlson (1981) Chlorine Oxide in the Stratospheric Ozone Layer: Ground-Based Detection and Measurement. Science, 211, 1158.
- Patel, C.K.N., E.G. Burkhardt and C.A. Lambert (1974) Spectroscopic Measurements of Stratospheric Nitric Oxide and Water Vapor. Science, 184, 1173-1176.
- Penkett, S.A., R.G. Derwent, P. Fabian, R. Borchers and U. Schmidt (1980) Methyl Chloride in the Stratosphere. Nature, 238, 58-60.
- Pyle, J.A. (1978) A Simple Calculation of Ozone Depletion by Chlorofluoromethanes Using a Two-Dimensional Model. Nature, 271, 42-43.
- Pyle, J.A. (1980) A Calculation of Possible Depletion of Ozone by Chlorofluorocarbons Using a Two-Dimensional Model. Pure Appl. Geophys., 118, 355-377.
- Pyle, J.A. and C.F. Rogers (1980) Stratospheric Transport by Stationary Planetary Waves - The Importance of Chemical Processes. Quart. J. Roy. Meteorol. Soc., 106, 421-446.
- Raper, O.F., C.B. Farmer, R.A. Tota and B.D. Robbins (1977) The Vertical Distribution of HCl in the Stratosphere. Geophys. Res. Lett., 4, 531.

- Rasmussen, R.A. and M.A.K. Khalil (1981) Atmospheric CH₄: Trends and Seasonal Cycles. J. Geophys. Res., 86, 9826-9832.
- Reed, R.J. and K.G. German (1965) A Contribution to the Problem of Stratospheric Diffusion by Large-Scale Mixing. Mon. Wea. Rev., 93, 313-321.
- Ridley, B.A. and L.C. Howlett (1974) An Instrument for Nitric Oxide Measurements in the Stratosphere. Revs. Sci., Instrum., 45, 742-746.
- Ridley, B.A., M. McFarland, J.T. Bruin, H.I. Schiff and J.C. McConnell (1977) Sunrise Measurements of Stratospheric Nitric Oxide. Can. J. Phys., 55, 212-221.
- Ridley, B.A. and H.I. Schiff (1981) Stratospheric Odd-Nitrogen: Nitric Oxide Measurements at 32° N in Autumn. J. Geophys. Res., 86, 3167.
- Ridley, B.A. and D.R. Hastie (1981) Stratospheric Odd-Nitrogen: NO Measurements at 51° N in Summer. J. Geophys. Res., 86, 316.
- Rowland, F.S. and Y. Makide (1982) Upper Stratospheric Photolysis of NaOH. Geophys. Res. Lett., 9, 473-475.
- Rowland, F.S. and P.J. Roger (1982) Upper Stratospheric Photolysis of NaCl and KCl. Proc. Nat'l. Acad. Sci., 79.
- Rudolph, J., D.H. Ehhalt, A. Tonnissen (1981) Vertical Profiles of Ethane and Propane in the Stratosphere. J. Geophys. Res., 86, 7267-7272.
- Sanford, M.C.W. and A.J. Gibson (1970) Laser Radar Measurements of Atmospheric Sodium Layer. J. Atmos. Terr. Phys., 32, 1423-1430.
- Schmidt, U., J. Rudolph, F.J. Johnen, D.H. Ehhalt, A. Volz, E.P. Roth, R. Borchers and P. Fabian (1980) The Vertical Distribution of CH₃Cl, CFCl₂ and CF₂Cl₂ in the Mid-Latitude Stratosphere. Preprint of paper submitted for Proceedings of International Ozone Symposium, Boulder, CO, August 3-8, 1980.
- Simonich, D.M., B.R. Clemescha and V.W.J.H. Kirchhoff (1979) The Mesospheric Sodium Layer at 23° S: Nocturnal and Seasonal Variations. J. Geophys. Res., 84, 1542-1550.
- Sze, N.D. (1978) Stratospheric Fluorine: A Comparison between Theory and Measurements. Geophys. Res. Lett., 5, 781.

- Sze, N.D., M.B. McElroy, S.C. Wofsy, D. Kong and R. Daesen (1978) Theoretical Models of Stratospheric Chemistry, Perturbations and Trace Gas Measurements. MCA Final Report.
- Sze, N.D., M.K.W. Ko, R. Specht, M. Livshits (1980) Modeling of Chemical Processes in the Troposphere and Stratosphere. Report to AFGL, AFGL-TR-80-0251.
- Sze, N.D., M.K.W. Ko, M. Livshits, R.E. Specht, P.B. Ryan, M.B. McElroy and S.C. Wofsy (1981) Annual Report to the Atmospheric Chemistry and Dynamics Program. Prepared for CMA.
- Sze, N.D. and M.K.W. Ko (1981) The Effects of the Rate for $\text{OH} + \text{HNO}_3$ and HO_2NO_2 Photolysis on Stratospheric Chemistry. Atmos. Environ., 15, 1301.
- Tung, K.K. (1981) On the 2-D Transport of Stratospheric Trace Gases in Isentropic Coordinates - Towards an Interactive Model of Dynamics and Photochemistry. (manuscript).
- Tyson, B.J., J.F. Vedder, J.C. Arveson and R.B. Brewer (1978) Stratospheric Measurements of CF_2Cl_2 and N_2O . Geophys. Res. Lett., 5, 369-372.
- Vedder, J.F., B.J. Tyson, R.B. Brewer, C.A. Boitnott and E.C.Y. Inn (1978) Lower Stratosphere Measurements of Variation with Latitude of CF_2Cl_2 , CFCl_3 , CCl_4 and N_2O . Geophys. Res. Lett., 5, 33-36.
- Vedder, J.F., E.C.Y. Inn, B.J. Tyson, C.A. Boitnott and D. O'Hara (1981) Measurement of CF_2Cl_2 , CFCl_3 and N_2O in the Lower Stratosphere between 2°S and 73°N Latitude. J. Geophys. Res., 86, 7363.
- Wang, W.C., M.K.W. Ko, N.D. Sze and F.M. Luther (1982) Influence of Infrared Absorption Band Treatment on the Calculated O_3 Increase due to Increased CO_2 . (manuscript).
- Wang, W.C., N.D. Sze, M.K.W. Ko and P.B. Ryan (1980) Coupled Effects of Atmospheric N_2O , CH_4 , CFMs and O_3 on the Earth's Climate. Quadrennial International Ozone Symposium, Boulder, CO.
- Waters, J.W., J.C. Hardy, R.F. Jamot and H.M. Pickett (1981) Chlorine Monoxide Radical, Ozone and Hydrogen Peroxide: Stratospheric Measurements by Microwave Limb Sounding. Science, 214, 61.

Weiss, R.F. (1981) The Temporal and Spatial Distribution of Tropospheric Nitrous Oxide. J. Geophys. Res., 86, 7185.

Williams, W.J., J.J. Kusters, A. Goldman and D.G. Murcray (1976) Measurements of the Stratospheric Mixing Ratio of HCl Using an Infrared Absorption Technique. Geophys. Res. Lett., 3, 383-385.

Wofsy, S.C. and M.B. McElroy (1973) On Vertical Mixing in the Stratosphere and Lower Mesosphere. J. Geophys. Res., 78, 2619-2624.

Zander, R., H. Leclercq and L.D. Kaplan (1981) Concentration of Carbon Monoxide in the Upper Stratosphere. Geophys. Res. Lett., 8, 365.

ACKNOWLEDGEMENTS

We wish to thank S. Piro and L. Gibson for assistance in the preparation of the report. We would like to take this opportunity to acknowledge the contribution of the late Robert E. Specht in developing the softwares for the AER 1-D and 2-D models. This work is supported by the Air Force Geophysics Laboratory under contract F19628-81-C-0016 and by the Chemical Manufacturers Association.

APPENDIX A

DOCUMENTATION OF 2-D MODEL

- A.1 Introduction
- A.2 The System of Equations
- A.3 Zonal Averaging
- A.4 Source Terms for the Zonal-Mean Trace-Gas Equation
- A.5 Numerical Solution of the Trace-Gas Equation
- A.6 Dynamical Variables Input
- A.7 Chemistry Scheme
- A.8 Model Algorithm

A.1 Introduction

The AER zonal-mean model is designed to simulate the zonal-mean behavior of atmospheric trace gases. The domain of the model covers the globe from pole to pole and up to an altitude of 60km. The horizontal and vertical resolutions are approximately 10^3 km and 3.5km respectively. The dynamic variables are governed by the system of equations obtained by taking the Eulerian zonal-mean of the simplified primitive equations which assumes geostrophic wind balance. Dynamic transport of trace gases is affected by advection from zonal-mean wind and eddy transport parameterized by a symmetric diffusion tensor. The photochemical scheme used in the 2-D model is based on the grouping techniques and calculates over 35 species affecting the O_3 balance. A 24-hour averaging of the photolysis rate calculation is used to simulate diurnal average condition. The behavior of the trace gases in the atmosphere is governed by the trace gas equation

$$N \left(\frac{\partial f_i}{\partial t} + \underline{v} \cdot \nabla f_i \right) = Q_i(f_j) \quad (\text{A.1})$$

where N is the bulk air density, \underline{v} is the velocity field of bulk motion, f_i is the volume mixing ratio and Q_i the local net production/loss rate of the i^{th} species.

Equation (A.1) is to be considered as a system of equations giving the time rate of change of the Eulerian field variables f_i 's as functions of the spatial coordinates in

in three dimensions. To solve the system, one requires knowledge of N , which depends on atmospheric conditions, pressures and temperature: the velocity wind field v and knowledge of the chemical interactions. To reduce the equations to two dimensions, a method for averaging must be specified. Each of these will be discussed in the following sections.

The structure of the dynamic framework in the model follows closely that of the Oxford model (Harwood and Pyle 1975). The Oxford model was originally designed to calculate the dynamic variables together with the trace gas concentrations. At the present stage of the development, the AER model uses pre-specified dynamic variables as input and solve only the trace gas equations. The assumptions used in arriving at the system of dynamic equations in the zonal model will be reviewed in Section A.2 and A.3. The discussion on the treatment and method of solution of the system of dynamic equations is kept to a minimum. The reader is referred to in the original paper of Harwood and Pyle (1975). The treatment of the trace gas equations will be discussed in more detail in Section A.4 through Section A.7. The overall model algorithm will be discussed in Section A.8.

A.2 The System of Equations

The atmospheric circulation is governed by the coupled system of dynamic and thermodynamic equations (cf. Lorentz,

1967):

momentum equation

$$\frac{dy}{dt} = -2\Omega xy - \frac{1}{NM} \nabla p - \nabla \phi \quad (\text{A.2})$$

thermodynamic equation

$$\frac{d\theta}{dt} = J \quad (\text{A.3})$$

continuity equation

$$\frac{dN}{dt} = -N\nabla \cdot y \quad (\text{A.4})$$

equation of state: ideal gas law

$$p = NRT \quad (\text{A.5})$$

where $\frac{d}{dt} = \frac{\partial}{\partial t} + y \cdot \nabla$ is the total time derivative

Ω = angular velocity of Earth

M = average mass of an air molecule

p = pressure

ϕ = the geopotential gz where g is acceleration due to gravity, z is geometric altitude

θ = potential temperature related to temperature

T by $\theta = T \left(\frac{p_0}{p}\right)^K$ with $K = R/C_p$; R the gas constant and C_p the specific heat at constant pressure

J = the diabatic influence with $C_p J \frac{T}{\theta}$ the heating rate per unit mass

R = the gas constant

T = temperature

Note that frictional forces have been left out in the momentum equation (A.2) under the assumption that they are unimportant for large scale motion.

The system of equations (A.2) to (A.5) is coupled to the trace gas equation through the J term which depends on distribution of gases such as O₃, CO₂, N₂O and CH₄ in the atmosphere. Thus, in principle, equations (A.1) through (A.5) should be solved simultaneously as a system. The following physical assumptions are usually adopted to obtain the so-called primitive equations (cf. Holten, 1975):

- A) Replacement of the vertical momentum equation by the hydrostatic equilibrium condition

$$\frac{\partial p}{\partial z} = -MN g \quad (\text{A.6})$$

- B) Discard terms in the expression for the coriolis force that contain the vertical component of the velocity.
- C) Replace r in the resulting equation by the mean distance from the earth's center.

In order to write the momentum equation in scalar form, it is convenient to introduce a coordinate system where the pressure p is used as the vertical coordinates in conjunction with λ the longitude and ϕ the latitude. In this coordinate system, the components of the velocity vectors are;

$$u = a \cos\phi \frac{d\lambda}{dt} \quad (\text{A.7})$$

$$v = a \frac{d\phi}{dt}$$

$$w = \frac{dp}{dt}$$

With the hydrostatic equilibrium assumption, the continuity equation and the trace gas equation take the form

$$\frac{1}{a \cos\phi} \frac{\partial u}{\partial \lambda} + \frac{1}{a \cos\phi} \frac{\partial}{\partial \phi} (v \cos\phi) + \frac{\partial w}{\partial p} = 0 \quad (\text{A.8})$$

$$\frac{\partial f_i}{\partial t} + \frac{1}{a \cos\phi} \frac{\partial}{\partial \lambda} (f_i u) + \frac{1}{a \cos\phi} \frac{\partial}{\partial \phi} (f_i v \cos\phi) + \frac{\partial}{\partial p} (f_i w) = \frac{Q_i}{N} \quad (\text{A.9})$$

The primitive equations can be written (cf. Lorentz, 1967; Holten, 1975)

$$\frac{\partial u}{\partial t} + \frac{1}{a \cos\phi} \frac{\partial}{\partial \lambda} (u^2) + \frac{1}{a \cos\phi} \frac{\partial}{\partial \phi} (uv \cos\phi) + \frac{\partial}{\partial p} (uw) \quad (\text{A.10})$$

$$- \frac{uv \tan\phi}{a} - 2\Omega v \sin\phi - \frac{g}{a \cos\phi} \frac{\partial z}{\partial \lambda} = 0$$

$$\frac{\partial v}{\partial t} + \frac{1}{a \cos\phi} \frac{\partial}{\partial \lambda} (vu) + \frac{1}{a \cos\phi} \frac{\partial}{\partial \phi} (v^2 \cos\phi) + \frac{\partial}{\partial p} (vw) \quad (\text{A.11})$$

$$+ \frac{u^2 \tan\phi}{a} + 2\Omega u \sin\phi - \frac{g}{a} \frac{\partial z}{\partial \phi} = 0$$

$$\frac{\partial \theta}{\partial t} + \frac{1}{a \cos\phi} \frac{\partial}{\partial \lambda} (\theta u) + \frac{1}{a \cos\phi} \frac{\partial}{\partial \phi} (\theta v \cos\phi) + \frac{\partial}{\partial p} (\theta w) = J$$

(A.12)

$$\frac{1}{a \cos \phi} \frac{\partial u}{\partial \lambda} + \frac{1}{a \cos \phi} \frac{\partial}{\partial \phi} (v \cos \phi) + \frac{\partial w}{\partial p} = 0 \quad (\text{A.13})$$

$$p = N R T \quad (\text{A.14})$$

$$g \frac{\partial z}{\partial p} = - \frac{1}{N M} \quad (\text{A.15})$$

In the above equations, the terms $\frac{uv \tan \phi}{a}$ and $\frac{u^2 \tan \phi}{a}$ are curvature terms arising from the non-Euclidean nature of the coordinate frames. The geopotential term $\frac{1}{a} \frac{\partial \phi}{\partial \phi}$ and $\frac{1}{a \cos \phi} \frac{\partial \phi}{\partial \lambda}$ has been written out explicitly with $\phi = gz$.

In this arrangement, equations (A.9) through (A.12) are prognostic equations for f , u , v and θ respectively, while equations (A.13) and (A.14) can be considered as diagnostic equations for w and N . Since p is being used as an independent variable, equation (A.15) serves the purpose of transforming between geometrical altitude and the pressure coordinate.

A.3 Zonal Averaging

We will now discuss ways of reducing the system of primitive equations to 2 dimensions for numerical modeling. Given any of the dependent Eulerian variables in the primitive equations, e.g., f , by averaging over one of the spatial coordinates, one obtains $\bar{f}(t, \mathbf{y})$ where \mathbf{y} is the vector representing the two remaining coordinates.

The corresponding equations governing the averaged variables can be obtained by applying the averaging operation to the primitive equations. In atmospheric modeling studies, one is interested in averaging over the longitudinal coordinate to obtain \bar{f} as a function of time, latitude and altitude, which can be viewed as the zonal-mean concentration. However, the exact physical interpretation of \bar{f} must depend on the averaging process involved.

In the Eulerian-mean model, the averaging process is performed over Eulerian field quantities by integrating over the longitude while holding all other coordinates fixed. Thus, given $g(t, \phi, p, \lambda)$, (where t is time, ϕ the latitude, p the pressure height coordinates and λ the longitude), one obtains

$$\bar{g}(t, \phi, p) = \frac{\int g(t, \phi, p, \lambda) d\lambda}{\int d\lambda} \quad (\text{A.16})$$

It is convenient to define g' , the deviations from the mean, by

$$g'(t, \phi, p, \lambda) = \bar{g}(t, \phi, p) - g(t, \phi, p, \lambda) \quad (\text{A.17})$$

It follows from equation (A.16) that

$$\overline{g'(t, \phi, p, \lambda)} = 0 \quad (\text{A.18})$$

and

$$\overline{gh} = \overline{g\bar{h}} + \overline{g'h'} \quad (\text{A.19})$$

Before applying the Eulerian-mean operation to the primitive equations, the geostrophic wind balance assumption will be used to replace (A.11) by

$$2\Omega\bar{u}\sin\phi - \frac{g}{a} \frac{\partial \bar{z}}{\partial \phi} = 0 \quad (\text{A.20})$$

Using the fact that the "—" operation commutes with the coordinate differential operators, we have

$$\frac{\partial \bar{f}_i}{\partial t} + \frac{1}{a \cos\phi} \frac{\partial}{\partial \phi} (\bar{f}_i \bar{v} \cos\phi) + \frac{\partial}{\partial p} (\bar{f}_i \bar{w}) = \left(\frac{\bar{Q}_i}{\bar{N}}\right) - F_{f_i} \quad (\text{A.21})$$

$$\frac{\partial \bar{u}}{\partial t} + \frac{1}{a \cos^2\phi} \frac{\partial}{\partial \phi} (\bar{u} \bar{v} \cos^2\phi) + \frac{\partial}{\partial p} (\bar{u} \bar{w}) - 2\Omega\bar{v} \cos\phi = -F_u \quad (\text{A.22})$$

$$2 \bar{u} \sin\Omega - \frac{g}{a} \frac{\partial \bar{z}}{\partial \phi} = 0 \quad (\text{A.23})$$

$$\frac{\partial \bar{\theta}}{\partial t} + \frac{1}{a \cos\phi} \frac{\partial}{\partial \phi} (\bar{\theta} \bar{v} \cos\phi) + \frac{\partial}{\partial p} (\bar{\theta} \bar{w}) = \bar{J} - F_\theta \quad (\text{A.24})$$

$$\frac{1}{a \cos\phi} \frac{\partial}{\partial \phi} (\bar{v} \cos\phi) + \frac{\partial \bar{w}}{\partial p} = 0 \quad (\text{A.25})$$

$$\bar{N} = \frac{p}{R\bar{T}} \quad (\text{A.26})$$

$$g \frac{\partial \bar{z}}{\partial p} = -\frac{1}{\bar{M}\bar{N}} = -\frac{R\bar{T}}{M\bar{p}} \quad (\text{A.27})$$

where

$$F_{f_i} = \frac{1}{a \cos\phi} \frac{\partial}{\partial \phi} (\overline{f_i'v'}) \cos\phi + \frac{\partial}{\partial p} (\overline{f_i'w'})$$

$$F_u = \frac{1}{a \cos^2 \phi} \frac{\partial}{\partial \phi} (\overline{v' u'} \cos^2 \phi) + \frac{\partial}{\partial p} (\overline{u' w'})$$

$$F_\theta = \frac{1}{a \cos \phi} \frac{\partial}{\partial \phi} (\overline{\theta' v'} \cos \phi) + \frac{\partial}{\partial p} (\overline{\theta' w'})$$

Equations (A.21, A.22 and A.24) are to be considered as prognostic equations for \bar{f} , \bar{u} and $\bar{\theta}$ respectively. Equation (A.25) implies existence of a stream function ψ , where

$$\bar{v} = -\frac{1}{\cos \phi} \frac{\partial \psi}{\partial p} \tag{A.28}$$

$$\bar{w} = \frac{1}{a \cos \phi} \frac{\partial \psi}{\partial \phi}$$

By differentiating w.r.t. p and using the hydrostatic equation (A.27), Equation (A.23) can be rewritten as the thermal wind relation

$$p \frac{\partial \bar{u}}{\partial p} = -\frac{\left(\frac{R}{M}\right) \left(\frac{p}{p_0}\right)^k}{2\Omega \sin \phi} \frac{1}{a} \frac{\partial \bar{\theta}}{\partial \phi} \tag{A.29}$$

To obtain an equation for ψ , one notes that (A.22) and (A.24) is of the form

$$\frac{\partial \bar{u}}{\partial t} = A \tag{A.30}$$

$$\frac{\partial \bar{\theta}}{\partial t} = B \tag{A.31}$$

where A and B contains only spatial derivatives. By differentiating (A.30) w.r.t. p and (A.31) w.r.t. ϕ and using the thermal wind relation, we obtain

$$p \frac{\partial A}{\partial p} = - \frac{\left(\frac{R}{M}\right) \left(\frac{p}{p_0}\right)^k}{2\Omega \sin\phi} \frac{1}{a} \frac{\partial B}{\partial \phi} \quad (\text{A.32})$$

Equation (A.32) is a diagnostic equation for ψ in terms of \bar{u} , $\bar{\theta}$, F_u , \bar{J} and F_θ and their spatial derivative. Summarizing, the system of zonal mean equations are (cf. Harwood and Pyle, 1975):

Prognostic Equation:

$$\frac{\partial \bar{f}_i}{\partial t} + \frac{1}{a \cos\phi} \frac{\partial}{\partial \phi} (\bar{f}_i \bar{v} \cos\phi) + \frac{\partial}{\partial p} (\bar{f}_i \bar{w}) = \left(\frac{\bar{Q}_i}{N}\right) - F_{f_i} \quad (\text{A.33})$$

$$\frac{\partial \bar{u}}{\partial t} + \frac{1}{a \cos^2\phi} \frac{\partial}{\partial \phi} (\bar{u} \bar{v} \cos^2\phi) + \frac{\partial}{\partial p} (\bar{u} \bar{w}) - 2\Omega \bar{v} \cos\phi = -F_u \quad (\text{A.34})$$

$$\frac{\partial \bar{\theta}}{\partial t} + \frac{1}{a \cos\phi} \frac{\partial}{\partial \phi} (\bar{\theta} \bar{v} \cos\phi) + \frac{\partial}{\partial p} (\bar{\theta} \bar{w}) = \bar{J} - F_\theta \quad (\text{A.35})$$

Diagnostic Equation for ψ :

$$p \frac{\partial A}{\partial p} = - \frac{\left(\frac{R}{M}\right) \left(\frac{p}{p_0}\right)^k}{2\Omega \sin\phi} \frac{1}{a} \frac{\partial B}{\partial \phi} \quad (\text{A.36})$$

Definitions

$$\left. \begin{aligned} \bar{v} &= - \frac{1}{\cos\phi} \frac{\partial \psi}{\partial p} \\ \bar{w} &= \frac{1}{a \cos\phi} \frac{\partial \psi}{\partial \phi} \end{aligned} \right\} \quad (\text{A.37})$$

$$\bar{N} = \frac{p}{RT} \quad (\text{A.38})$$

Conversion to geometrical altitude:

$$\frac{\partial \bar{z}}{\partial p} = - \frac{R\bar{T}}{Mgp} \quad (\text{A.39})$$

Given the variables \bar{f}_i , \bar{u} , \bar{T} , at time t , if the sources terms $(\frac{\bar{Q}_i}{N})$, F_{f_i} , \bar{J} , F_θ and F_u are known, (A.36) can be used to solve for ψ . The velocity field \bar{v} and \bar{w} are specified by (A.37). Equations (A.33), (A.34) and (A.35) can then be used to solve for \bar{f}_i , \bar{u} and \bar{T} at a later time $t + \Delta t$. Thus the whole system can be propagated forward in time.

A.4 Source Terms for Zonal-Mean Trace-Gas Equations

We shall now restrict our discussion to the treatment of the trace-gas equations. A discussion on the treatment of the dynamic equations can be found in Harwood and Pyle (1975). Solution to (A.33) depends on knowledge of \bar{v} , \bar{w} , $(\frac{\bar{Q}_i}{N})$ and F_{f_i} . As pointed out in the introduction, \bar{v} and \bar{w} are obtained from input files. The term F_{f_i} is parameterized by mean of an eddy diffusion tensor (Reed and German, 1965). In the present coordinate system,

$$\begin{pmatrix} \overline{v'f_i'} \\ \overline{w'f_i'} \end{pmatrix} = - \begin{pmatrix} K^{\phi\phi} & K^{\phi p} \\ K^{p\phi} & K^{pp} \end{pmatrix} \begin{pmatrix} \frac{1}{a} \frac{\partial \bar{f}_i}{\partial \phi} \\ \frac{\partial \bar{f}_i}{\partial p} \end{pmatrix} \quad (\text{A.40})$$

where $K^{p\phi} = K^{\phi p}$. Note that it is assumed that the same diffusion tensor can be used for all species.

The formulation of Reed and German (1965) is based on mixing length type argument. Let the motion in a fluid be given by a mean motion \bar{v} with deviation v' . For a quantity x which is conserved along the mean flow, it is reasonable to argue that the deviation from the mean x' is given by

$$x' = - \underline{l}' \cdot \nabla \bar{x}$$

where \underline{l}' is the displacement vector associated with the deviation velocity v' . If one further assumes that \underline{l}' and v' are linearly related, i.e.

$$\underline{l}' = v' \Delta t$$

where Δt is the characteristic time-scale of the deviation from the mean motion, it follows that

$$\overline{v'x'} = - \overline{v'(\underline{l}' \cdot \nabla \bar{x})} = - \Delta t \overline{\underline{l}'\underline{l}'} \cdot \nabla \bar{x} \quad (\text{A.41})$$

where $\overline{\underline{l}'\underline{l}'}$ is a symmetry tensor. In scalar form, we have

$$\begin{pmatrix} \overline{v'x'} \\ \overline{w'x'} \end{pmatrix} = - \begin{pmatrix} K^{\phi\phi} & K^{\phi p} \\ K^{p\phi} & K^{pp} \end{pmatrix} \begin{pmatrix} \frac{1}{a} \frac{\partial \bar{x}}{\partial \phi} \\ \frac{\partial \bar{x}}{\partial p} \end{pmatrix} \quad (\text{A.42})$$

If one assumes that the eddy fluxes of potential temperature can be parameterized this way, one can deduce the values for the tensor component by examining the temperature and wind field statistics (cf. Reed and German, 1965; Luther 1973).

The exact form of the term Q_i will be discussed in Section A.6. The discussion here will be restricted to the treatment of the averaging processes. The term Q/N consists of sums of terms each of which take one of the following forms

$$J_i f_i; N k_{ij}(T) f_i f_j; N^2 k_{ijk}(T) f_i f_j f_k$$

for photolytic processes and two-body and three-body reactions respectively. Note that the temperature dependence of the reaction rates k_{ij} and k_{ijk} are explicitly displayed. The longitudinal behavior of J_i and f_i arise from the diurnal effect since each longitude is at a different local time at any instant in time. In the present model, the term $\left(\frac{\bar{Q}}{N}\right)$ is formed by taking the corresponding products of the zonal-mean quantities. No attempt is made to take into account for the covariance of the individual terms making up the product.

A.5 Numerical Solution of the Trace-Gas Equations

In finding the numerical solution of the equation, it is more convenient to use the log-pressure coordinate $\xi = \ln(p_0/p)$ where p_0 is taken to be 1000 mb. In this coordinate system, the vertical velocity is given by

$$\omega = \frac{d\xi}{dt} \tag{A.43}$$

Equation (A.33) can be rewritten in the form:

$$\frac{\partial \bar{f}_i}{\partial t} + \frac{1}{a \cos \phi} \frac{\partial}{\partial \phi} (\bar{f}_i \bar{v} \cos \phi) + e^\xi \frac{\partial}{\partial \xi} (e^{-\xi} \bar{f}_i \bar{\omega}) = \left(\frac{\bar{Q}_i}{N}\right) - F_{f_i} \quad (\text{A.44})$$

where

$$F_{f_i} = \frac{1}{a \cos \phi} \frac{\partial}{\partial \phi} (\bar{f}_i \bar{v}' \cos \phi) + e^\xi \frac{\partial}{\partial \xi} (e^{-\xi} \bar{f}_i \bar{\omega}')$$

with

$$\begin{pmatrix} \bar{f}_i \bar{v}' \\ \bar{f}_i \bar{\omega}' \end{pmatrix} = - \begin{pmatrix} K^{\phi\phi} & K^{\phi\xi} \\ K^{\xi\phi} & K^{\xi\xi} \end{pmatrix} \begin{pmatrix} \frac{1}{a} \frac{\partial \bar{f}_i}{\partial \phi} \\ \frac{\partial \bar{f}_i}{\partial \xi} \end{pmatrix}$$

$$K^{\phi\xi} = K^{\xi\phi} = -K^{\phi p} e^\xi$$

$$K^{\xi\xi} = K^{pp} \left(\frac{\partial \xi}{\partial p}\right)^2 = K^{pp} e^{2\xi}$$

To obtain a numerical solution of the equations, the differential operators are first converted to finite difference form. The two-dimension space is divided into a 19 x 17 grid. The globe is covered by 19 latitude belts each 9.5° (10³ km) wide. The vertical resolution is constant in $\xi = \ln p_0/p$ with $\Delta\xi = 0.5$ or $\Delta z = 3.5$ km. The top boundary corresponds to 0.3 mb level or ~60 km.

The grid is schematically represented in Figure A-1. Within each box, the variables are defined at different positions so that all the individual terms entering into Equation (A.44) are defined at the center of the grid. This is summarized in Table A-1.

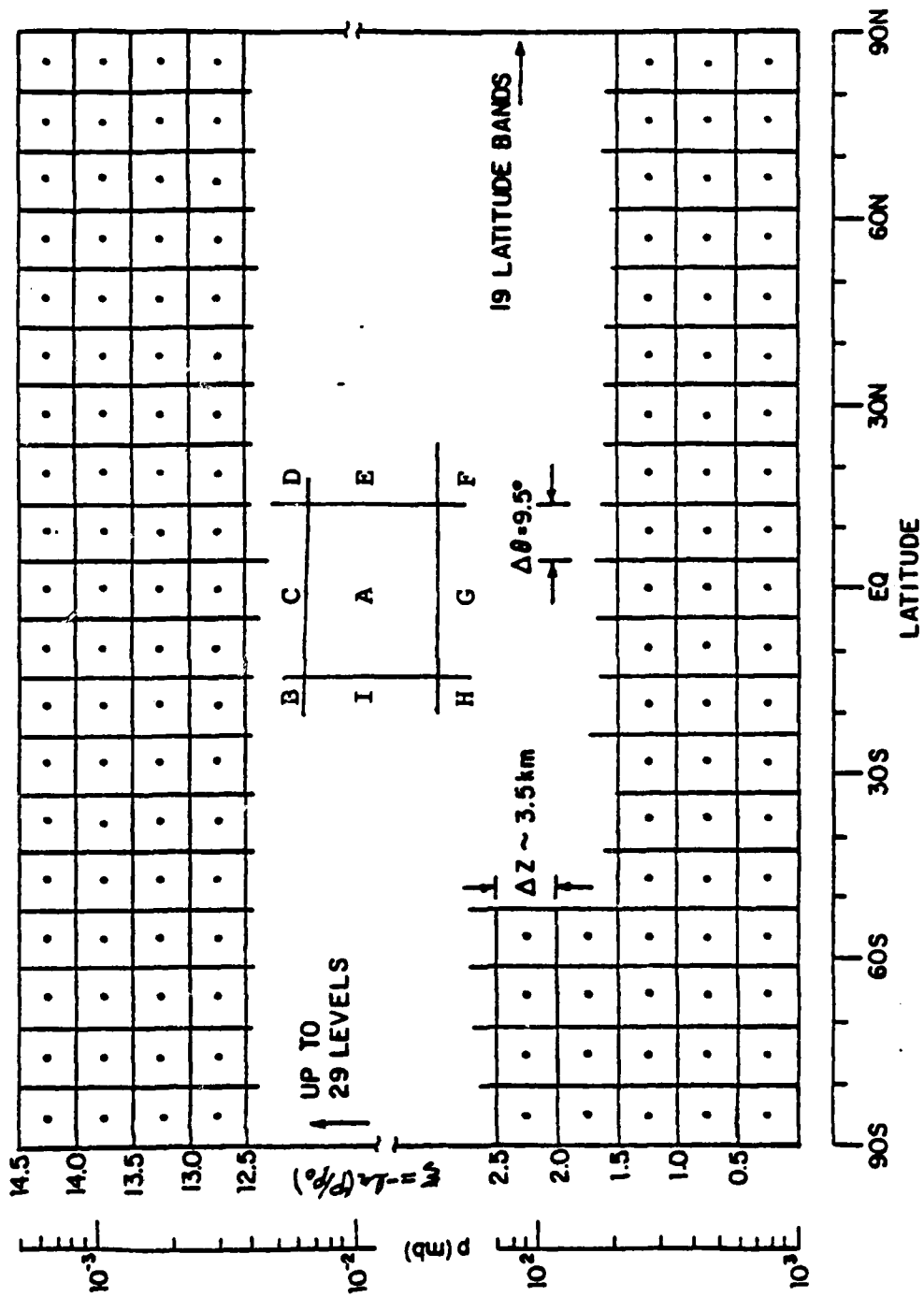


Figure A-1
Schematic diagram showing the grid sizes in the 2-D model.

Table A-1

Table showing the positions where each of the variables are defined in the finite difference scheme. The positions refer to those marked in Figure A-1.

Position	Variables
Center of Box A	$\bar{f}_i, \frac{\partial \bar{f}_i}{\partial t}, \bar{T}, \left(\frac{Q_i}{N}\right), \bar{N}$
C & G	$\bar{\omega}, \frac{\partial \bar{f}_i}{\partial \xi}, K^{\xi\xi},$
	$\overline{f_i \omega} = K^{\xi\phi} \frac{1}{a} \frac{\partial \bar{f}}{\partial \phi} + K^{\xi\xi} \frac{\partial \bar{f}_i}{\partial \xi}$
B, D, F, H	$\psi, K^{\phi\xi}, K^{\xi\phi}$
E, I	$K^{\phi\phi}, \bar{v}, \frac{\partial \bar{f}_i}{\partial \phi}$
	$\overline{f_i \omega} = K^{\phi\phi} \frac{1}{a} \frac{\partial \bar{f}}{\partial \phi} + K^{\xi\phi} \frac{\partial \bar{f}}{\partial \xi}$

Equation (A.33) is used to define $\frac{\partial \bar{f}_i}{\partial t}$ at each time step. The R.H.S. is evaluated using \bar{v} , $\bar{\omega}$ and K's from input files, $(\frac{\bar{O}}{N})$ calculated from the chemistry scheme and values of \bar{f}_i 's at the current time step. The Adam-Bashford scheme is used to calculate the \bar{f}_i at the next time step, i.e.:

$$\bar{f}_i(t + \Delta t) = (1.5 \frac{\partial \bar{f}_i}{\partial t}(t) - 0.5 \frac{\partial \bar{f}_i}{\partial t}(t - \Delta t))\Delta t$$

Adjustments are made at each time step to simulate the appropriate boundary condition at the top and bottom of the atmosphere. These will be discussed in Section A.7.

The Adam-Bashford scheme is a second order accuracy in time. To ensure stability, Δt must be sufficiently small, with the present grid size, Δt is taken to be 4 hours.

A.6 Dynamical Variables Input

The dynamical variables input necessary for solving (A.44) are the temperature field, the stream function for generating \bar{v} and $\bar{\omega}$ and the eddy diffusion coefficients. The values for the components of the eddy diffusion coefficients are from Luther (1973). The temperature and ψ -function are from previous calculations of Harwood and Pyle (1977).

a) Eddy diffusion tensor:

The values of the symmetric tensor are compiled by Luther (1973) using the procedure similar to the one described by Reed and German (1965). The heat transfer, temperatures and wind variance data of Oort and Rasmussen (1971) are

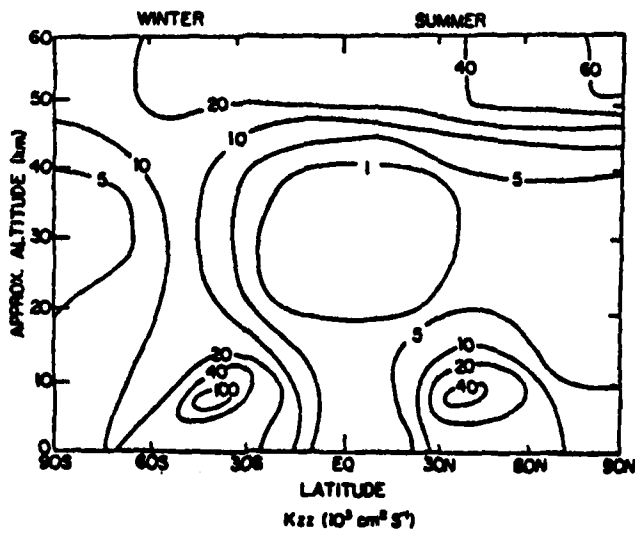
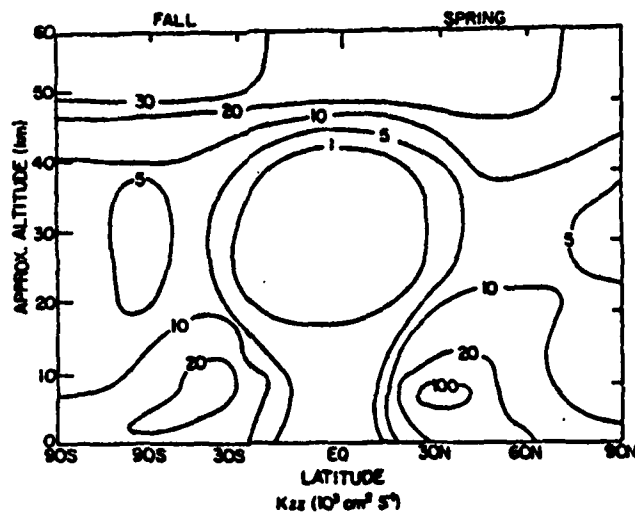


Figure A-2

Latitude-altitude cross-section plots of K_{22} for different seasons. Values are from Luther (1973).

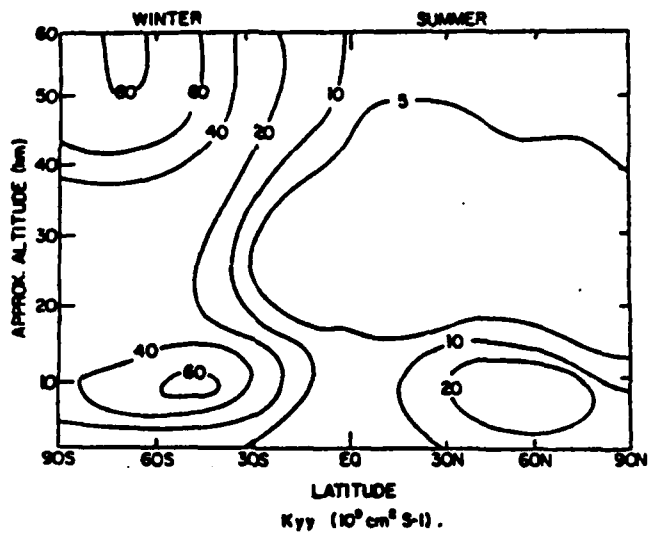
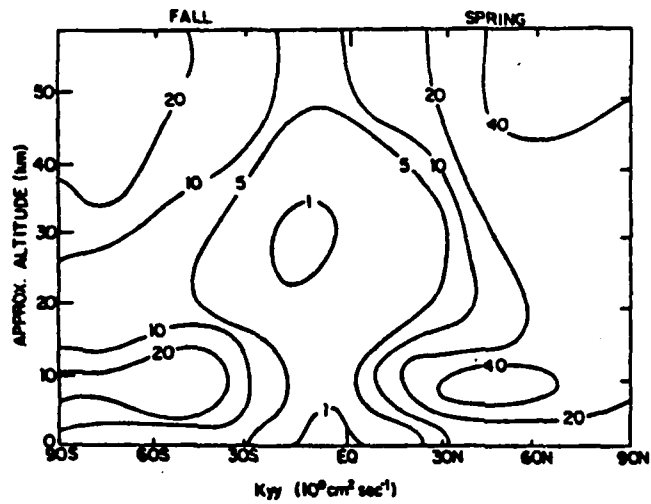


Figure A-3

Latitude-altitude cross-section plots of K_{yy} for different seasons. Values are from Luther (1973).

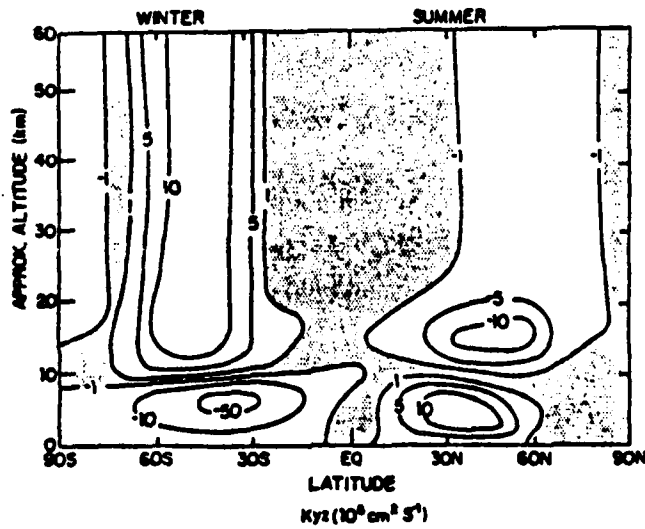
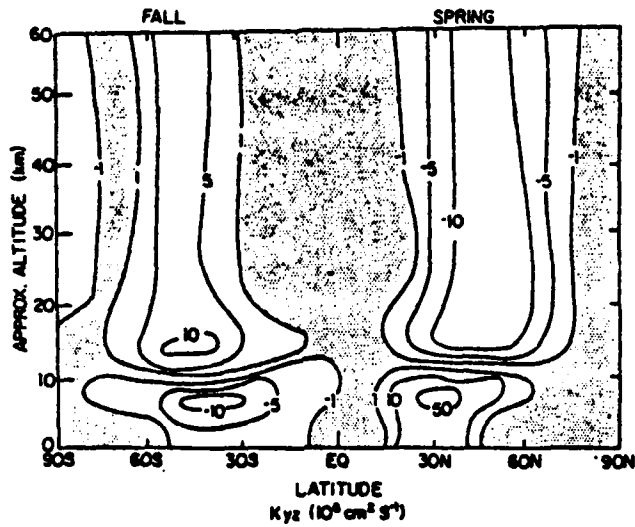


Figure A-4

Latitude-altitude cross-section plots of K_{yz} for different seasons. Values are from Luther (1973).

analyzed to derive a set of values as functions of time and space. The original data only covers part of the northern hemisphere. The results of Newell et al. (1966) and Wofsy and McElroy (1973) are used to extrapolate the values at places where there is no data. The values for $K^{\phi\phi}$, $K^{\phi\xi}$ and $K^{\xi\xi}$ for the northern hemisphere written on files as function of latitude and altitude with a set of values for each month. The values of the southern hemisphere is obtained by using the northern hemisphere values shifted by six months. The values for the K's are read from input file and kept constant over the whole month. Values for K's are plotted in Figure A-2 through A-4 for different seasons.

b) Temperature and ψ -field:

The values of T and ψ are tabulated as functions of latitude and altitude around the year with one set of values every 10 days. A simple linear interpolation scheme is used to obtain the values for each time-step as required. Plots of the values of the variables for different seasons are given in Figure A-5, A-6 and A-7.

The values are from model calculations of the Oxford model in which the dynamic equations are solved together with the O_3 equation. A detail of the model calculation can be found in Harwood and Pyle (1977); only a brief summary will be given here.

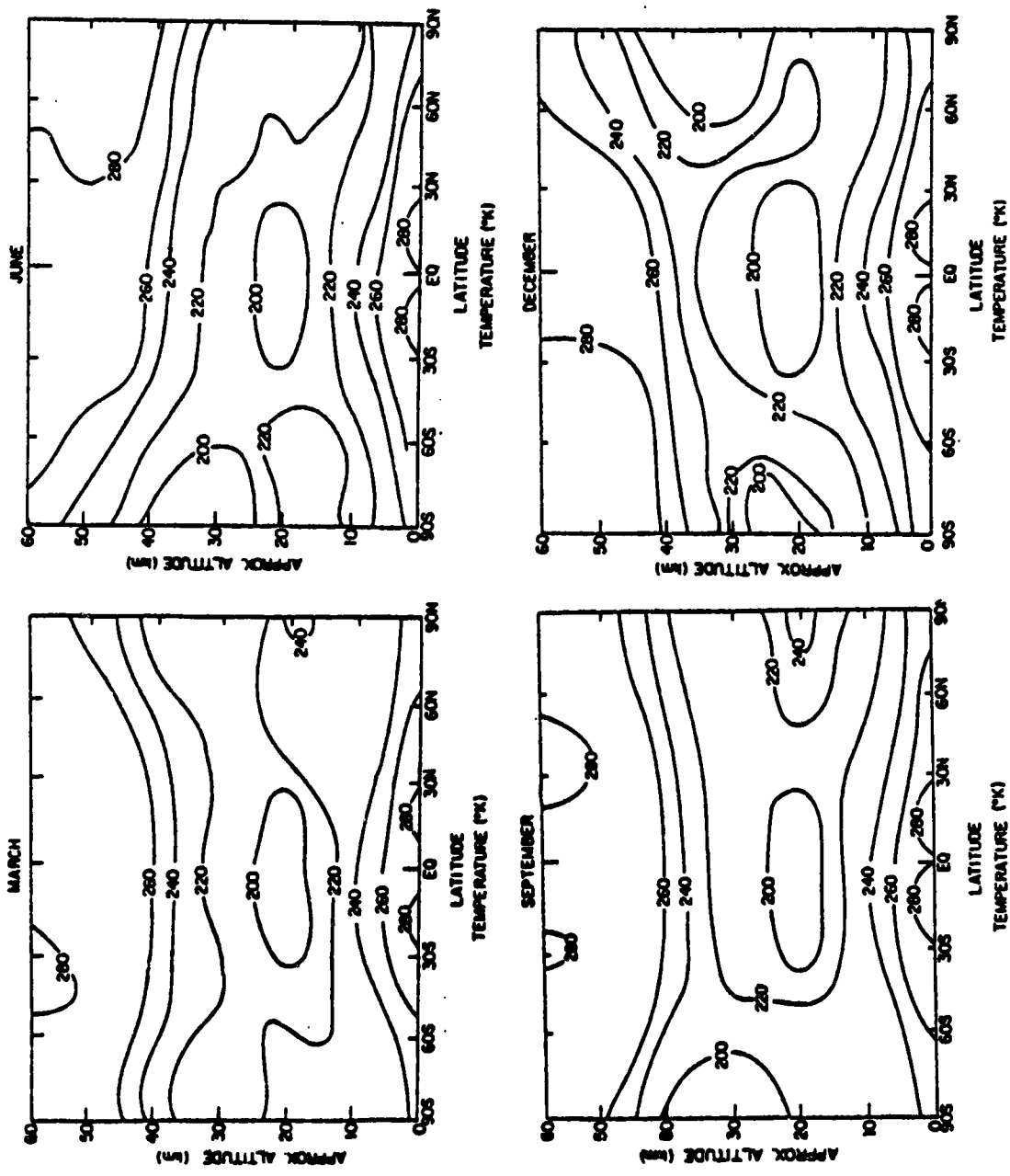


Figure 7-5
 Latitude-altitude cross-section plots of the temperature for different seasons
 Values are from Harwood and Pyle (1977).

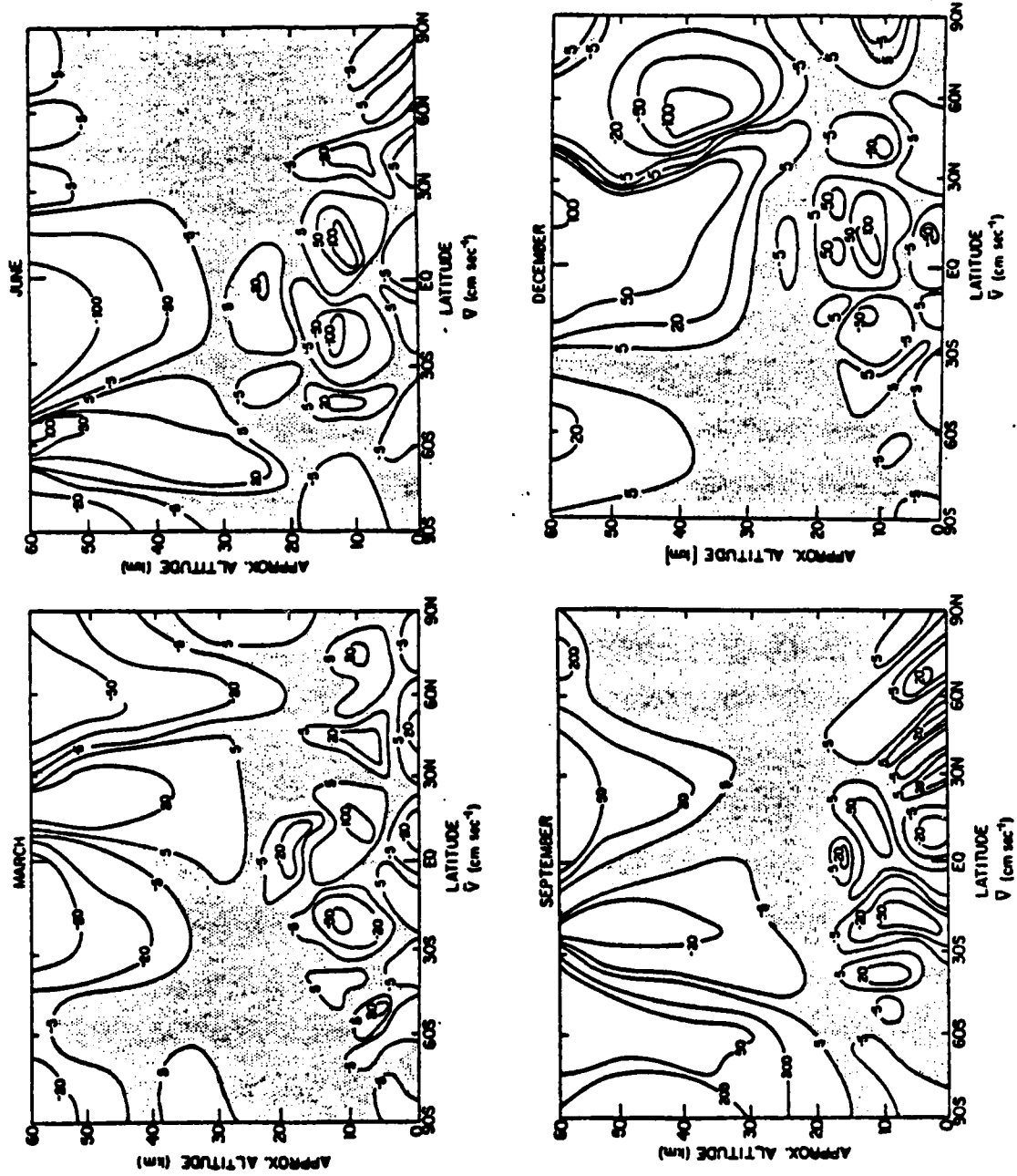


Figure A-6

Latitude-altitude plots of horizontal velocity for different seasons. Values are from Harwood and Pyle (1977).

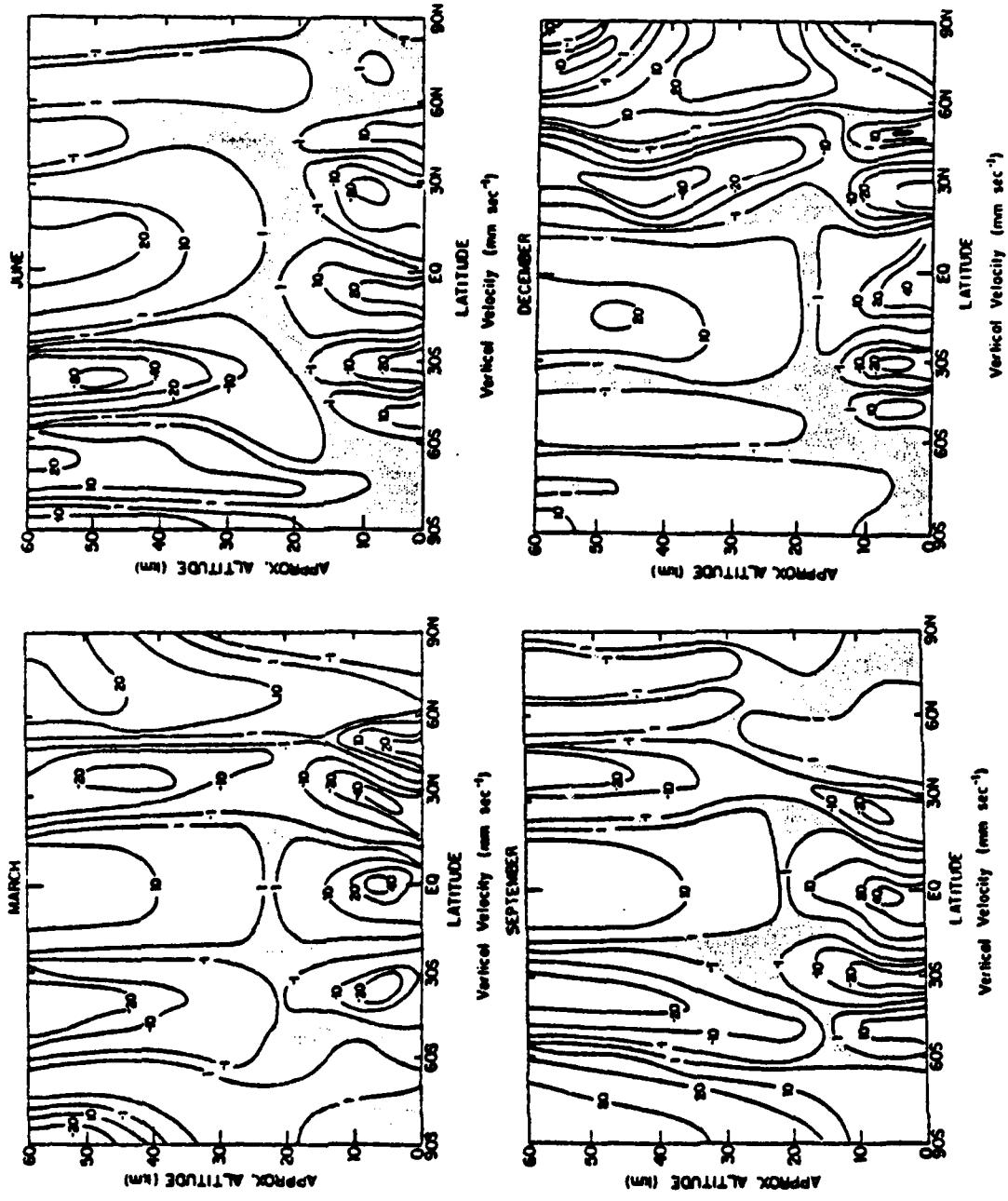


Figure A-7

Latitude-altitude cross-section plots of the vertical velocity for different seasons. Values are from Harwood and Pyle (1977).

(i) Treatment of Ozone equation in Harwood and Pyle (1977):

It is assumed that deviations from the photochemical equilibrium concentration of O_3 ($[O_3]_e$) decay with a chemical lifetime τ . In terms of the parameters used in (A.44)

$$Q_{O_3} = \frac{[O_3]_e - [O_3]}{\tau}$$

In the 1977 model run, $[O_3]_e$ and τ are precalculated and tabulated. A chemical scheme involving OH and NOX is used where $[O_3]_e$ and τ are calculated from given latitudinal independent altitude profile of OH, NOX and reaction rates.

The eddy fluxes for O_3 are parameterized by eddy diffusion tensor. A zero mixing ratio boundary condition is imposed at the lower boundary to simulate rapid destruction at the ground.

(ii) Treatment of temperature equation in Harwood and Pyle (1977):

The heating/cooling rate is treated as follows:

Solar heating: Heating by O_3 absorption using the parameterization of Kennedy (1964) and model calculated O_3

Thermal radiation:
for troposphere (up to 12km), constant lapse rate from climatology is assumed

1.5 K/day 0-8 km
.75 K/day 9-12 km

for lower stratosphere (12km-24km), thermal cooling is set equal to solar heating so that there is no net heating

for stratosphere (above 24km) long wave cooling by CO_2 and O_3 each parameterized by two altitude dependent coefficients.

Eddy fluxes of potential temperature are parameterized by eddy diffusion tensor. The heat flux across the lower boundary is calculated as functions of wind and temperature via the method of Clarke (1970). The underlying surface is assumed to be at fixed temperature with infinite heat capacity.

(iii) Treatment of angular momentum equation:

The momentum flux across the boundary simulating frictional drag is calculated from the wind and temperature via the method of Clarke (1970). The values for horizontal eddy momentum fluxes are deduced from the observation of Nimbus-V SCR data. Vertical eddy momentum is ignored.

A.7 Chemistry Scheme

The design of the chemistry scheme is based on the grouping technique. The trace gases are separated into the radical species and the long-lived species. For the radical species, local photochemical equilibrium is assumed. Thus the concentrations are given by the system of algebraic equations:

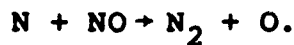
$$Q_i(N_j) = 0 \quad i = 1, \dots, NR \quad \text{where } NR \text{ is the number of radical species} \quad (A.45)$$

$$j = 1, \dots, NS \quad \text{where } NS \text{ is the total number of trace species in the model}$$

The radical species treated in the model is listed in Table A-2 and grouped into families.

In the grouping technique, the solution to Equation (A.45) provides the partition of the radical species within each family. The abundance of each family group is related to long-lived species. The abundance of the oxygen family is to a large extent controlled by O_2 concentration, while the hydrogen and methyl family depends on water vapor concentrations. The treatment of O_2 and H_2O concentration is summarized in Table A-3.

The sums of the nitrogen radicals (NOX) and the chlorine radicals (ClX) are each treated as a long-lived species. The ClX concentration is obtained from the solution of the trace gas equation with photo-oxidation of CCl_4 , $CFCl_3$, CF_2Cl_2 , CH_3Cl and CH_3CCl_3 as the source and tropospheric washout as sink. In the case of NOX, photo-oxidation of N_2O constitutes the source while the sink consists of tropospheric washout and stratospheric removal via the reaction.



The production/loss rates of the long-lived species are expressed in the form

$$Q_i = P_i - L_i \bar{N} f_i - L_i^{(2)} (\bar{N} f_i)^2$$

where P_i is the production rate, L_i and $L_i^{(2)}$ are the linear and quadratic loss frequency respectively.

Table A-2

Group of Radical Species

Family	Species
Oxygen	O, O('D)
Hydrogen	H, OH, HO ₂ , H ₂ O ₂
Methyl family	CH ₃ , CH ₃ O ₂ , CH ₃ O, CH ₂ O, HCO
Nitrogen	NO, NO ₂ , NO ₃ , N ₂ O ₅ HNO ₃ , ClNO ₃ , N, HNO ₄
Chlorine	Cl, ClO, ClNO ₃ , HCl, HOCl

Table A-3

Fixed Species

Fixed Species	Remark
\bar{N}	Calculated from ideal gas law using \bar{T}
$\overline{O_2}$	Set equal to 21% of \bar{N}
$\overline{H_2O}$	Stratospheric value of 5 ppmv is assumed Tropospheric mixing ratio is calculated from latitudinal dependent relative humidity profile (see Table A-5).

A zero flux boundary condition is imposed at the poles and the top boundary for all long-lived species except O_3 for which photochemical equilibrium is assumed at the top of the atmosphere. Lower boundary conditions are specified to simulate appropriate exchange with the surface. The list of long-lived species in the model is given in Table A-4 together with the lower boundary conditions.

The reaction rate constants are taken from NASA/WMO workshop. Tropospheric washout is parameterized by a first order loss frequency with effective lifetime of 10 days. A 24-hour averaging is used to calculate the photolysis rate to simulate diurnal averaged condition.

A.8 Model Algorithm

The model algorithm employed in the present model is schematically represented in Figure A-8. For our numerical studies, the radical species concentrations and the production rates and loss frequencies of the long-lived species are calculated once every 10 days. The long-lived species solutions are propagated forward in time for 10 days with the production rates and loss frequencies held fixed. The values for the eddy diffusion tensor is updated once a month. The temperature and ψ field is read in and interpolation for each time step.

Table A-4

Long-Lived Species and Lower Boundary Condition

Species	Lower Boundary Condition
N_2O	300 ppbv
NOX	.1 ppbv
CH_3Cl	.8 ppbv
CCl_4	.12 ppbv
CH_3CCl_3	.12 ppbv
CFC-11 } CFC-12 }	Time-dependent release rate from CMA (1980) and spread uniformly between 24°N and 60°N
ClX	1 ppbv
H_2	500 ppbv
CO	90°S-50°S 60 ppbv 40°S-Eq. 70 ppbv Eq-40°N 140 ppbv 80°N-90°N 190 ppbv
CH_4	1.5 ppmv
O_3	30 ppbv

Table A-5
Relative Humidity

Lat. \ Alt.			24S	5S	5N		
	90S-45S	42S-24S	↓ 5S	↓ 5N	↓ 24N	24N-42N	42N-90N
$\xi = 0 \rightarrow$ $\xi = 0.5$.65	.5	.6			.5	.65
$\xi = 0.5 \rightarrow$ $\xi = 1.5$.5	.38	.43			.38	.5
$\xi = 1.5 \rightarrow$ $\xi = 2$.55	.58			.55	
$\xi = 2 \rightarrow$ $\xi = 2.5$		Summer 7	Smr .8	.8	Smr .8	Summer .7	



Stratospheric value of 5 ppmv is used.

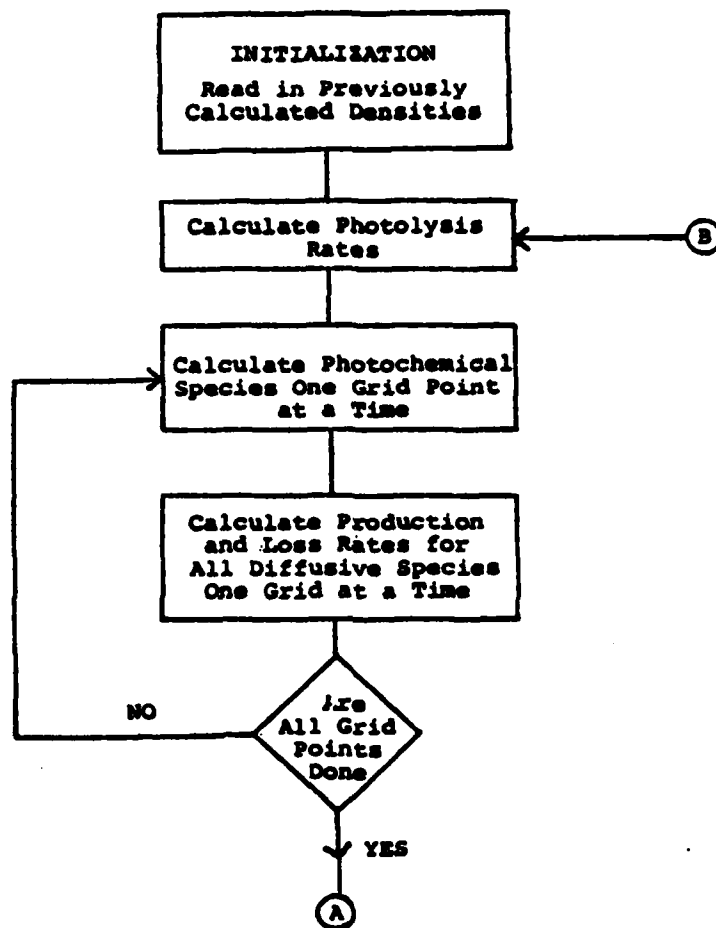


Figure A-8
Schematic Flow Chart for 2-D Model

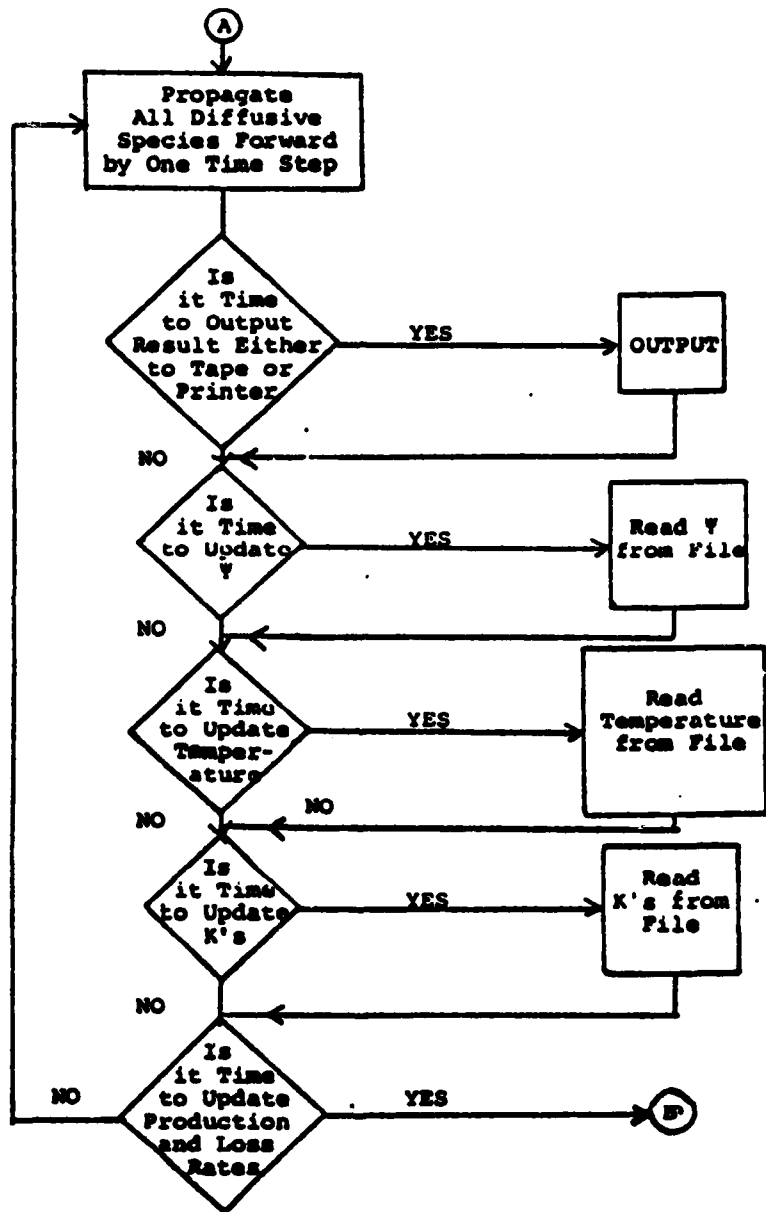


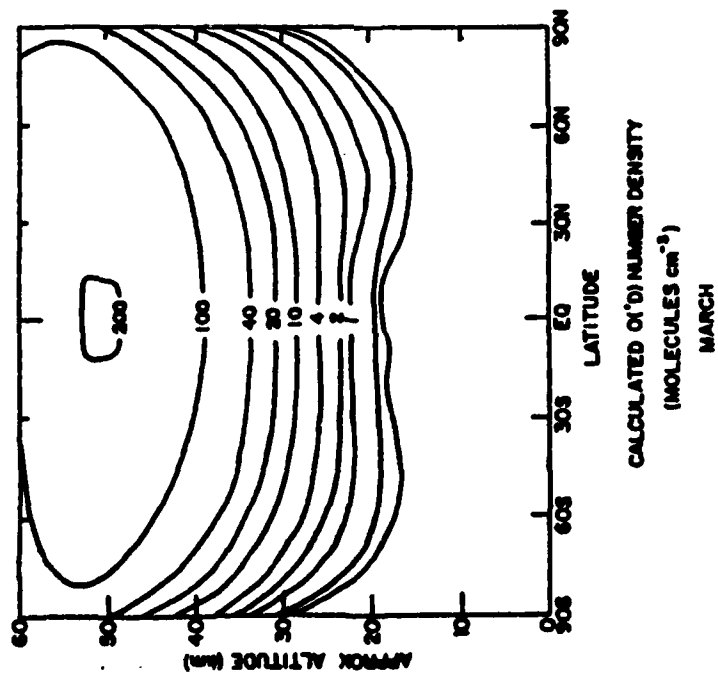
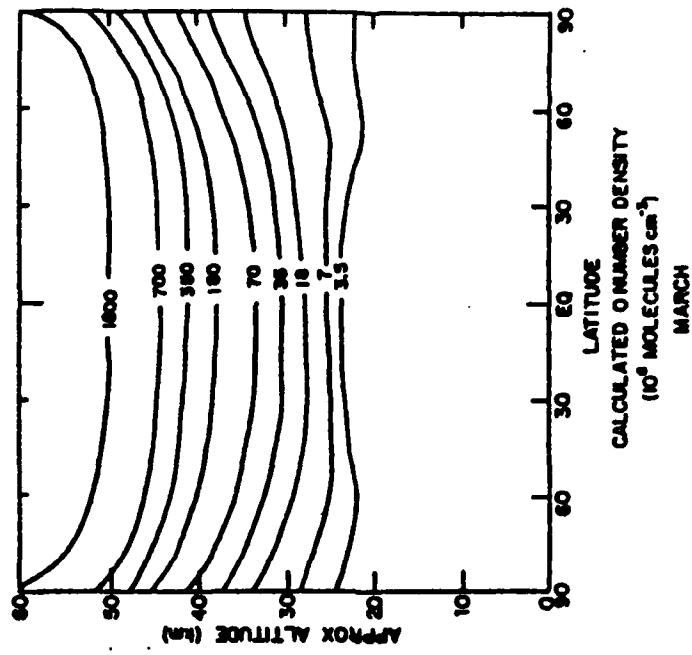
Figure A-8 (cont.)

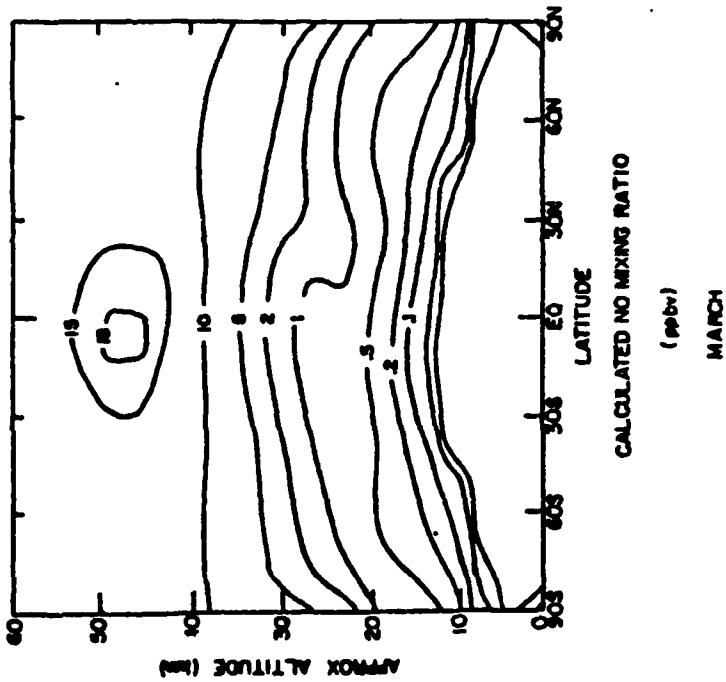
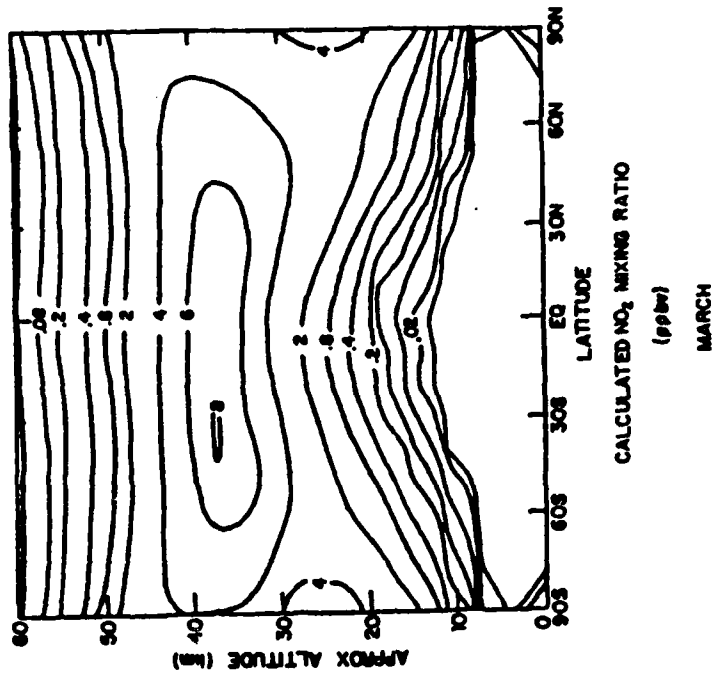
APPENDIX B

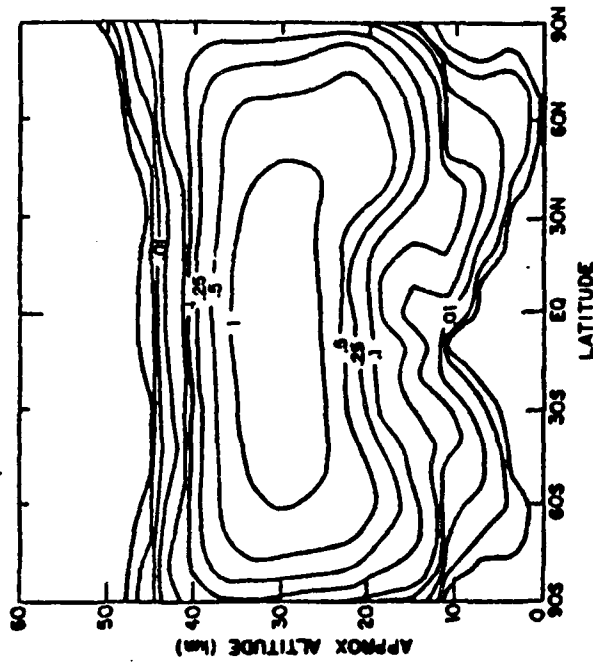
LATITUDE-ALTITUDE CROSS-SECTIONS
FOR RADICAL SPECIES

Presented here are the calculated latitude-altitude cross-sections for some of the radical species from the AER 2-D model corresponding to March conditions. The concentrations, which are computed using 24-hour averaged photolysis rates, can be interpreted as the diurnal average species concentrations. This should be taken into account in comparing the calculated results with available measurements.

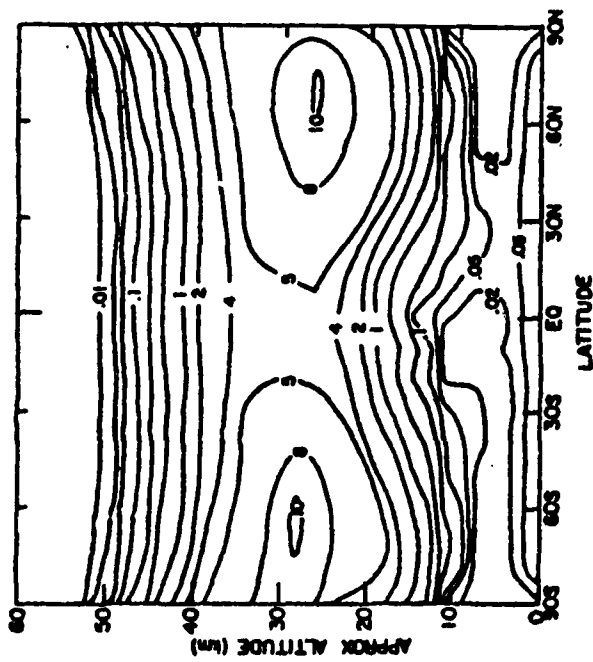
The behavior of the species in the upper stratosphere can, to a large extent, be explained in terms of photochemical interactions. Some of the species exhibit sizeable latitudinal variations in the lower stratosphere. In the case of the radical species with longer photochemical lifetimes (HCl , HNO_3), the effect of transport is evident.







CALCULATED HO₂/NO₂ MIXING RATIO
(ppbv)
MARCH



CALCULATED HNO₃ MIXING RATIO
(ppbv)
MARCH

